DISSERTATION / DOCTORAL THESIS

Titel der Dissertation /Title of the Doctoral Thesis

Spacetime Simulation and Metrology with Bose-Einstein Condensates

verfasst von / submitted by

Daniel Hartley

angestrebter akademischer Grad / in partial fulfilment of the requirements for the degree of

Doktor der Naturwissenschaften (Dr. rer. nat.)

Wien, 2019 / Vienna 2019

Studienkennzahl lt. Studienblatt / degree programme code as it appears on the student record sheet:	A 796 605 411
Dissertationsgebiet lt. Studienblatt / field of study as it appears on the student record sheet:	Physik
Betreut von / Supervisor:	Prof. Dr. Ivette Fuentes

To Dad

Abstract

After thousands of years of access only to light based astronomy, the rapidly accelerating march of technological progress has brought direct measurements of gravity beyond Newton into the realm of reality. From tests of the equivalence principle in satellites and even on the Moon to the first detection of gravitational waves, these measurements are expanding human capabilities for observing the Universe and strongly constraining our models of physical reality.

Cold atoms are starting to play an important role in tests and measurements of gravity. The low noise and high degree of control afforded by cold atom system make them an attractive platform for precision metrology. Many of these gravitational tests are already being made with cold atoms and the next generation of gravitational wave detectors with cold atom systems is currently under construction.

The natural limit of "cold" for most atoms is a Bose-Einstein condensate (BEC). In a BEC the atoms are cooled to the ground state, their wavefunctions spread out to overlap completely, and quantum phenomena occur over macroscopic distances (a typical experimental BEC has the width of a human hair). Control of the quantum state of a BEC adds another powerful tool to the toolbox of the precision metrologist.

In this thesis, a BEC-based detector for constraining models beyond General Relativity is proposed, alongside techniques for various analogue simulations. The models considered here are fifth force models where the force is "screened" in areas of high ambient matter density. Such models appear in many extensions to General Relativity e.g. string theory, and are currently most tightly bounded by atom interferometry experiments.

The two analogue simulations described in this thesis, comprising these screened fifth-force models and gravitational waves, are both fundamentally interesting for tests of computationally challenging parameter spaces. They are also useful for (and originally motivated by) testing the metrological schemes of the detector proposed in this thesis and a BEC-based gravitational wave detector proposed in 2014.

If all of the atoms in a BEC are in the ground state, low energy excitations take the form of collective oscillations i.e. sound waves. In this manifestly quantum system, sound waves only occur in a quantised manner and quantised sound waves are called "phonons". The evolution of the phonon field is a key process studied in this thesis. The analogue simulation techniques described in this thesis are achieved by modifying the experimental parameters of a BEC such that the equations of motion for the phonon field on a flat static background become identical to those on the desired non-trivial background.

For the gravitational wave simulation, explicit expressions are given for the experimental parameters needed to simulate the effect of any generic far-field gravitational wave profile. For the screened fifth force simulation, these parameters are derived for many of the most commonly studied screening mechanisms including chameleon, symmetron, dilaton, galileon and D-BIon models.

The detector proposed in this thesis consists of a guided BEC interferometer scheme. The sensitivity of this detector is optimised and the resulting constraints on two of the simplest screening mechanisms; the chameleon and symmetron mechanisms, are calculated. It is shown that a single run of this detector could entirely eliminate the remaining interesting parameter space of the simplest chameleon model, as well as substantially improving existing bounds on other models by many orders of magnitude.

Zusammenfassung

Nach Tausenden von Jahren von alleinig lichtbasierter Astronomie bringen die rasanten technologischen Fortschritte des letzten Jahrhunderts die direkte Messung der Gravitation jenseits von Newton an die Schwelle des Machbaren. Tests des Äquivalenzprinzips in Satelliten und sogar auf dem Mond sowie die ersten Erfassungen von Gravitationswellen erweitern die menschlichen Fähigkeiten zur Beobachtung des Universums. Die gewonnen hochpräzisen Daten werden verwendet um einige physikalische Modelle zu falsifizieren und andere zu untermauern.

Aufgrund ihrer hohen erreichbaren Präzision und Kontrollierbarkeit sind ultrakalte Atomsysteme dabei zu einem wichtigen Bestandteil von Gravitationstests zu werden. Ultrakalte Atomsysteme werden bereits in vielen solcher Tests und der im Bau befindlichen nächsten Generation von Gravitationswellendetektoren eingesetzt.

Werden Atome sehr stark gekühlt, entsteht bei den meisten Elementen ein Bose-Einstein-Kondensat (BEK). Ein BEK besteht aus Atomen im quantenmachanischen Grundzustand, deren Wellenfunktionen sich ausdehnen, einander überlappen und somit ein makroskopisches Quantenobjekt bilden. Die genaue Kontrolle über diesen Quantenzustand kann ein wichtiges Werkzeug für den Präzisionsmetrologe sein.

In dieser Doktorarbeit wird ein BEK-Detektor zur Parameterbeschränkung von über die allgemeine Relativitätstheorie hinausgehenden Modellen vorgeschlagen und Methoden zur analogen Simulation dieser Modelle sowie von Gravitationswellen vorgestellt. Bei den hier betrachteten Modellen handelt es sich um “abgeschirmte” Fünfte-Wechselwirkungsmodelle, deren Stärke von der Umgebungsstoffdichte abhängt und in vielen Erweiterungen der allgemeinen Relativitätstheorie wie z.B. Stringtheorie vorkommen. Die derzeit strengsten Einschränkungen dieser Modelle stammen von der Atominterferometrie.

Die in dieser Doktorarbeit vorgestellten analogen Simulationen sind, ihrer ursprünglichen Motivation entsprechend, für das Testen der metrologischen Schemata des in dieser Dissertation vorgeschlagenen Detektors und eines 2014 vorgeschlagenen Gravitationswellendetektors auf BEK-Basis geeignet. Zusätzlich konnen sie für analoge Tests in rechnerisch anspruchsvollen Teilen ihrer jeweiligen Parameterräume genutzt werden.

Die Anregungen eines im Grundzustand befindlichen BEK nehmen die Form von kollektiven Schwingungen, also Schallwellen, an. Diese Schwingungen sind quantisiert und werden Phononen genannt. Die Zeitentwicklung dieses Phononenfeldes steht im Mittelpunkt dieser Arbeit, wobei die BEK-Durchschnittsfeldparameter und die Hintergrundmetrik der Raumzeit beide eine direkte Rolle spielen. Durch die Modifizierung der experimentellen Parameter des BEK können die Bewegungsgleichungen des im flachen statischen Hintergrund eingebetteten Phononenfeldes denen eines anderen Feldes auf einem nichttrivialen Hintergrund angeglichen werden.

Es werden explizite Ausdrücke der für die Simulation eines generischen Gravitationswellenprofiles benötigten experimentellen Parameter des BEK angegeben. Für die Simulation abgeschirmter Fünfte-Wechselwirkungsmodelle werden die experimentellen BEK-Parameter für viele der am häufigsten untersuchten Abschirmungsmechanismen hergeleitet, einschließlich Chamäleons, Symmetronen, Dilatonen, Galileonen und D-BIonen.

Der in dieser Doktorarbeit vorgeschlagene Detektor basiert auf einem gelenkten BEK-Interferometerschema. Die Präzision dieses Detektors wird optimiert und die daraus resultierenden prognostizierten Einschränkungen des Chamäleon- bzw.

Symmetron-Abschirmungsmechanismus werden berechnet. Nach diesen Ergebnissen könnte ein einzelner Durchlauf dieses Detektors den verbleibenden interessanten Parameterraum des einfachsten Chamäleonmodells vollständig eliminieren und bestehende Grenzen bei anderen Modellen um viele Größenordnungen verbessern.

List of Publications

[1] Daniel Hartley, Tupac Bravo, Dennis Rätzel, Richard Howl, Ivette Fuentes

Analogue simulation of gravitational waves in a $3+1$-dimensional Bose-Einstein condensate

Physical Review D **98**, 025011 (2018)

arXiv:1712.01140

[2] Daniel Hartley, Christian Käding, Richard Howl, Ivette Fuentes

Quantum simulation of dark energy candidates

Physical Review D **99**, 105002 (2019)

arXiv:1811.06927

[3] Daniel Hartley, Christian Käding, Richard Howl, Ivette Fuentes

Quantum-enhanced screened dark energy detection

Submitted on 04.09.2019

arXiv:1909.02272

Contents

Part I

Preamble

Introduction

Light based astronomy has been pivotal to determining human understanding of the Universe for almost all of human history. The importance of understanding the phases of the Moon for planning life on Earth was already demonstrably clear to the Mesolithic peoples of Scotland; they built the recently rediscovered oldest known lunar calendar in Warren Field, Aberdeenshire around 8000 BCE. The movement of the Sun, Moon and stars are known to have been tracked by civilisations throughout Europe, Asia, Mesoamerica, Northern Africa and the Middle East from at least the Early Bronze Age.

Over time, the study of astronomy became highly mathematical and sophisticated. Examples include the star catalogues of 12$^{\text{th}}$ century BCE Babylon and 4$^{\text{th}}$ century BCE China, detailed calculation tables in Mayan codices, the precise astrological alignment of the Ancient Egyptian pyramids, the plethora of Ancient Indian and Greek models of the planets (*πλανήται* or "wanderers") and the astoundingly complex Antikythera mechanism amongst many others. Light based astronomy has been our only way of accessing the Universe beyond the Earth until very recently. As such, many models of the Universe have had to rely on only these observations and measurements to test predictions and validate or falsify theories.

The last few decades have brought with them paradigm-shifting advances in technology. Amongst many other examples, the development of this technology has led to the first ever successful detection of gravitational waves (GWs) by the LIGO collaboration [4]. This detection marks the first direct measurement of anything beyond our solar system with something other than light. Following this discovery, the first simultaneous detection with waves of both light and gravity was the 2017 detection of a neutron star merger [5, 6]. A worldwide intensive analysis of this event revealed that neutron star mergers can produce heavier elements than supernovae, and are now the first and only known observationally confirmed source in the Universe of many of the elements heavier than iron [7, 8] (and are likely to be the primary source of most of these elements). The various observations of GWs [4, 5, 9–12] have also validated the last major prediction of Einstein's General Relativity (GR), namely the existence of GWs, and have strongly constrained or entirely eliminated many alternative gravitational theories.

The interferometer schemes used by the LIGO and VIRGO collaborations [13, 14] involve many kilometres of evacuated chambers, are incredible technical achievements and continue to produce fundamentally important results. However, these detectors suffer from problems of cost and scalability. The low noise and high degree of control of cold atoms systems makes them an ideal platform for precision metrology, and the march of technological progress is bringing these systems ever further into the realm of measuring gravity. Cold atom systems are already being used for tests of the equivalence principle [15, 16], high precision gravity gradiometry [17] and constraining models beyond GR [18]. The metrological benefits of cold atoms are being exploited in the next generation of GW detectors, from proposals such as satellite-based atom interferometry [19] to experiments currently under construction such as the MAGIS-100 very long baseline atom interferometer [20] and the optical cavity coupled array of atom interferometers of the MIGA collaboration [21]. This thesis will present results relevant to the measurement of gravitational phenomena with cold atom systems.

One of the GW detector proposals relevant to the results of this thesis is that of a Bose-Einstein condensate (BEC) based resonant detector proposed by Sabín et. al. in 2014 [22]. A BEC is a cloud of atoms cooled to such a low temperature that the majority of the atoms fall into the motional ground state. When this happens, the wavefunctions of these atoms spread out and overlap completely and quantum effects such as wavefunction interference can be observed on a macroscopic scale. The size of a typical experimental BEC is on the order of the width of a human hair, which is very much in the realm of macroscopic objects.

The operating principle of this detector is the amplification of persistent gravitational waves through resonance, a principle which was also used in the earliest (unfortunately unsuccessful) GW detectors, namely Weber bars. The frequencies of the GWs detected by the LIGO and VIRGO collaborations are on the order of 10^2 Hz [4, 5, 9–12]. The wavelength of light needed to match this frequency in free space is on the order of 10^3 km. However, the detector proposed in [22] involves using sound waves travelling through the BEC, for which the corresponding speed of sound is on the order of mm/s[1]. As a BEC is a manifestly quantum system, these sound waves appear in a quantised manner and the sound wave quanta are called "phonons". To match and resonate with the 10^2 Hz gravitational wave frequency, the phonon wavelength must be on the order of $10 - 100$ μm which corresponds to the width of the cloud of atoms in a typical BEC experiment.

The transformation induced by a GW on this proposed detector produces mode-mixing and phonon creation in a phenomenon resembling the dynamical Casimir effect, making the final state distinguishable from the initial probe state. Such a detector requires extensive testing and verification procedures, and the first results presented in this thesis are a contribution towards this effort. The results described in [1] present a framework for simulating the effects of a GW in a BEC, which allows the metrological scheme of the detector proposal in [22] to be tested, amongst other applications in analogue gravity.

As mentioned briefly above, cold atoms are being used to constrain models beyond GR. While it is clear that GR has limitations (such as the cosmological constant problem) and that GR and quantum mechanics cannot be reconciled, all current attempts to construct models beyond GR suffer from a lack of experimental evidence. The results presented in [3] consist of a proposed BEC-based interferometric detector used to greatly improve the current constraints on a wide array of models beyond GR and the Standard Model (SM). This is achieved by constraining a class of fifth-force models with a so-called "screening mechanism," which allows the fifth force to be weak within our solar system but cosmologically significant on inter-galactic scales. Such a model may thus be tested at many different scales, and the parameter space will be simultaneously constrained from different directions. The viable parameter space may even eventually be eliminated; a crucial feature of any realistic model proposal sadly missing from many models beyond GR.

Fifth-force models arise from many extensions and modifications of GR, from the simplest scalar-tensor gravity theories to low energy limits of proposed Theories of Everything such as string theory and supergravity. Screening mechanisms may be used to partially explain why no distinguishing features of any of these models

[1]See Chapter 1 and references therein for a justification of this estimate through data from experimental literature.

have yet been observed. Therefore, screening mechanisms are currently arguably the most viable (and, crucially, testable) fifth-force models in the current scope of fundamental physics research.

As demonstrated in [3], a null result from a single run of this proposed detector would immediately eliminate the remaining interesting parameter space of the simplest of these screened models. The current bounds on other screened models would also be substantially improved by many orders of magnitude.

As with the above GW detector proposal, the central result of [2] is a scheme for simulating the effects of these screened fifth-force models in a BEC. Such a simulation is interesting both for testing the detector proposed in [3] and for the otherwise computationally challenging analogue simulation of the evolution of matter fields under the influence of a screened fifth force.

The formalism used in [1–3] is quantum field theory in curved space-time (QFTCS). QFTCS consists of quantum fields evolving on a (generally) curved background, where the back-reaction of these fields on the metric is small enough to be ignored. Well known results of this theory include Hawking radiation [23] and the Unruh effect [24]. An overview of BEC physics in the framework of QFTCS is presented in Chapter 1, alongside other relevant results. Chapters 2-4 cover introductions and basic useful results for GWs, screened scalar field models and quantum metrology respectively. The results of this thesis are presented in the publications in Part II.

Basic definitions and conventions

Throughout this thesis, the following conventions will be used unless stated otherwise:

- Bold symbols $\boldsymbol{g}$ are used to denote vectors, matrices and tensors, whereas non-bold symbols g are scalars,
- The Einstein summation convention will be used throughout,
- Greek indices (e.g. α, β, μ, ν) run from 0 to 3 while Latin indices (e.g. i, j, k) run from 1 to 3,
- Commas and semicolons in indices represent normal and covariant derivatives respectively e.g. $x_{\mu;\nu} = \nabla_\nu x_\mu$,
- Partial derivatives $\partial/\partial x^\mu$ are otherwise written in short hand as ∂_μ,
- n-dimensional integrals $\int \cdots \iint [\cdot]\, dx^1 dx^2 \cdots dx^n$ are written in short hand as $\int [\cdot]\, d^n\boldsymbol{x}$ where $\boldsymbol{x} = \left(x^1, x^2, \cdots, x^n\right)$,
- T is used exclusively to denote a matrix or vector transpose, e.g. $(\cdot,\cdot)^T$,
- † is used exclusively to denote a conjugate transpose,
- The Kronecker delta is given by δ_{ij} where $\delta_{ij} = 1$ if $i = j$ and 0 otherwise,
- $\mathbb{I}_n$ is the $n \times n$ identity matrix,
- The signature of the space-time metric is $(-,+,+,+)$,
- The coordinates used are Minkowski coordinates given by (ct, x, y, z),
- The Minkowski metric in these coordinates is given by $\boldsymbol{\eta} = \mathrm{diag}\,(-1,1,1,1)$,
- The Riemann curvature tensor $\boldsymbol{R}$ has indices ordered such that $R_{\mu\nu} = R^{\rho}{}_{\mu\rho\nu}$ are the elements of the Ricci curvature tensor.

A note on analogue gravity

A sizeable part of this thesis concerns the field of analogue gravity. When creating an analogue system, the applicability of that analogy must be kept in mind. A discussion of this point is found in the Introduction of [2], but will be reiterated here as it is an important point and is not often considered in the literature.

Since no analogue system is identical to the system it is mimicking (by construction), no new effects or features can be said to be independently discovered in an analogue system. Any effects or features of an original system can only be confirmed conclusively by direct measurement of that original system, although an analogue system may provide clues for what to look for and/or how to look for it. Great care must be taken to ensure that any new or unexpected observation of an analogue model is not just an artefact of the analogue system. An analogue system can also perform important self-consistency checks and demonstrate effects that are only reliant on a partial analogy. In being used to test metrological schemes of detectors, the results of [1] and [2] are examples of the latter two cases.

Chapter 1

Bose-Einstein condensation in curved space-time

A *Bose-Einstein condensate* (BEC) is a fundamentally different form of matter to those conventionally experienced in everyday life. A BEC is formed when the quantum mechanical wavefunctions of a collection of indistinguishable particles (bosons) completely overlap, which leads to microscopic quantum phenomena becoming apparent on a macroscopic scale. The most easily visible quantum effect most alien to our everyday experience of reality is that of wavefunction interference. This effect can be demonstrated with clouds of atoms in a BEC larger than the width of human hair [25], which definitively puts this effect into the realm of macroscopicity. Other blatantly quantum effects can be seen in superfluids which flow up the walls and out of containers they are placed in, a state of matter for which the BEC condensation mechanism is fundamental [26].

A combination of low internal noise and a high degree of control make cold atom systems a very attractive platform for precision metrology, from practical applications such as ultra-high precision clocks [27] to fundamental tests of the equivalence principle [15, 16]. The condensation of a cold atom system into a BEC adds a degree of control of the internal state of a macroscopic quantum system to the toolbox of the precision metrologist. Taking advantage of the benefits of quantum metrology (explained in detail in Chapter 4) is an obvious improvement to the current cold atom based metrological systems, although technically challenging.

The utilisation of a BEC as a tool of precision quantum metrology is relevant to all publications presented in Part II, and this chapter introduces the basic theory of the BEC in the context of measuring and constraining interesting space-time geometries.

1.1 Bose-Einstein condensation

In this section, basic properties of Bose-Einstein condensation will be covered including the physical mechanism which produces a BEC, the long range correlations observed and the Bogoliubov approximation; most widely used BEC approximation.

Basic definitions

A complex scalar field can be represented by a *field operator* $\hat{\Psi}$. This object is an operator valued distribution. When evaluated at a point in space $\boldsymbol{r}$ it resolves to an operator acting on the Hilbert space of states of the scalar field, producing a 1-particle position eigenstate. Explicitly,

$$|\boldsymbol{r}\rangle = \hat{\Psi}^{\dagger}(\boldsymbol{r})\,|0\rangle \tag{1.1}$$

where $|0\rangle$ is the vacuum state of the scalar field. Accordingly, a 1-particle state distributed in space with the wavefunction ψ can be described by

$$|\psi\rangle = \int \psi(\boldsymbol{r})\,\hat{\Psi}^{\dagger}(\boldsymbol{r})\,d\boldsymbol{r}\,|0\rangle\,. \tag{1.2}$$

All derivation and calculation in this chapter will be done in the Heisenberg picture, so the operator $\hat{\Psi}(\boldsymbol{r})$ evaluated at the point in space $\boldsymbol{r}$ is also a function of time.

If the scalar field is confined to a finite volume, then it has a discrete energy spectrum and the field operator evaluated at a point can be written as

$$\hat{\Psi}(\boldsymbol{r}) = \sum_{\boldsymbol{p}} \psi_{\boldsymbol{p}}(\boldsymbol{r})\,\hat{a}_{\boldsymbol{p}} \tag{1.3}$$

where the momentum $\boldsymbol{p}$ indexes the energy levels in the spectrum, $\psi_{\boldsymbol{p}}(\boldsymbol{r})$ is the wave function for a particle of momentum $\boldsymbol{p}$ evaluated at $\boldsymbol{r}$, and $\hat{a}_{\boldsymbol{p}}$ is an annihilation operator in momentum space. This construction suggests the definition of a *one body density*

$$n^{(1)}\left(\boldsymbol{r},\boldsymbol{r}'\right) = \langle\hat{\Psi}^{\dagger}\left(\boldsymbol{r}'\right)\hat{\Psi}(\boldsymbol{r})\rangle \tag{1.4}$$

where the expectation $\langle\cdot\rangle$ has been taken over the state of the field. The *diagonal density* can then be defined as

$$n(\boldsymbol{r}) = n^{(1)}(\boldsymbol{r},\boldsymbol{r})\,. \tag{1.5}$$

This is the usual number density evaluated at a point $\boldsymbol{r}$. Since the field is scalar, it follows Bose statistics and

$$\left[\hat{\Psi}(\boldsymbol{r}),\hat{\Psi}^{\dagger}\left(\boldsymbol{r}'\right)\right] = \delta\left(\boldsymbol{r}-\boldsymbol{r}'\right)\,,\ \left[\hat{\Psi}(\boldsymbol{r}),\hat{\Psi}\left(\boldsymbol{r}'\right)\right] = 0 \tag{1.6}$$

where $[\cdot,\cdot]$ is the usual commutator, and all field operators are evaluated at the same time.

Long range order

If a scalar field with N excitations is confined to a volume Ω and the state of the field is uniformly and isotropically distributed across that volume, then the diagonal density simply reduces to $n = N/\Omega$. In the thermodynamic limit where $N,\Omega \to \infty$ but n is kept constant, the one body density is no longer dependent on position but instead on the magnitude of the difference between positions $\boldsymbol{s} = \boldsymbol{r} - \boldsymbol{r}'$. This is given by

$$n^{(1)}(s) = \frac{1}{\Omega}\int n(\boldsymbol{p})\,e^{-i\boldsymbol{p}\cdot\boldsymbol{s}/\hbar}d\boldsymbol{p} \tag{1.7}$$

where $s = |\boldsymbol{s}|$ and $n(\boldsymbol{p})$ is the Fourier transform of $n(\boldsymbol{r})$ from position to momentum space. For a normal system, the momentum density is approximately smooth for $\boldsymbol{p} \to 0$ and $n^{(1)}(s)$ vanishes for $s \to \infty$. However, if there is some substantial fraction of the excitations of the field in the momentum ground state, then

$$n(\boldsymbol{p}) = N_0\delta(\boldsymbol{p}) + \tilde{n}(\boldsymbol{p}) \tag{1.8}$$

where $\delta(\cdot)$ is the Dirac delta function, and

$$\lim_{s\to\infty} n^{(1)}(s) = \frac{N_0}{\Omega} \neq 0. \tag{1.9}$$

The physical interpretation of this observation is that the wave functions of all of the excitations of the field overlap and the entire field is spatially coherent. This is called *long range order*, and is the characteristic property of a BEC. The quantity N_0/N is called the *condensed fraction*.

It should be noted that this derivation fails in 1 dimension, as the one body density $n^{(1)}(s)$ diverges logarithmically when $s \to \infty$, and there is no condensation mechanism. Despite this, quasi-1-dimensional bosonic systems (higher dimensional systems strongly constrained in all but 1 dimension by external potentials) exhibit condensation and 1-dimensional bosonic systems with macroscopically occupied ground states still have interesting properties. This is derived and discussed in detail in [26].

Creating a Bose-Einstein condensate

The physical mechanism for the realisation of the momentum distribution in Eq. (1.8) depends on the *chemical potential*, which is defined as

$$\mu = \frac{\partial E}{\partial N}, \tag{1.10}$$

i.e. the energy needed to add an excitation to the field. For a Bose field with N excitations and energy levels indexed by i with energies E_i, the average occupation of each energy level $\bar{n}_i$ follows the Bose-Einstein distribution [26, 28]

$$\bar{n}_i = \frac{1}{\exp\left[\beta\left(E_i - \mu\right)\right] - 1}, \tag{1.11}$$

where $\beta = 1/k_B T$, k_B is the Boltzmann constant and T is the temperature. The occupation of the lowest energy state must physically be positive or zero, so the chemical potential μ must be less than the ground state energy E_0 at any temperature. When the temperature T of the field decreases, the chemical potential similarly decreases in magnitude as less energy is needed to add more excitations to the field.

The BEC condensation mechanism is described as follows: at some *critical temperature* T_c, μ is positive and becomes comparable to E_0 and the ground state occupation rapidly increases with further cooling. Above this critical temperature, the field momentum distribution smoothly goes to zero at zero momentum. Below this critical temperature, the momentum distribution is more accurately described by Eq. (1.8) and Bose-Einstein condensation occurs. For the uniform non-interacting Bose field with N excitations in a box of volume Ω introduced above, the critical temperature is given by [28]

$$T_c \approx \frac{2\pi\hbar^2}{k_B m}\left(\frac{N}{\zeta\left(3/2\right)\Omega}\right)^{2/3} \tag{1.12}$$

where ζ is the Riemann zeta function. This expression is calculated by setting the chemical potential to the ground state energy of the field, and then setting the ground state energy to zero. Changes to the geometry and dimensionality of the trapping volume modify this expression slightly. Additional corrections to this expression from the zero point energy and from an exact expression for μ, as well as a more detailed derivation of the BEC condensation mechanism can be found in [26] and [28].

Typical atom densities in a BEC experiment are $10^{14} - 10^{15}$ cm^{-3} [25]. At these densities, the critical temperature in a box potential is on the order of $T_c \sim 500$ nK$-2\,\mu$K.

The Bogoliubov approximation

The ground state contribution to the field operator $\hat{\Psi}$ can be separated out of Eq. (1.3) as

$$\hat{\Psi}\left(\boldsymbol{r}\right) = \psi_0\left(\boldsymbol{r}\right)\hat{a}_0 + \sum_{\boldsymbol{p}\neq 0}\psi_{\boldsymbol{p}}\left(\boldsymbol{r}\right)\hat{a}_{\boldsymbol{p}}. \tag{1.13}$$

At temperatures below the critical temperature for which the momentum density of the field is well described by Eq. (1.8), the mean occupation of the ground state far exceeds the occupation of any higher energy states. Since the field follows Bose statistics,

$$\left[\hat{a}_0, \hat{a}_0^\dagger\right] = 1 \tag{1.14}$$

but the occupation of the ground state is $N_0 \gg 1$. Hence, the *Bogoliubov approximation* consists of ignoring the non-commutativity of $\hat{a}_0$ and replacing it with $\sqrt{N_0}$. This is equivalent to stating that N_0 is so large that the difference between two states with ground state occupations of N_0 and $N_0 + 1$ respectively is small enough to be ignored. The field operator is then expressed as

$$\hat{\Psi} = \Psi_0 + \delta\hat{\Psi} \tag{1.15}$$

where Ψ_0 represents the ground state condensed fraction of the BEC, and is called the *order parameter*. Note that Ψ_0 is no longer an operator valued distribution, but instead becomes a distribution of complex functions.

1.2 The Gross-Pitaevskii equation

Given that $\hat{\Psi}$ represents a complex scalar field, the evolution in time of each $\hat{\Psi}\left(\boldsymbol{r}\right)$ can be described by the Hamiltonian density [26]

$$\hat{\mathcal{H}}_P\left(\boldsymbol{r}\right) = \frac{\hbar^2}{2m}\nabla\hat{\Psi}^\dagger\left(\boldsymbol{r}\right)\cdot\nabla\hat{\Psi}\left(\boldsymbol{r}\right) + \hat{\mathcal{V}}\left(\boldsymbol{r}\right) \tag{1.16}$$

which is the simplest non-trivial positive definite Hamiltonian density equivalent to a point transformation invariant Lagrangian density[1]. ∇ is the gradient operator in this section. $\hat{\mathcal{V}}$ is the total potential, and can be written as

$$\hat{\mathcal{V}}\left(\boldsymbol{r}\right) = \hat{\Psi}^\dagger\left(\boldsymbol{r}\right)V\left(\boldsymbol{r}\right)\hat{\Psi}\left(\boldsymbol{r}\right) + \int\hat{\Psi}^\dagger\left(\boldsymbol{r}\right)\hat{\Psi}^\dagger\left(\boldsymbol{r}'\right)U\left(\boldsymbol{r}'-\boldsymbol{r}\right)\hat{\Psi}\left(\boldsymbol{r}\right)\hat{\Psi}\left(\boldsymbol{r}'\right)d\boldsymbol{r}' + \cdots \tag{1.17}$$

where $V\left(\boldsymbol{r}\right)$ is the external potential applied to the field. $U\left(\boldsymbol{r}\right)$ is the two-body potential, and is the lowest order field self-interaction term. All higher order potential terms are ignored as a first approximation[2]. The time evolution of the field operator $\hat{\Psi}$ is generated by the Hamiltonian as

$$i\hbar\partial_t\hat{\Psi} = \left[\hat{\Psi}, \hat{H}_P\right] = \int\left[\hat{\Psi}, \hat{\mathcal{H}}_P\right]d^3\boldsymbol{r} \tag{1.18}$$

[1] Lorentz invariance is only necessary when considering fields in special relativity

[2] Higher order terms are not always irrelevant and become important at very high densities, e.g. three-body recombination strongly limits the atom density achievable in experiments [28].

which can be evaluated as

$$i\hbar\partial_t \hat{\Psi}(\boldsymbol{r}) = \left[-\frac{\hbar^2}{2m}\nabla^2 + V(\boldsymbol{r}) + \int \hat{\Psi}^\dagger(\boldsymbol{r}') U(\boldsymbol{r}'-\boldsymbol{r}) \hat{\Psi}(\boldsymbol{r}') d\boldsymbol{r}' \right] \hat{\Psi}(\boldsymbol{r}). \tag{1.19}$$

Interactions

The two body potential $U(\boldsymbol{r})$ parameterises two-body interactions at both short and long length scales. However, not all of these length scales are relevant for a realistic description of a BEC that can be produced in a lab. To progress past this point, it is necessary to choose a particular form of boson and investigate its interaction properties; BECs produced in experiments overwhelmingly consist of atoms so the field $\hat{\Psi}$ will be considered to represent the bosonic behaviour of a collection of atoms for the remainder of this thesis.

It would not be appropriate in general to replace $\hat{\Psi}$ with Ψ_0 for the full potential $U(\boldsymbol{r})$, but this substitution is appropriate when only considering variations in $\hat{\Psi}$ longer than the range of interatomic forces. This is effectively a restriction on the density of the field applicable to this analysis, as a high density of atoms forces those atoms close together, making short range effects more important even in the ground state. When only considering relatively long range variations in $\hat{\Psi}$, it is also appropriate to make the replacement $\Psi_0(\boldsymbol{r}') \to \Psi_0(\boldsymbol{r})$. When only considering "long wavelength" interactions between atoms, the potential can be replaced by an *effective potential* $U_0(\boldsymbol{r})$ with which the relevant integral in Eq. (1.17) is evaluated as

$$\hat{\mathcal{V}} \to V(\boldsymbol{r}) \Psi_0^\dagger \Psi_0 + g_{NR} \Psi_0^\dagger \Psi_0^\dagger \Psi_0 \Psi_0 + \cdots. \tag{1.20}$$

The interaction strength is parameterised by

$$g_{NR} = \int U_0(\boldsymbol{r})\, d^3\boldsymbol{r} = \frac{4\pi\hbar^2 a}{m} \tag{1.21}$$

where m is the atomic mass and a is the s-wave scattering length. For a derivation of the form of $U_0(\boldsymbol{r})$ and a detailed evaluation of this integral, see [28]. The label "NR" is added to the usual notation for this interaction strength to avoid notational confusion in later parts of this thesis.

Typical s-wave scattering lengths are on the order of a fraction of a Bohr radius to a hundred Bohr radii ($0.3a_0$ in hydrogen [29], $52a_0$ in sodium-23 [30], $98a_0$ in rubidium-87 [31])[3], although scattering lengths of several thousand Bohr radii are not impossible ($> 2500a_0$ in triplet state caesium-133 [32, 33]).

The Gross-Pitaevskii equation

With a total potential given by Eq. (1.20), Eq. (1.19) becomes

$$i\hbar\partial_t \Psi_0(\boldsymbol{r}) = \left[-\frac{\hbar^2}{2m}\nabla^2 + V(\boldsymbol{r}) + g_{NR} \left|\Psi_0(\boldsymbol{r})\right|^2 \right] \Psi_0(\boldsymbol{r}). \tag{1.22}$$

This is the *Gross-Pitaevskii equation* (GPE) as derived independently by Gross [34] and Pitaevskii [35] in 1961, and is one of the most utilised and most widely applicable tools for studying Bose-Einstein condensation.

[3] Scattering lengths do not have to be positive (and are often not), but a negative scattering length implies an attractive interaction which precludes the formation of a stable BEC.

Since it is widely applicable, it is important to keep in mind the assumptions under which this equation has been derived. Firstly, the total number of atoms should be sufficiently high to define Bose-Einstein condensation. Secondly, the density and temperature of these atoms should be sufficiently low that the Bogoliubov approximation $\hat{\Psi} \to \Psi_0$ is reasonable. Thirdly, the distances of interest must be much greater than the s-wave scattering length a so that the interaction potential can be replaced by an effective potential.

The continuity equation

It is trivial to show that the Hamiltonian density in Eq. (1.16) and its corresponding Lagrangian density $\mathcal{L}$ have a $U(1)$ symmetry, i.e. they are invariant under a global phase shift $\hat{\Psi} \to e^{i\alpha}\hat{\Psi}$. As in the preceding discussion, the Bogoliubov approximation will be made and assumed to hold sufficiently strongly that $\hat{\Psi}$ can be replaced by Ψ_0. Noether's theorem states that this symmetry corresponds to a conserved current J^μgiven by

$$\begin{aligned} J^\mu &= \frac{\partial \mathcal{L}}{\partial \left(\partial_\mu \Psi_0\right)} \delta\Psi_0 + \frac{\partial \mathcal{L}}{\partial \left(\partial_\mu \Psi_0^\dagger\right)} \delta\Psi_0^\dagger \\ &= -\hbar \Psi^\dagger \Psi \delta^{0\mu} + i\frac{\hbar^2}{2m}\left[\Psi_0^\dagger \partial_j \Psi_0 - \Psi_0 \partial_j \Psi_0^\dagger\right]\delta^{j\mu}, \end{aligned} \tag{1.23}$$

where $\delta\Psi_0$ and $\delta\Psi_0^\dagger$ are the infinitesimal transformations of Ψ_0 and $\Psi_0^\dagger$ respectively generated by the global phase shift. In the *Madelung representation*, the field Ψ_0 is separated into two real fields consisting of a density ρ and a phase θ as $\Psi_0 = \sqrt{\rho}e^{i\theta}$. The conservation equation for the current J^μ can then be written as

$$\partial_t \rho + \nabla \cdot \left(\frac{\hbar \rho}{m} \nabla \theta\right) = 0. \tag{1.24}$$

This has the form of a fluid continuity equation [36], and motivates the definition of the *flow velocity* $\boldsymbol{v}$ as

$$\boldsymbol{v} = \frac{\hbar}{m} \nabla \theta. \tag{1.25}$$

1.3 Excitations

Quasi-particle spectrum

The energy spectrum of excitations of a BEC can be calculated in at least two different ways, both of which are covered in [28]. The first method involves diagonalising the Hamiltonian corresponding to Eq. (1.16) in momentum space, with the potential given in Eq. (1.17) where V is a uniform external potential, as was originally done by Bogoliubov [37]. The second method uses a hydrodynamic approach where Ψ_0 describes a homogeneous gas, deriving the spectrum of perturbations to Ψ_0 from the GPE.

In both cases after some tedious but straightforward algebra, the energy E of an excitation is given by [28]

$$E^2(\boldsymbol{k}) = \frac{\hbar^2 g_{NR} n}{m} |\boldsymbol{k}|^2 + \frac{\hbar^4 |\boldsymbol{k}|^4}{4m^2}, \tag{1.26}$$

where $n = |\Psi_0|^2$ is the condensate number density and $\boldsymbol{k}$ is the wave vector of the excitation. Since the external potential is uniform, the excitations of the BEC are effectively free quasi-particles[4] and their momentum is given by $\boldsymbol{p}(\boldsymbol{k}) = \hbar\boldsymbol{k}$.

Low and high energy limits

At low momenta, the $|\boldsymbol{k}|^2$ term is dominant and the energy of an excitation is

$$E(\boldsymbol{k}) \approx \sqrt{\frac{g_{NR} n}{m}} |\boldsymbol{p}(\boldsymbol{k})| . \tag{1.27}$$

This spectrum describes quantised density perturbations (with their own phase) with a linear spectrum, which is exactly a description of *phonons* travelling at the *speed of sound*

$$c_s = \sqrt{\frac{g_{NR} n}{m}}. \tag{1.28}$$

When the hydrodynamic approach is used to derive this spectrum, this result seems obvious as sound waves are a well established excitation of a hydrodynamic system. As mentioned above, typical atom number densities in BEC experiments are $n \sim 10^{14} - 10^{15}$ cm^{-3} and typical values for the s-wave scattering length are $a_s \sim 10^0 - 10^2\, a_0$, so the corresponding speed of sound in these parameter ranges is $c_s \sim 2 - 30$ mm/s.

At high momenta, the first two terms in an expansion of Eq. (1.26) are

$$E(\boldsymbol{k}) \approx \frac{|\boldsymbol{p}(\boldsymbol{k})|^2}{2m} + g_{NR} n. \tag{1.29}$$

This is the spectrum of a *free particle* plus some mean field potential contribution. Inspection of the Hamiltonian diagonalisation scheme described above reveals that the Hamiltonian corresponding to Eq. (1.16) already becomes diagonal at high energies, so high momentum excitations of the field can be directly interpreted as strongly excited atoms. Physically, this implies that atoms in a BEC move collectively at low energies but more freely at high energies.

The transition between these regimes occurs when the kinetic term $|\boldsymbol{p}(\boldsymbol{k})|^2/2m$ becomes comparable to the potential term $g_{NR} n$. Setting these two potentials to be equal, solving for the wave number $|\boldsymbol{k}|$ and inverting it results in a length scale at which this transition occurs. This length scale is given by

$$\xi = \sqrt{\frac{\hbar^2}{2m g_{NR} n}}, \tag{1.30}$$

and coincides with the *healing length*. The healing length will shortly be derived as the distance over which a condensate is approximately uniform near a hard potential boundary. Since this length scale corresponds to the transition between the low and high momentum regimes, or equivalently the phonon and excited atom regimes, any excitation that is considered to be a phonon must have a wavelength much greater than the healing length ξ.

[4] Both perturbative approaches for deriving Eq. (1.26) are taken to first order. Interactions between quasi-particles appear in higher order corrections. These corrections are assumed to be negligible as a first approximation, as the number of excitations must be much smaller than the ground state population for condensation to occur in the first place. Quasi-particle interactions can be relevant in experiments as Landau and Belaiev damping (e.g. [38, 39]).

Healing length

Two-body interactions significantly modify the ground state density of a BEC, which will now be demonstrated with a simple example. Consider a BEC confined to an external box potential with infinitely high walls. While the GPE (Eq. (1.22)) cannot easily be solved analytically, its form can be used to deduce the shape of the ground state density.

Far from the walls, the external potential V is constant so the density of any BEC with non-trivial interactions should approach a constant "bulk" value n. At the walls, the condensate density must vanish. Near a wall corresponding to the direction x, the form of the solution to the GPE with these two constraints is [26]

$$\Psi_0(x) \approx \sqrt{n}\tanh\left(\sqrt{\frac{mg_{NR}n}{\hbar^2}}x\right) = \sqrt{n}\tanh\left(\frac{x}{\sqrt{2}\xi}\right) \tag{1.31}$$

where ξ is defined as above in Eq. (1.30). Hence, the density of the condensate rises from zero to its bulk value in a distance of the order of the *healing length* ξ. This name comes from the observation that the condensate can be said to "heal" from defects over this length scale. In the limit where interactions are turned off ($g_{NR} \to 0$), the healing length diverges and the normal "particle in a box" wave functions become the solutions of the GPE. This is to be expected from the observation that the atoms in the BEC are effectively free particles in a box if there are no interactions.

At the typical densities ($n \sim 10^{14} - 10^{15}\ \mathrm{cm}^{-3}$) and scattering lengths ($a_s \sim 10^0 - 10^2\, a_0$) mentioned above, the typical healing length found in a BEC experiment is on the order of $\xi \sim 0.1 - 5\,\mu\mathrm{m}$.

When considering length scales much greater than the healing length, a condensate in a box potential has an effectively constant density everywhere. As derived above, phonons have wavelengths much greater than the healing length by definition, so the phonons of a condensate in a box potential do not "see" the non-uniform density near the walls of the box and thus present a particularly mathematically simple system.

1.4 The acoustic metric

Under certain approximations, the evolutions of phonons in a BEC can be described by a massless non-interacting Klein-Gordon equation with an effective metric, called an *acoustic metric*. The acoustic metric depends on both the mean-field properties of the BEC and the underlying space-time. Surprisingly, the acoustic metric has a pseudo-Riemannian signature even when derived in the flat space Newtonian limit. This type of equation was first derived for "normal" BECs in [40] in 1998 and for "relativistic" BECs in [41, 42] in 2010. However, these derivations either do not consider a background metric that is not flat or consider only classical perturbations of the BEC. Thus, they cannot be used to describe the interaction of phonons on a BEC (especially in interesting and useful quantum states) with interesting gravitational phenomena.

The QFTCS version of this acoustic metric was derived collaboratively by myself, Tupac Bravo, Richard Howl, Dennis Rätzel and Joel Lindkvist and was published in the appendix of [1]. As it is relevant to both [1] and [2], this derivation is reproduced here. The outline of the two derivations from [41] and [42] are also briefly outlined here for clarity and comparison.

It is important to point out that there is nothing necessarily "relativistic"[5] about the BECs considered in [1] and [2]. This acoustic metric derivation is presented in a generally covariant formalism to introduce the background space-time in a natural way, and does also describe manifestly "non-relativistic" BECs as demonstrated in experiments. Explicit non-relativistic limits are taken in the results of [1] and [2] to apply these results to realistic experiments.

1.4.1 Sound in explicitly non-relativistic Bose-Einstein condensates

A pseudo-Riemannian geometry for sound waves in a BEC was first derived in [40] and this derivation is reproduced schematically here.

Hydrodynamic equations

The derivation starts by considering the BEC as an inhomogeneous, barotropic, inviscid and irrotational fluid. Since the BEC is approximately entirely condensed, it is at zero temperature and therefore automatically barotropic [40]. It is clear from the definition of the flow velocity $\boldsymbol{v}$ in Eq. (1.25) that the flow is irrotational.

With these assumptions, the *Euler equations* for the BEC have the form

$$\partial_t \rho + \nabla \cdot (\rho \boldsymbol{v}) = 0, \tag{1.32}$$

$$\rho \left[\partial_t \boldsymbol{v} + (\boldsymbol{v} \cdot \nabla) \boldsymbol{v}\right] = -\nabla p + \rho \nabla \Phi, \tag{1.33}$$

where ρ is the density, p is the pressure and Φ is total potential of all external driving forces (including the Newtonian gravity potential). Note that Eq. (1.32) is exactly the continuity equation derived above as Eq. (1.24). Since $\boldsymbol{v}$ is irrotational, a velocity potential can be defined as $\boldsymbol{v} = \nabla \theta$.

Linearisation

The entire system can then be linearised around some "bulk" or "mean-field" behaviour by defining

$$\begin{aligned} \theta &= \theta_0 + \epsilon \theta_1 + \mathcal{O}\left(\epsilon^2\right), && (1.34)\\ \rho &= \rho_0 + \epsilon \rho_1 + \mathcal{O}\left(\epsilon^2\right), && (1.35)\\ p &= p_0 + \epsilon p_1 + \mathcal{O}\left(\epsilon^2\right), && (1.36) \end{aligned}$$

for some $\epsilon \ll 1$, where the amplitude of high frequency perturbations is small. Straightforward but tedious rearrangement and linearisation of Eqs. (1.32)-(1.33) to first order in ϵ leads to the systems of equations

$$\begin{aligned} \partial_t \rho_0 + \nabla \cdot (\rho_0 \boldsymbol{v}_0) &= 0, && (1.37)\\ -\partial_t \theta_0 + \int^{p_0} \frac{dp'}{\rho_0 (p')} + \frac{1}{2} v_0^2 + \Phi &= 0, && (1.38) \end{aligned}$$

[5] e.g. high excitation energies, high flow velocities, strong coupling...

for the bulk components where $v_0 = \nabla\theta_0$, and

$$\begin{aligned}
p_1 &= -\rho_0 \left(\partial_t\theta_1 + v_0 \cdot \nabla\theta_1\right) && (1.39)\\
\rho_1 &= -\frac{\rho_0}{c_0^2} \left(\partial_t\theta_1 + v_0 \cdot \nabla\theta_1\right) && (1.40)\\
0 &= -\partial_t \left(\frac{\rho_0}{c_0^2} \left[\partial_t\theta_1 + v_0 \cdot \nabla\theta_1\right]\right) \\
&\quad + \nabla \cdot \left(\rho_0\nabla\theta_1 - \frac{\rho_0}{c_0^2} v_0 \left[\partial_t\theta_1 + v_0 \cdot \nabla\theta_1\right]\right) && (1.41)
\end{aligned}$$

for the first order perturbations, where the speed of sound c_0 is defined in the standard way as

$$\frac{1}{c_0^2} = \frac{\partial\rho}{\partial p}. \tag{1.42}$$

This system of equations can be completely solved by evaluating the final equation for θ_1, which can be written in the form

$$\partial_\mu \left(f^{\mu\nu}\partial_\nu\theta_1\right) = 0 \tag{1.43}$$

where f is a tensor with components $f_{\mu\nu}$, its inverse f^{-1} has components $f^{\mu\nu}$ given by

$$\boldsymbol{f}^{-1} = \frac{\rho_0}{c_0^2} \begin{pmatrix} -1 & -v_0^T \\ -v_0 & c_0^2\mathbb{I}_3 - v_0 v_0^T \end{pmatrix} \tag{1.44}$$

and the coordinates are defined as (t, x, y, z). Eq. (1.43) is very visually similar to the Klein-Gordon equation for a massless non-interacting scalar field. To complete the analogy, the tensor f is equated to an effective acoustic metric $\boldsymbol{G}^{NR}$ and metric density G^{NR} as

$$f^{\mu\nu} = \sqrt{-G^{NR}} \left(G^{NR}\right)^{\mu\nu}. \tag{1.45}$$

Solving this equation and inverting the resulting inverse acoustic metric, the acoustic metric is finally given by

$$\boldsymbol{G}^{NR} = \frac{\rho_0}{c_0} \begin{pmatrix} -\left(c_0^2 - v_0^2\right) & -v_0^T \\ -v_0 & \mathbb{I}_3 \end{pmatrix}. \tag{1.46}$$

It is clear that this acoustic metric is pseudo-Riemannian, despite the fact that this derivation is entirely explicitly non-relativistic and does not consider the geometry of the underlying space-time. For a BEC without any bulk flows ($v_0 \to 0$), this acoustic metric is conformal to a $3+1$ dimensional Minkowski metric with the speed of light replaced by the speed of sound. Hence, the solutions of Eq. (1.43) in this case represent freely evolving wave-like phase perturbations travelling at the speed of sound c_0, i.e. sound waves.

1.4.2 Relativistic Bose-Einstein condensates: two approaches

The acoustic metric derived in [40] starts from non-relativistic fluid equations. This derivation was generalised to relativistic BECs in 2010 with two different approaches; firstly from a scalar field Lagrangian in special relativity in [41] and secondly from relativistic fluid equations in [42]. These derivations will be briefly outlined here for comparison with Chapter 1.4.3.

1.4.2.1 Bosons as a scalar field

Scalar field evolution in special relativity

To derive an equation governing the evolution of phonons on a BEC that may have relativistic properties as in [41], the Lagrangian density corresponding to the Hamiltonian density in Eq. (1.16) must be generalised to special relativity. Rather than point transformation invariance, all terms must now be invariant under Lorentz transformations. For convenient interpretation, the mass energy is split from the lowest order term of the potential $\hat{\mathcal{V}}$. The extended Lagrangian density is given by

$$\mathcal{L}_{SR} = -\eta^{\mu\nu}\partial_\mu\hat{\Phi}^\dagger\partial_\nu\hat{\Phi} - \left(\frac{m^2c^2}{\hbar^2} + V\right)\hat{\Phi}^\dagger\hat{\Phi} - U. \tag{1.47}$$

This is the standard Lagrangian density used for spin 0 quantum fields in special relativity [43, 44]. Different symbols (i.e. $\hat{\Psi} \to \hat{\Phi}$) are used in this chapter to distinguish the fields here from those in Chapter 1.2, which generally differ by a factor of $\exp\left(imc^2t/\hbar\right)$. As in Chapter 1.2, the interaction potential U is approximated by an effective two-body scattering potential

$$U \approx \frac{\lambda}{2}\hat{\Phi}^\dagger\hat{\Phi}^\dagger\hat{\Phi}\hat{\Phi}. \tag{1.48}$$

The Euler-Lagrange equation for $\hat{\Phi}^\dagger$ derived from Eq. (1.47) is

$$\left[\Box_\eta - \left(\frac{m^2c^2}{\hbar^2} + V\right) - \lambda\hat{\Phi}^\dagger\hat{\Phi}\right]\hat{\Phi} = 0, \tag{1.49}$$

where $\Box_\eta$ is the *Laplace operator* for the Minkowski metric $\boldsymbol{\eta}$, and can be expanded as $\Box_\eta\psi = \eta^{\mu\nu}\partial_\mu\partial_\nu\psi$.

Linearisation

As in Chapter 1.2, the Bogoliubov approximation is made. However, the excited component of the field operator $\hat{\psi}$ is normalised by the order parameter ϕ for mathematical convenience later. The full field $\hat{\Phi}$ is replaced by

$$\hat{\Phi} = \phi\left(1 + \hat{\psi}\right). \tag{1.50}$$

It is assumed that the order parameter obeys Eq. (1.49) for $\hat{\Phi} \to \phi$. This assumption will be more rigorously formalised in Chapter 1.4.3. Expressed in the Madelung representation where $\phi = \sqrt{\rho}e^{i\theta}$, this equation can be split into the two equations

$$\partial_\mu\left(\rho u^\mu\right) = 0, \tag{1.51}$$

$$|\boldsymbol{u}|^2 = -\eta_{\mu\nu}u^\mu u^\nu = c^2 + \frac{\hbar^2}{m^2}\left[V + \lambda\rho - \frac{\Box_\eta\sqrt{\rho}}{\sqrt{\rho}}\right], \tag{1.52}$$

where

$$u^\mu = \frac{\hbar}{m}\eta^{\mu\nu}\partial_\nu\theta \tag{1.53}$$

is the *flow 4-velocity*, whose components will be labelled $\boldsymbol{u} = \left(u^0, \bar{\boldsymbol{u}}\right)$. Eq. (1.51) is a generalisation of the continuity equation (Eq. (1.24)) to special relativity, Eq. (1.52) relates the normalisation of the flow velocity to the external and interaction potentials and Eq. (1.53) is a generalisation of the flow velocity (Eq. (1.25)) to a 4-vector.

The remaining component of Eq. (1.49) for $\hat{\psi}$ is given by

$$\Box_\eta \psi + 2\eta^{\mu\nu}\left(\frac{1}{2}\partial_\mu \ln\rho + i\partial_\mu\theta\right)\partial_\nu\hat{\psi} - \lambda\rho\left(\hat{\psi}+\hat{\psi}^\dagger\right) = 0. \tag{1.54}$$

With some straightforward manipulation, Eq. (1.54) can be converted into the form

$$\left(\left[i\hbar u^\mu\partial_\mu + \hat{T}_\rho\right]\frac{1}{c_0^2}\left[-i\hbar u^\mu\partial_\mu + \hat{T}_\rho\right] + 2m\hat{T}_\rho\right)\hat{\psi} = 0 \tag{1.55}$$

where

$$\hat{T}_\rho\hat{\psi} = -\frac{\hbar^2}{2m\rho}\eta^{\mu\nu}\partial_\mu\left(\rho\partial_\nu\hat{\psi}\right) \tag{1.56}$$

is a generalised kinetic operator and

$$c_0^2 = \frac{\hbar^2}{2m^2}\lambda\rho. \tag{1.57}$$

Dispersion

For a BEC with homogeneous bulk properties and no flows (i.e. ρ, λ and u^0 are constant and $\bar{\boldsymbol{u}} = 0$), Eq. (1.55) can be solved exactly by plane waves of the form $\hat{\psi} \propto \exp\left(-i\omega t + i\boldsymbol{k}\cdot\boldsymbol{x}\right)$. The dispersion relation of these plane waves at low momenta is well approximated by

$$\omega^2 = c_s^2\left|\boldsymbol{k}\right|^2 \tag{1.58}$$

where

$$c_s^2 = \frac{c^2c_0^2}{c_0^2 + \left|\boldsymbol{u}\right|^2} \tag{1.59}$$

can be interpreted as the speed of sound. The "low momentum" criterion is given by

$$\left|\boldsymbol{k}\right| \ll \frac{mu^0}{\hbar}\left(1+\left(\frac{c_0}{u^0}\right)^2\right)\min\left\{1, \frac{2c_0}{u^0}\right\}. \tag{1.60}$$

In the non-relativistic limit, $\left|\boldsymbol{u}\right|^2 \to c^2$ so $c_s^2 \to c_0^2$. Hence, c_0 can be interpreted as the non-relativistic limit of the speed of sound.

For high momenta, the dispersion relation becomes $\omega^2 = c^2\left|\boldsymbol{k}\right|^2$ which is that of a massless free particle[6]. Hence, low momentum excitations of the BEC are collective oscillations (quantised as phonons) travelling at the speed of sound c_s, whereas high momentum excitations are free particles no longer acting collectively. Note that this is exactly the relativistic version of the conclusions reached in Chapter 1.3.

Acoustic metric

With some further assumptions that will be covered in more detail in Chapter 1.4.3, Eq. (1.55) can be converted into the form

$$\partial_\mu\left(f^{\mu\nu}\partial_\nu\hat{\psi}\right) = 0 \tag{1.61}$$

[6]This dispersion relation describes an excitation of $\hat{\psi}$. However, the physical field is $\phi\hat{\psi}$, restoring the expected massive free particle dispersion relation.

for a tensor $\boldsymbol{f}^{-1}$ (with components $f^{\mu\nu}$) given by

$$\boldsymbol{f}^{-1} = \frac{\rho}{c_0^2}\begin{pmatrix} -\left(c_0^2 + \left(u^0\right)^2\right) & -u^0\bar{\boldsymbol{u}}^T \\ -u^0\bar{\boldsymbol{u}} & c_0^2\mathbb{I}_3 - \bar{\boldsymbol{u}}\bar{\boldsymbol{u}}^T \end{pmatrix}. \tag{1.62}$$

Defining the normalised flow velocity as

$$v^\mu = \frac{cu^\mu}{|\boldsymbol{u}|} \tag{1.63}$$

and equating $\boldsymbol{f}^{-1}$ to an acoustic metric and its density by $f^{\mu\nu} = \sqrt{-G^{(\eta)}}\left(G^{(\eta)}\right)^{\mu\nu}$ as in Chapter 1.4.1, the acoustic metric $\boldsymbol{G}^{(\eta)}$ has components

$$G^{(\eta)}_{\mu\nu} = \frac{\rho c}{c_s}\left[\eta_{\mu\nu} + \left(1 - \frac{c_s^2}{c^2}\right)\frac{v_\mu v_\nu}{c^2}\right]. \tag{1.64}$$

1.4.2.2 Bosons as a fluid

Relativistic fluid equations

The hydrodynamic formalism of [40] can be generalised to relativistic fluids as in [42]. The relativistic equivalents of the Euler equations (Eqs. (1.32)-(1.33)) are

$$\nabla_\mu\left(\varrho V^\mu\right) + p\nabla_\mu V^\mu = 0, \tag{1.65}$$

$$\left(\varrho + p\right)V^\mu\nabla_\mu V^\nu + \left(g^{\nu\sigma} + V^\nu V^\sigma\right)\nabla_\sigma p = 0, \tag{1.66}$$

where ϱ is the *energy density* (cf. mass density ρ in Chapter 1.4.1), $\boldsymbol{V}$ is the normalised flow 4-velocity, $\boldsymbol{g}$ is the background space-time metric and ∇ is now the *covariant derivative* associated with the metric $\boldsymbol{g}$. Note that these equations apply to classical fluids on generally curved backgrounds. This is to be contrasted with the derivation in [41], where the BEC is a quantum field (possibly with relativistic properties) on a flat background. As before, the flow is irrotational which is expressed covariantly as

$$V^\mu = \frac{g^{\mu\nu}\nabla_\nu\theta}{\sqrt{-g^{\rho\sigma}\nabla_\rho\theta\nabla_\sigma\theta}} \tag{1.67}$$

for some velocity potential θ. It is also assumed again that the BEC is barotropic. With this assumption, Eq. (1.65) can be written as

$$\nabla_\mu\left(\exp\left[\int_{\varrho_{p=0}}^{\varrho}\frac{d\varrho'}{\varrho' + p\left(\varrho'\right)}\right]V^\mu\right) = 0 \tag{1.68}$$

which suggests the definition of the *particle number density* as

$$n\left(p\right) = n_{p=0}\exp\left[\int_{\varrho_{p=0}}^{\varrho(p)}\frac{d\varrho'}{\varrho' + p\left(\varrho'\right)}\right]. \tag{1.69}$$

Linearisation

The BEC properties ϱ, p and θ may be linearised as in Chapter 1.4.1. Linearisation and manipulation of Eqs. (1.65)-(1.69) eventually leads to the system of equations

$$p_1 = \left.\frac{dp}{d\varrho}\right|_{\varrho_0} \varrho_1 = \frac{c_s^2}{c^2}\varrho_1 \tag{1.70}$$

$$\varrho_1 = -\frac{n_0 c^2}{n_{p=0}c_s^2}\varrho_{p=0}V_0^\mu \nabla_\mu \theta_1 \tag{1.71}$$

$$0 = \nabla_\mu \left(\frac{n_0^2}{\varrho_0 + p_0} \left[g^{\mu\nu} + \left(1 - \frac{c^2}{c_s^2}\right) V_0^\mu V_0^\nu \right] \nabla_\nu \theta_1 \right) \tag{1.72}$$

The last of these equations is of the form $\nabla_\mu \left(f^{\mu\nu}\nabla_\nu\theta_1\right) = 0$. Equating $f^{\mu\nu} = \sqrt{-G^{(c)}}\left(G^{(c)}\right)^{\mu\nu}$ as in previous sections and solving for the components $G^{(c)}_{\mu\nu}$ of $\boldsymbol{G}^{(c)}$ in $3+1$ dimensions, the acoustic metric components are given by

$$G^{(c)}_{\mu\nu} = \frac{n_0^2 c \varrho_{p=0}}{(\varrho_0 + p_0)\, c_s n_{p=0}} \left[g_{\mu\nu} + \left(1 - \frac{c_s^2}{c^2}\right) (V_0)_\mu (V_0)_\nu \right]. \tag{1.73}$$

Equivalence of results

It is straightforward to show that the acoustic metrics from [41] (Eq. (1.64)) and [42] (Eq. (1.73)) are identical when $\boldsymbol{g} \to \boldsymbol{\eta}$. The flow velocity $\boldsymbol{V}_0$ is normalised to 1 whereas the equivalent flow velocity $\boldsymbol{v}$ in [41] is normalised to c^2, so

$$V_0^\mu = c v^\mu. \tag{1.74}$$

Comparison of Eqs. (1.51) and (1.68) suggests

$$n_0 = |\boldsymbol{u}|\, \rho. \tag{1.75}$$

In the process of going from Eqs. (1.65)-(1.66) to Eqs. (1.70)-(1.72), it is shown in [42] that

$$\sqrt{-g^{\mu\nu}\nabla_\mu\theta\nabla_\nu\theta} = \exp\left[\int_0^p \frac{dp'}{\varrho(p') + p'}\right] = \frac{(\varrho(p) + p)\, n_{p=0}}{n(p)\, \varrho_{p=0}}. \tag{1.76}$$

In terms of $\boldsymbol{u}$, this can be written as

$$|\boldsymbol{u}| = \left[\frac{(\varrho_0 + p_0)\, n_{p=0}}{n_0 \varrho_{p=0}}\right]_{g\to\eta}. \tag{1.77}$$

Eqs. (1.74)-(1.77) can be combined to immediately show

$$\frac{\rho c}{c_s} = \frac{n_0^2 c \varrho_{p=0}}{(\varrho_0 + p_0)\, c_s n_{p=0}} \tag{1.78}$$

and Eqs. (1.64) and (1.73) are identical when $\boldsymbol{g} \to \boldsymbol{\eta}$.

1.4.3 Quantum fields in curved space-time

The derivation in Chapter 1.4.2.1 can be extended to non-Minkowski space-times by considering a generally covariant Lagrangian density. This derivation, derived collaboratively by myself, Tupac Bravo, Richard Howl, Dennis Rätzel and Joel

Lindkvist and published in the appendix of [1], is reproduced here as it is relevant to both [1] and [2]. Many of the details of the derivation are relevant to the derivation in Chapter 1.4.2.1, but are presented here in much greater detail.

The Lagrangian density in curved space-time

The special relativistic Lagrangian density $\mathcal{L}_{SR}$ for an interacting complex scalar field $\hat{\Phi}$ is given in Eq. (1.47). The *action functional* generated by this Lagrangian density is

$$S_{SR} = \int \mathcal{L}_{SR}(\boldsymbol{x})\, d^4\boldsymbol{x} \tag{1.79}$$

where $\boldsymbol{x}$ is a position 4-vector.

This Lagrangian density can be extended to a more general non-Minkowski space-time described by a metric $\boldsymbol{g}$, which may have non-zero curvature. For this extension, derivatives are generalised to covariant derivatives and all tensors are contracted to vierbeins (which has the effect of replacing $\boldsymbol{\eta}$ with $\boldsymbol{g}$ in Eq. (1.47)) such that the action is generally covariant. The scalar field $\hat{\Phi}$ may also couple directly to the curvature; the only possible generally covariant local scalar coupling to the curvature is given by $\xi R\hat{\Phi}^\dagger\hat{\Phi}$ [44] where R is the Ricci scalar and ξ is a constant numerical factor. Finally, the volume element is replaced by the covariant volume element $\sqrt{-g}d\boldsymbol{x}$, where g is the determinant of $\boldsymbol{g}$. With all of these modifications, the action takes the form

$$S = -\int \left[g^{\mu\nu}\nabla_\mu\hat{\Phi}^\dagger\nabla_\nu\hat{\Phi} + \left(\frac{m^2c^2}{\hbar^2} + V\right)\hat{\Phi}^\dagger\hat{\Phi} + U + \xi R\hat{\Phi}^\dagger\hat{\Phi}\right]\sqrt{-g}d^4\boldsymbol{x}. \tag{1.80}$$

Note that ∇ is a covariant derivative as in Chapter 1.4.2.2, and not the gradient operator as was used in Chapter 1.2. Since $\hat{\Phi}$ is a scalar field, the covariant derivative ∇_μ reduces to the standard partial derivative ∂_μ. The metrics considered in [1, 2] have very weak curvature, so it is appropriate to neglect the direct coupling of the scalar field to the curvature without having to decide on a value for ξ[7]. This assumption restricts this derivation to metrics with weak curvature. It is not immediately obvious that a Bose-Einstein condensate may exist in very strongly curved space-time, which may be an interesting topic of future research. With these assumptions and using Eq. (1.79) to define the Lagrangian density, the form of the generally covariant weakly curved space-time version of Eq. (1.47) is given by

$$\mathcal{L}_G = -\sqrt{-g}\left\{ g^{\mu\nu}\partial_\mu\hat{\Phi}^\dagger\partial_\nu\hat{\Phi} + \left(\frac{m^2c^2}{\hbar^2} + V\right)\hat{\Phi}^\dagger\hat{\Phi} + U\right\}. \tag{1.81}$$

Derivations of this "minimal substitution" in greater detail can be found in [43] and [44].

It is important to keep in mind that there does not have to be anything inherently "relativistic" about the excitations of the field $\hat{\Phi}$ despite this being allowed in the theory; this derivation is simply a natural way to introduce the effect of the space-time geometry into the dynamics of $\hat{\Phi}$. This is to be contrasted with the derivations in [41] and [42], where the purpose of the extension of [40] was to consider explicitly relativistic scenarios.

[7]This term cannot be immediately ignored as an interacting scalar field is not necessarily renormalisable when $\xi = 0$, see e.g. [45]. An argument could be made that this is irrelevant for finitely confined fields, as considered here.

Averaged equation of motion

As in Chapter 1.2, the interaction strength can be greatly simplified by considering only two particle contact interactions such that

$$U \approx \frac{\lambda}{2!}\hat{\Phi}^\dagger\hat{\Phi}^\dagger\hat{\Phi}\hat{\Phi}. \tag{1.82}$$

The Euler-Lagrange equation for $\hat{\Phi}^\dagger$ derived from the Lagrangian density in Eq. (1.81) is

$$\left[\Box_g - \left(\frac{m^2c^2}{\hbar^2} + V\right) - \lambda\hat{\Phi}^\dagger\hat{\Phi}\right]\hat{\Phi} = 0 \tag{1.83}$$

where $\Box_g$ is the Laplace operator for the metric g and can be expanded as

$$\Box_g\hat{\Phi} = g^{\mu\nu}\nabla_\mu\nabla_\nu\hat{\Phi} = \frac{1}{\sqrt{-g}}\partial_\mu\left(\sqrt{-g}g^{\mu\nu}\partial_\nu\hat{\Phi}\right). \tag{1.84}$$

When $\hat{\Phi}$ represents a boson field in a condensed state, several approximations can be made to simplify the calculation of the field dynamics. As in Chapter 1.4.2.1, the Bogoliubov approximation is made and the field operator $\hat{\Phi}$ is split into a "condensed fraction" order parameter ϕ and the normalised excited field operator $\hat{\psi}$ as

$$\hat{\Phi} = \phi\left(1 + \hat{\psi}\right). \tag{1.85}$$

Due to the Bogoliubov approximation, the non-equilibrium average $\langle\cdot\rangle$ of $\hat{\Phi}$ is given by

$$\langle\hat{\Phi}\rangle \approx \phi \implies \langle\hat{\psi}\rangle \approx 0. \tag{1.86}$$

Taking this average of Eq. (1.83),

$$\left[\Box_g - \left(\frac{m^2c^2}{\hbar^2} + V\right) - \lambda\left|\phi\right|^2\right]\phi - \lambda\left|\phi\right|^2\phi\left[\langle\hat{\psi}\hat{\psi}\rangle + 2\left\langle\hat{\psi}^\dagger\hat{\psi}\right\rangle + \left\langle\hat{\psi}^\dagger\hat{\psi}\hat{\psi}\right\rangle\right] = 0. \tag{1.87}$$

Since the occupation number of the excited $\hat{\psi}$ field should be much smaller than that of the condensed ϕ field, it is reasonable to make the approximation that

$$\left\langle\hat{\psi}^\dagger\hat{\psi}\right\rangle \ll 1, \tag{1.88}$$

i.e. the number of excitations in the $\hat{\psi}$ field is sufficiently small that it does not affect the dynamics of ϕ. Terms proportional to $\hat{\psi}\hat{\psi}$ involve spontaneous creation and destruction of pairs of excitations with opposite momenta. If the temperature of the BEC is sufficiently low then these terms (and higher order terms) can be ignored, i.e.

$$\langle\hat{\psi}\hat{\psi}\rangle \approx 0 \approx \left\langle\hat{\psi}^\dagger\hat{\psi}\hat{\psi}\right\rangle. \tag{1.89}$$

The temperature of the BEC is automatically sufficiently low enough to make this assumption when the density of excitations can be ignored.

With these approximations, the equation of motion for ϕ is simply

$$\left[\Box_g - \left(\frac{m^2c^2}{\hbar^2} + V\right) - \lambda\left|\phi\right|^2\right]\phi = 0. \tag{1.90}$$

It is obvious that these approximations can be more simply stated as ignoring the back-reaction of excitations on the ground state wave function of the condensate.

Aside: recovering the Gross-Pitaevskii equation

Eq. (1.90) is valid for any general properties of ϕ. However, this is often more generality than is necessary for describing the dynamics of real systems. Consider replacing ϕ on a flat Minkowski background ($\boldsymbol{g} \to \boldsymbol{\eta}$) with a field

$$\phi = \varphi e^{-imc^2 t/\hbar}. \tag{1.91}$$

Expanding Eq. (1.90),

$$\left[-\frac{1}{c^2}\partial_t^2 + 2i\frac{m}{\hbar}\partial_t + \nabla^2 - V - \lambda\left|\varphi\right|^2\right]\varphi = 0 \tag{1.92}$$

Making the approximation $\left|\partial_t^2\varphi\right| \ll c^2$ and rearranging terms[8], what is left becomes

$$i\hbar\partial_t\varphi = \left[-\frac{\hbar^2}{2m}\nabla^2 + V_{NR} + g_{NR}\left|\varphi\right|^2\right]\varphi \tag{1.93}$$

which is exactly the GPE (cf. Eq. (1.22)), where $V_{NR} = \left(\hbar^2/2m\right)V$ and $g_{NR} = \left(\hbar^2/2m\right)\lambda$ are the usual external potential and interaction strength respectively.

Continuity and flow velocity

The field ϕ is more useful (especially for physical interpretation) in the Madelung representation; $\phi = \sqrt{\rho}e^{i\theta}$ where ρ and θ are real scalar fields. With this form, a flow velocity can be defined as

$$u^\mu = \frac{\hbar}{m}g^{\mu\nu}\partial_\nu\theta \tag{1.94}$$

which is motivated in the same way as in Chapter 1.2. Expanding Eq. (1.90) into real and imaginary components and substituting the above definition, the resulting two equations are

$$\nabla_\mu\left(\rho u^\mu\right) = 0 \tag{1.95}$$

and

$$|\boldsymbol{u}|^2 = -g_{\mu\nu}u^\mu u^\nu = c^2 + \frac{\hbar^2}{m^2}\left\{V + \lambda\rho - \frac{\Box_g\sqrt{\rho}}{\sqrt{\rho}}\right\}. \tag{1.96}$$

The first of these equations is the continuity equation also seen in Eq. (1.24) in the non-relativistic limit and Eq. (1.51) for $\boldsymbol{g} \to \boldsymbol{\eta}$[9]. The second of these equations describes the normalisation of the flow velocity, generalising Eq. (1.52) to non-flat metrics.

Excited field equations of motion

Returning finally to Eq. (1.83), combining it with Eqs. (1.85) and (1.90) results in

$$\left[i\hbar u^\mu\partial_\mu - \hat{T}_\rho - mc_0^2\right]\hat{\psi} = mc_0^2\hat{\psi}^\dagger \tag{1.97}$$

[8] i.e. the usual "non-relativistic" approximation, alternatively and equivalently taking $c \to \infty$.

[9] This equation can also be equivalently derived as the conserved Noether current associated to the global phase invariance of the Lagrangian in Eq. (1.81) as in Chapter 1.2

where

$$c_0^2 = \frac{\hbar^2}{2m^2}\lambda\rho \tag{1.98}$$

as in Eq. (1.57), and

$$\hat{T}_\rho \hat{\psi} = -\frac{\hbar^2}{2m\rho\sqrt{-g}}\partial_\mu\left(\rho\sqrt{-g}g^{\mu\nu}\partial_\nu\hat{\psi}\right). \tag{1.99}$$

Note that $\hat{T}_\rho$ reduces to the standard kinetic operator $T = -\left(\hbar^2/2m\right)\nabla^2$ when ρ is constant in the "non-relativistic" flat space-time limit, so $\hat{T}_\rho$ is a generalised kinetic operator. With the equivalent of Eq. (1.97) for $\hat{\psi}^\dagger$ combined with Eq. (1.97) to eliminate $\hat{\psi}^\dagger$,

$$\left(\left[i\hbar u^\mu\partial_\mu + \hat{T}_\rho\right]\frac{1}{c_0^2}\left[-i\hbar u^\nu\partial_\nu + \hat{T}_\rho\right] + 2m\hat{T}_\rho\right)\hat{\psi} = 0. \tag{1.100}$$

This equation can be split into four terms as

$$\hat{T}_1 + \hat{T}_2 + \hat{T}_3 + \hat{T}_4 = 0 \tag{1.101}$$

where

$$\begin{aligned} \hat{T}_1 &= i\hbar u^\mu\partial_\mu\frac{1}{c_0^2}\left[-i\hbar u^\nu\partial_\nu\right]\hat{\psi}, & \hat{T}_3 &= \hat{T}_\rho\frac{1}{c_0^2}\hat{T}_\rho\hat{\psi}, \\ \hat{T}_2 &= i\hbar\left[u^\mu\partial_\mu\frac{1}{c_0^2}\hat{T}_\rho - \hat{T}_\rho\frac{1}{c_0^2}u^\mu\partial_\mu\right]\hat{\psi}, & \hat{T}_4 &= 2m\hat{T}_\rho\hat{\psi}. \end{aligned} \tag{1.102}$$

To proceed past this point, an eikonal approximation is needed. If ω is the frequency of a mode in $\hat{\psi}$, then as in [41],

$$\left|\frac{\partial_t\rho}{\rho}\right| \ll \omega, \left|\frac{\partial_t c_0}{c_0}\right| \ll \omega, \left|\frac{\partial_t u^\mu}{u^\mu}\right| \ll \omega \tag{1.103}$$

and the corresponding relations for variations in space. In the more general curved space-time case, it is also required that the metric is not changing too rapidly, so

$$\left|\frac{\partial_t g_{\mu\nu}}{g_{\mu\nu}}\right| \ll \omega\forall\mu,\nu, \left|\frac{\partial_t g}{g}\right| \ll \omega \tag{1.104}$$

and the corresponding relations for variations in space, without summation of indices. As in Chapters 1.3 and 1.4.2.1, the interesting "phononic" part of the excitation spectrum is at low momenta (wavelength longer than the healing length), so terms quartic in the momentum of $\hat{\psi}$ can be ignored to first order. With these approximations, $\hat{T}_2$ and $\hat{T}_3$ are negligible and the remaining equation is

$$\left[u^\mu\partial_\mu\frac{1}{c_0^2}u^\nu\partial_\nu + \frac{2m}{\hbar^2}\hat{T}_\rho\right]\hat{\psi} = 0 \tag{1.105}$$

or

$$\partial_\mu\left(\rho\sqrt{-g}\left[g^{\mu\nu} - \frac{u^\mu u^\nu}{c_0^2}\right]\partial_\nu\hat{\psi}\right) = 0. \tag{1.106}$$

This equation is now close to a Klein-Gordon-like equation and the only thing that remains to be done is to separate out the effective metric determinant. Writing Eq.

(1.106) as $\partial_\mu \left(f^{\mu\nu} \partial_\nu \hat{\psi} \right) = 0$, the equation to solve is

$$f^{\mu\nu} = \sqrt{-G} G^{\mu\nu} \tag{1.107}$$

for some tensor $\boldsymbol{G}$. Taking the determinant of this equation[10],

$$G = -\left(-f\right)^{\frac{2}{n-2}} \tag{1.108}$$

where n is the total number of dimensions[11]. Taking the determinant of $\boldsymbol{f}$ and combining it with Eq. (1.108) results in

$$\sqrt{-G} = \sqrt{-g} \rho^{\frac{n}{n-2}} \left(\frac{c}{c_s} \right)^{\frac{2}{n-2}} \tag{1.109}$$

where the speed of sound c_s is defined as in Eq. (1.59). Separating the determinant G from the tensor $\boldsymbol{f}$, the acoustic metric $\boldsymbol{G}$ is given by

$$G_{\mu\nu} = \left(\frac{\rho c}{c_s} \right)^{\frac{2}{n-2}} \left[g_{\mu\nu} + \left(1 - \frac{c_s^2}{c^2} \right) \frac{v_\mu v_\nu}{c^2} \right]. \tag{1.110}$$

Comparison with previous results

As shown in Chapter 1.4.2.2, it is clear that Eq. (1.110) is equivalent to the acoustic metric in [42] for quantised phonons. In the case where $\boldsymbol{g} \to \boldsymbol{\eta}$, Eq. (1.110) immediately reduces to the acoustic metric in [41]. In the non-relativistic flat spacetime limit in $3+1$ dimensions, $|\boldsymbol{u}| \to c$ so $c_s \to c_0$ and

$$u_0 \to c + \sum_i \frac{u_i^2}{c} \tag{1.111}$$

to first order. Consequently,

$$\begin{aligned} G_{\mu\nu} \to & \frac{\rho c}{c_0} \left[\left\{ -\frac{c_0^2}{c^2} + \left(1 - \frac{c_0^2}{c^2} \right) \sum_j \frac{u_j^2}{c^2} \right\} \delta^0{}_\mu \delta^0{}_\nu \right. \\ & \left. - \left(1 - \frac{c_0^2}{c^2} \right) \left(1 + \sum_j \frac{u_j^2}{c^2} \right) \frac{u_i}{c} \left(\delta^i_\mu \delta^0_\nu + \delta^0_\mu \delta^i_\nu \right) + \left\{ 1 + \left(1 - \frac{c_0^2}{c^2} \right) \frac{u_i u_j}{c^2} \right\} \delta^i{}_\mu \delta^j{}_\nu \right]. \end{aligned} \tag{1.112}$$

Rescaling the coordinate x^0 by $ct \to t$, the acoustic metric becomes

$$G'_{\mu\nu} = \frac{\rho}{c_0} \left[\left(-c_0^2 + \sum_j u_j^2 \right) \delta^0{}_\mu \delta^0{}_\nu - u_i \left(\delta^i_\mu \delta^0_\nu + \delta^0_\mu \delta^i_\nu \right) + \delta^i{}_\mu \delta^j{}_\nu \right] + \mathcal{O}\left(\frac{1}{c^2} \right) \tag{1.113}$$

which, to lowest order in c^{-1}, is exactly the non-relativistic acoustic metric given in [40].

It is stated in Chapter 1.4.2.1 that c_0 is the non-relativistic limit of the speed of sound; this will now be shown explicitly. In the non-relativistic limit, the time component of the flow velocity u^0 goes to c. It is clear from Eq. (1.59) that $c_s \to c_0$

[10] Note that f is the determinant of $\boldsymbol{f}$ with components $f^{\mu\nu}$, while G is the determinant of $\boldsymbol{G}$ with components $G_{\mu\nu}$.

[11] Note that this diverges in $1+1$ dimensions. Eq. (1.106) remains valid for any n.

in this limit. As shown earlier in this section when reconstructing the GPE, the interaction strengths λ and g_{NR} are related by

$$g_{NR} = \frac{\hbar^2}{2m}\lambda. \tag{1.114}$$

Comparison of the definition of c_0 in Eq. (1.57) and the non-relativistic speed of sound in Eq. (1.28) with the above expression for the interaction strengths immediately leads to the conclusion that they are identical.

Chapter 2

Gravitational waves

When Einstein proposed his theory of General Relativity (GR) in 1915 [46], it was quickly converted into a series of predictions for experimental tests. These predictions were shown to be consistent with observations made in the following century without fail. The last major prediction of GR to be observed in an experiment is that of gravitational radiation; ripples in the fabric of space-time caused by the motion of massive objects.

The fact that gravity is so much weaker than the three other fundamental forces observed in the Universe is not difficult to demonstrate. For example, the gravitational effect of all six trillion trillion kilograms of the Earth's mass on a human body can be countered by the electromagnetic force of a few small magnets on the order of a few centimetres long each. Because of the relatively weak nature of gravity, the magnitude of gravitational waves is astronomically tiny. This can be demonstrated by considering the first ever detection of gravitational waves [4]. The effective change in distance measured by the LIGO detectors is equivalent to detecting a difference in the distance from the Earth to Proxima Centurai (the nearest known star to the Sun) of a single human hair. These inconceivably small numbers serve to make the now almost routine detection of gravitational waves by the LIGO and VIRGO collaborations a phenomenally impressive feat of experimental physics and engineering.

The demonstrated technical feasibility of detecting gravitational waves has prompted an outpouring of proposals and in-progress implementations of gravitational wave detectors across a wide range of frequencies (see [20, 21, 47] amongst many other examples). Some of these proposals aim to address the most prohibitive drawbacks of the LIGO and VIRGO projects, namely the large size and cost. One such example is the proposal by Sabín et. al. to build resonant gravitational wave detectors with Bose-Einstein condensates [22]. The technical implementation studies of this proposal are currently in progress (e.g. in [48–51]) and must necessarily include schemes for testing the metrological scheme. The theoretical foundation for one such testing scheme is presented in [1].

The material presented in this chapter serves as an introduction to the theory of gravitational waves and Fermi normal coordinates and is relevant to [1].

2.1 Linearised gravity

The metric perturbation

Consider a region of space-time which is almost flat. In this region, there are no large objects producing strong gravitational fields. The phrase "almost flat" can be made more exact by defining the metric as

$$g_{\mu\nu} = \eta_{\mu\nu} + h_{\mu\nu} : \left|h_{\mu\nu}\right| \ll 1 \forall \mu, \nu. \tag{2.1}$$

Problems involving weak gravitational curvature may be solved perturbatively with $\boldsymbol{h}$ parameterising the perturbation; this approach is called *linearised gravity*. All calculations in the remainder of this section will be implicitly truncated to first order in $\boldsymbol{h}$ unless otherwise stated. As $\boldsymbol{g}$ must still be a valid metric, this perturbation $\boldsymbol{h}$ is constrained to fulfil the Einstein field equations (EFE) [52]

$$G_{\mu\nu} + \Lambda g_{\mu\nu} = \kappa T_{\mu\nu} \tag{2.2}$$

where $\boldsymbol{G}$ is the Einstein tensor, $\boldsymbol{T}$ is the stress-energy tensor, Λ is the cosmological constant and κ is the Einstein constant. The Einstein tensor for $\boldsymbol{g}$ as defined in Eq. (2.1) is

$$G_{\mu\nu} = \left(\delta^{\gamma}{}_{\mu}\delta^{\zeta}{}_{\nu} - \frac{1}{2}g_{\mu\nu}g^{\gamma\zeta}\right)\frac{1}{2}\eta^{\epsilon\eta}\left(h_{\eta\zeta,\gamma\epsilon} - h_{\eta\epsilon,\gamma\zeta} - h_{\gamma\zeta,\eta\epsilon} + h_{\gamma\epsilon,\eta\zeta}\right). \tag{2.3}$$

This expression can be somewhat simplified by introducing the *trace reversed perturbation*

$$\bar{h}^{\mu\nu} = h^{\mu\nu} - \frac{h}{2}\eta^{\mu\nu} \tag{2.4}$$

where $h = g^{\mu\nu}h_{\mu\nu} = \eta^{\mu\nu}h_{\mu\nu} + \mathcal{O}\left(h^2\right)$ is the trace of $\boldsymbol{h}$. The Einstein tensor then reduces to

$$G_{\mu\nu} = -\frac{1}{2}\left(\bar{h}_{\mu\nu,\eta}{}^{,\eta} + \eta_{\mu\nu}\bar{h}_{\eta\gamma}{}^{,\eta\gamma} - \bar{h}_{\mu\eta,\nu}{}^{,\eta} - \bar{h}_{\nu\eta,\mu}{}^{,\eta}\right). \tag{2.5}$$

Gauge transformations

As in non-perturbative GR, physical laws in linearised gravity must be invariant under coordinate transformations. Consider a coordinate transformation

$$x^{\mu} \to x'^{\mu} = x^{\mu} + \xi^{\mu} \tag{2.6}$$

where $\boldsymbol{\xi}$ is some "small" vector. Under such a coordinate transformation, the metric transforms as

$$g_{\mu\nu} \to g'_{\mu\nu} = \eta_{\mu\nu} + h_{\mu\nu} - \xi_{\mu,\nu} - \xi_{\nu,\mu} + \mathcal{O}\left(\xi^2\right) + \mathcal{O}\left(\xi h\right). \tag{2.7}$$

Defining

$$h'_{\mu\nu} = h_{\mu\nu} - \xi_{\mu,\nu} - \xi_{\nu,\mu} \tag{2.8}$$

makes the precise definition of the "smallness" restriction on $\boldsymbol{\xi}$ obvious; this coordinate transformation should not be large enough to disturb the "smallness" condition $\left|h_{\mu\nu}\right| \ll 1$. As such a coordinate transformation has a similar effect on the metric perturbation $\boldsymbol{h}$ as a gauge transformation of the electromagnetic 4-potential, this type of coordinate transformation is usually also called a *gauge transformation*.

It is straightforward to show that the Einstein tensor is invariant under such a gauge transformation (e.g. [52]). As mentioned above, this is required in GR, even when linearised. However, $\bar{\boldsymbol{h}}$ does not have this gauge invariance. Hence, without any loss of generality, a gauge can be chosen such that

$$\bar{h}_{\mu\nu}{}^{,\nu} = 0 \forall \mu. \tag{2.9}$$

In analogy to electromagnetic gauges, this is called the *Lorentz gauge*. The Lorentz gauge condition is preserved under gauge transformations satisfying $\Box\xi^{\mu} = 0\forall\mu$.

2.2 Linearised waves

The wave equation

In the Lorentz gauge, the Einstein tensor has the particularly simple form

$$G_{\mu\nu} = -\frac{1}{2}\bar{h}_{\mu\nu,\eta}{}^{,\eta}. \tag{2.10}$$

The EFE are then

$$\Box\bar{h}_{\mu\nu} = -2\kappa T_{\mu\nu}. \tag{2.11}$$

It has been assumed that the acceleration of the expansion of the universe is sufficiently slow that it has no measurable effect on the metric perturbation, so Λ is ignored.

Eq. (2.11) is simply an inhomogeneous wave equation for $\bar{\boldsymbol{h}}$, where energy serves as a source of metric perturbation through the stress-energy tensor. Hence, it can be concluded that weak perturbations to the metric must take the form of waves, i.e. *gravitational waves* (GWs). In a region of space-time with no significant matter or energy concentrations (effectively a vacuum), $\boldsymbol{T} \sim 0$ so the EFE reduce to

$$\Box\bar{h}_{\mu\nu} = 0. \tag{2.12}$$

Wave properties

As the EFE take the form of a wave equation, the most obvious potential solution to test is a plane wave. If

$$\tilde{h}_{\mu\nu} = A_{\mu\nu}\exp\left(ik_{\alpha}x^{\alpha}\right) \tag{2.13}$$

for some pseudotensor of constants $\boldsymbol{A}$, the EFE are fulfilled if and only if $k_{\alpha}k^{\alpha} = 0$. Hence $\tilde{\boldsymbol{h}}$ is only a valid solution for null momentum waves, i.e. GWs must travel at the speed of light[1]. The substitution of this solution into the Lorentz gauge condition reveals that

$$k_{\mu}A^{\mu\nu} = 0\forall\nu, \tag{2.14}$$

so the amplitude of a GW is entirely transverse to its propagation direction in the Lorentz gauge.

2.3 Specific gauges

As mentioned in Chapter 2.1, the Lorentz gauge condition does not fully specify a set of coordinates. Any transformation of the form of Eq. (2.6) such that $\Box\xi^{\mu} = 0\forall\mu$ still obeys the Lorentz gauge condition, but the observed physical properties of GWs in these different coordinates can be very different.

[1]This is not true for many extensions of GR. The recent simultaneous light and GW observations of a neutron star merger [6] have strongly constrained the speed of GWs to be within a small interval around the speed of light, ruling out many models beyond GR, e.g. [53].

2.3.1 The transverse-traceless gauge

Suppose $\bar{\boldsymbol{h}} : \bar{h}_{\mu\nu} = A_{\mu\nu} \exp\left(ik_\alpha x^\alpha\right)$ is a solution of the EFE, and a gauge transformation is performed where $\boldsymbol{\xi}$ is chosen as

$$\xi^\mu = B^\mu \exp\left(ik_\alpha x^\alpha\right) \tag{2.15}$$

for some amplitude vector $\boldsymbol{B}$. Choosing

$$B_\mu = -\frac{i}{k_0}\left[A_{\mu 0} - \frac{k_\mu}{2k_0}A_{00} + \left(\eta_{\mu 0} + \frac{k_\mu}{2k_0}\right)\frac{A^\mu_\mu}{n-2}\right] \tag{2.16}$$

in $n \neq 2$ dimensions (or an equivalent expression for $n = 2$), the resulting amplitude $\boldsymbol{A}'$ obeys the properties

$$A'^\mu{}_\mu = 0\,,\; A'_{\mu\nu}u^\nu = 0 \tag{2.17}$$

for $\boldsymbol{u} = (1, 0, 0, \cdots)$. In words, the GW amplitude is now traceless and transverse to $\boldsymbol{u}$, so these coordinates are called the *transverse-traceless gauge* (TT gauge)[2]. The above procedure can be performed for any arbitrary $\boldsymbol{u}$ with a corresponding amplitude $\boldsymbol{B}$.

In the TT gauge, the form of $\boldsymbol{h}$ is particularly simple. By construction, $h_{\mu\nu} = \bar{h}_{\mu\nu}$. If $\boldsymbol{u}$ is chosen to be $(1, 0, 0, 0)^T$ in $3 + 1$ dimensions, then $A_{\mu 0} = A_{0\mu} = 0 \forall \mu$. If the coordinates are rotated such that the GW is travelling in the x^3 direction, $\boldsymbol{k} = (\omega, 0, 0, \omega)^T$ for some ω and $A_{\mu 3} = A_{3\mu} = 0 \forall \mu$. The remaining degrees of freedom are constrained by metric symmetry and the traceless condition, so that only two free parameters remain:

$$\boldsymbol{h}^{TT} = \begin{pmatrix} 0 & 0 & 0 & 0 \\ 0 & h_+ & h_\times & 0 \\ 0 & h_\times & -h_+ & 0 \\ 0 & 0 & 0 & 0 \end{pmatrix}. \tag{2.18}$$

Since $\bar{h}_{\mu\nu} = h_{\mu\nu}$ by construction and the components $\bar{h}_{\mu\nu}$ have the form of plane waves, the components of the metric perturbation $\boldsymbol{h}^{TT}$ are themselves simply plane waves with two orthogonal polarisations. The functions $h_+(t, z)$ and $h_\times(t, z)$ are often called *strain functions*.

Particles in the TT gauge

If a test mass with the position $\boldsymbol{x}$ on a geodesic described by the world line $\mathscr{P}_0(s)$ is initially at rest in the TT gauge at $s = 0$, then $dx^i/ds = 0 \forall i$ and the geodesic equation for the 3-velocity of that mass has the form [52]

$$\left.\frac{d^2x^i}{ds^2}\right|_{s=0} = -\left[\Gamma^i{}_{00}\left(\frac{dx^0}{ds}\right)^2\right]_{s=0}. \tag{2.19}$$

The relevant Christoffel symbols $\Gamma^i{}_{00}$ for the metric given by Eq. (2.1) are

$$\Gamma^i{}_{00} = \frac{1}{2}\left(2\partial_0 h_{0i} - \partial_i h_{00}\right). \tag{2.20}$$

[2]It should be noted that the TT gauge does not exist for non-radiative gravitational perturbations (e.g. near a rotating spherical mass) as $\boldsymbol{h}$ cannot be written as a superposition of plane waves [52].

In the TT gauge, all of these components of $\boldsymbol{h}$ vanish at all values of s, so the Christoffel symbols vanish and

$$\frac{d^2x^i}{ds^2} = 0 \forall s. \tag{2.21}$$

It can thus be concluded that test particles initially at rest in the TT gauge remain at rest regardless of the form of any passing GWs. Hence, the coordinate distance between two test particles remains constant.

Consider two events separated by some vector $\boldsymbol{d} = (0,1,0,0)$. The proper distance between these events is

$$\int_{\boldsymbol{d}} ds = \sqrt{1 + h_+}. \tag{2.22}$$

While a passing GW does not alter the coordinate distance between two test particles in the TT gauge, this example shows that it may alter their proper distance depending on the relative orientation of the separation of the particles and the propagation vector of the GW.

2.3.2 Fermi normal coordinates

While the TT gauge is very useful for introducing GWs and deriving some basic properties, it is not the most useful for describing what a realistic observer would measure. A more useful frame for describing these observations is the proper comoving reference frame of an inertial time-like observer. This is defined as an orthonormal tetrad $\{\boldsymbol{e}_\alpha\}$ defined at some point such that the metric is locally flat at that point, extended along the observer's time-like world line $\mathscr{P}$ by parallel transport so that the axes follow those defined by local gyroscopes. Such coordinates are called *Fermi normal coordinates*, and represent the coordinates measured by any realistic experiment.

It is always possible to define a coordinate system that is locally flat at some point P in space-time. If an inertial observer with a world line $\mathscr{P}(s)$ is at the point P when $s = 0$, then the metric that this observer locally experiences at P is $\boldsymbol{\eta}$ by definition and the Christoffel symbols $\boldsymbol{\Gamma}(P)$ all vanish. Since the coordinates are then extended along the world line by parallel transport, the metric is locally flat and the Christoffel symbols are always zero at all points on the world line. This fact can be used to derive the form of the metric perturbatively near the observer's world line.

Perturbations around the world line

Near the world line $\mathscr{P}$, the metric can be expanded as a Maclaurin series in the distances along the tetrads of $\{\boldsymbol{e}_\alpha\}$ perpendicular to the world line, i.e. distances in space in comoving coordinates. This expansion has the form

$$g_{\mu\nu} = g_{\mu\nu}\big|_{\mathscr{P}} + g_{\mu\nu,i}\big|_{\mathscr{P}} x^i + \frac{1}{2!} g_{\mu\nu,jk}\big|_{\mathscr{P}} x^j x^k + \cdots . \tag{2.23}$$

Since the Christoffel symbols vanish on the world line, all first derivatives of the components of the metric also vanish on the world line. The second derivatives do not vanish, but are instead given by

$$g_{\mu\nu,\alpha\beta}\big|_{\mathscr{P}} = \eta_{\mu\sigma}\, \Gamma^\sigma{}_{\nu\alpha,\beta}\Big|_{\mathscr{P}} + \eta_{\sigma\nu}\, \Gamma^\sigma{}_{\mu\alpha,\beta}\Big|_{\mathscr{P}} \tag{2.24}$$

where

$$\begin{aligned}
\left.\Gamma^{\sigma}{}_{\mu\nu,0}\right|_{\mathscr{P}} &= 0 \forall \sigma, \mu, \nu, & (2.25)\\
\left.\Gamma^{\sigma}{}_{\mu 0,\nu}\right|_{\mathscr{P}} &= -\left.R^{\sigma}{}_{\mu\nu 0}\right|_{\mathscr{P}}, & (2.26)\\
\left.\Gamma^{\sigma}{}_{ij,k}\right|_{\mathscr{P}} &= \frac{1}{3}\left.\left(R^{\sigma}{}_{ijk} + R^{\sigma}{}_{jik}\right)\right|_{\mathscr{P}}. & (2.27)
\end{aligned}$$

These properties can be derived from the geodesic deviation equation and the definition of the Riemann curvature tensor when all Christoffel symbols are zero [54][3]. Combining Eqs. (2.23)-(2.27), the covariant line element has the form

$$\begin{aligned}
ds^2 = &-\left(1 + \left.R_{0i0j}\right|_{\mathscr{P}} x^i x^j\right) c^2 dt^2 \\
&- \left(\frac{2}{3}\left.R_{0jik}\right|_{\mathscr{P}} x^j x^k\right) 2cdtdx^i + \left(\delta_{ij} - \frac{1}{3}\left.R_{ikjl}\right|_{\mathscr{P}} x^k x^l\right) dx^i dx^j
\end{aligned} \qquad (2.28)$$

to lowest order in deviation from the world line $\mathscr{P}$, where $x^0 = ct$.

The problem of expressing the metric in Fermi normal coordinates is thus reduced to calculating the components of the Riemann curvature tensor $\boldsymbol{R}$. This tensor is generally covariant, but in linearised gravity with a metric of the form of Eq. (2.1) it is very straightforward to show that all components $R^{\rho}{}_{\sigma\mu\nu}$ are of magnitude $\mathcal{O}(h)$. Since gauge transformations perturb the coordinates by a term of order $\mathcal{O}(h)$, $\boldsymbol{R}$ is not just covariant but completely invariant to first order under gauge transformations. Hence, $\boldsymbol{R}$ can be calculated in any gauge that happens to be mathematically convenient. Since the metric is particularly simple in the TT gauge, it is a good choice for this calculation.

The metric form

Evaluating the components of $\boldsymbol{R}$ in the TT gauge, the Fermi normal coordinates line element in Eq. (2.28) is simply

$$ds^2 = \left(-1 + \frac{1}{2c^2}\left[2xy\partial_t^2 h_\times + \left(x^2 - y^2\right)\partial_t^2 h_+\right]\right) c^2 dt^2 + \delta_{ij} dx^i dx^j. \qquad (2.29)$$

While the other components of $\boldsymbol{R}$ appearing in Eq. (2.28) are not zero, they are proportional to a single or double spatial derivative of the GW strain functions in its direction of propagation. As this wavelength is typically far longer than the extent of any observer or detector[4], these terms are ignored for the purposes of describing a realistic observer.

[3]Everything is calculated on the world line $\mathscr{P}$; any strong and/or rapid changes of the metric close to this world line limit the applicability of this approximation.

[4]For example, the GW detection events of LIGO and VIRGO have peak detected frequencies on the order of 10^2 Hz [4, 5, 9–12], which corresponds to a wavelength of roughly half the radius of the Earth.

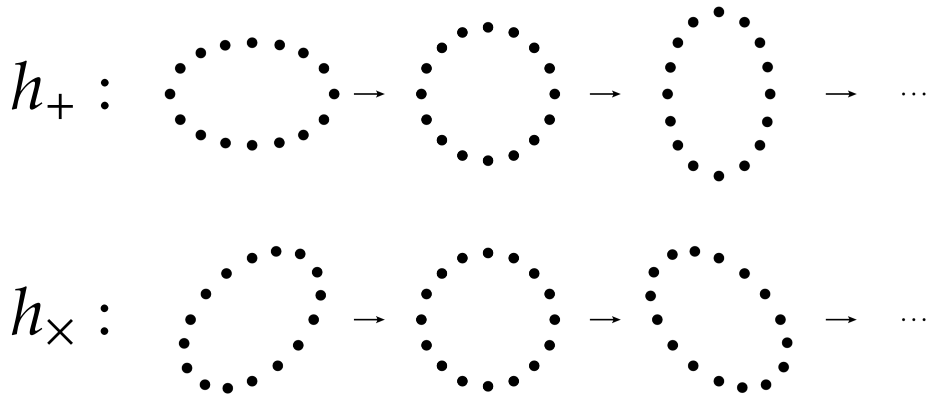

FIGURE 2.1: The greatly exaggerated evolution of a ring of test particles due to a GW in Fermi normal coordinates. The GW is propagating into or out of the page and the coordinate axes are arbitrarily chosen to match the direction of the text. The top row of diagrams corresponds to a GW with a purely h_+ polarisation, and the bottom row of diagrams corresponds to the orthogonal $h_\times$ polarisation.

Equivalence of gauges

There exists a gauge transformation between the TT gauge and Fermi normal coordinates. This is simply given by

$$\xi = \left(\frac{1}{4c}\left(2xy\partial_t h_\times + \left(x^2 - y^2\right)\partial_t h_+\right), -\frac{1}{2}\left(xh_+ + yh_\times\right), -\frac{1}{2}\left(xh_\times - yh_+\right), 0\right)^T \tag{2.30}$$

where ξ is defined as in Eq. (2.6). It is straightforward to show that $\Box\xi^\mu = 0$, so Fermi normal coordinates also describe GWs in the Lorentz gauge.

A non-inertial reference frame can similarly be constructed, and is useful for accurately describing e.g. Earth-bound GW detectors which have non-trivial acceleration and rotation. This frame is typically called the *proper detector frame*. A derivation of the form of this coordinate system and its associated metric near the world line can be found in [55].

Particles in Fermi normal coordinates

An initially stationary test mass A on a world line $\mathscr{P}_0(s)$ with an initial position $\boldsymbol{x}$ at $s = 0$ obeys the geodesic equation given in Eq. (2.19). However, Fermi normal coordinates are defined with respect to a particular world line, so the test particle will remain stationary in its own Fermi normal coordinates (all Christoffel symbols vanish on $\mathscr{P}_0$ so Eq. (2.19) has only trivial solutions). A more useful picture can be built from the geodesic deviation equation.

Given Fermi normal coordinates defined for the test mass A, denote the distance to a second test mass B as $\boldsymbol{\zeta}$ and suppose that these two particles follow geodesics such that $\boldsymbol{\zeta}(s = 0) = (0, \varepsilon, 0, 0)^T = \boldsymbol{\zeta}_{(0)}$. The value of ε is chosen to be small enough that the metric at A does not differ significantly from the metric at B. The geodesic deviation as measured from A is given by [52, 56]

$$\nabla_{\boldsymbol{u}}\nabla_{\boldsymbol{u}}\zeta^{\mu} = R^{\mu}{}_{\nu\alpha\beta}u^{\nu}u^{\alpha}\zeta^{\beta} \tag{2.31}$$

where $\boldsymbol{u}$ is the propagation vector along the geodesic of A and $\boldsymbol{R}$ is calculated at A. Since $\boldsymbol{u} = (1,0,0,0)^T$ and all Christoffel symbols vanish along the geodesic of A in Fermi normal coordinates, this equation can be simplified to

$$\frac{d^2\zeta^{\mu}}{dt^2} = -c^2 R^{\mu}{}_{0\nu 0}\zeta^{\nu}. \tag{2.32}$$

Evaluating these components of $\boldsymbol{R}$ (in the TT frame again),

$$R^{\mu}{}_{0\nu 0} = -\frac{1}{2}\eta^{\mu\rho}h^{TT}_{\rho\nu,00}. \tag{2.33}$$

Supposing that the particles would be at rest with respect to each other for $h \to 0$, then the solution of Eq. (2.32) reads

$$\zeta^{\mu} = \zeta^{\nu}_{(0)}\left(\delta^{\mu}{}_{\nu} + \frac{c^2}{2}\eta^{\mu\rho}h^{TT}_{\rho\nu,00}\right). \tag{2.34}$$

For the particular $\boldsymbol{\zeta}_{(0)}$ chosen above, this is

$$\boldsymbol{\zeta} = \left(0, \varepsilon\left[1 + \frac{1}{2}\partial_t^2 h_+\right], \frac{\varepsilon}{2}\partial_t^2 h_\times, 0\right)^T. \tag{2.35}$$

Unlike the TT frame, test masses in Fermi normal coordinates move with respect to each other under the influence of a passing GW.

It is immediately clear from Eq. (2.35) that the effect of the GW on two test masses is entirely transverse to its direction of propagation in Fermi normal coordinates. Expanding the above method to a ring of particles around the origin and considering a simple sinusoidal GW shows that the two polarisations h_+ and $h_\times$ of the GW have similar yet orthogonal effects. These effects are schematically plotted in Fig. (2.1).

Chapter 3

Conformally coupled screened scalar fields

There are two major motivating arguments for additional scalar fields in Nature, namely from extensions of general relativity (GR) and from extensions of the Standard Model (SM). It has recently been shown that some of these models are equivalent. This chapter will begin with an outline of the basic underlying arguments of each approach. The models outlined in this chapter are considered in [2] and [3].

3.1 Gravity as an incomplete description

This section will present the motivating arguments for screened scalar fields from the general relativity perspective.

Einstein's theory of GR has been one of the most phenomenally successful theories in the history of physics. Its predictions have been consistent with the barrage of experiments levied against it since its formulation in the early 1910's, from the famous 1919 measurement of the magnitude of gravitational lensing [57] to the ongoing lunar laser ranging experiments [58] and the recent first observations of gravitational waves [4]. However, GR is manifestly incompatible with the currently accepted quantum mechanical description of the other three fundamental forces in the Universe. This incompatibility is joined by other unsolved problems, such as the nature of curvature singularities in black holes, the cosmological constant problem, the accelerating expansion of the universe implying dark energy and galactic observations implying dark matter. Due to these issues, there have been many attempts to build theories beyond GR.

Scalar-tensor gravity

One of the simplest ways of extending GR is with a *scalar-tensor theory*. Such a theory introduces an extra scalar field ψ that couples to a metric theory of gravity through an action such as[1]

$$S = \int \sqrt{-g} \left[\xi \psi^2 R - \frac{1}{2} g^{\mu\nu} \partial_\mu \psi \partial_\nu \psi - V(\psi) \right] d^4 \boldsymbol{x} + S_m. \tag{3.1}$$

In Eq. (3.1), $g_{\mu\nu}$ are the elements of the metric $\boldsymbol{g}$ with an associated Ricci scalar R, ξ is a constant parameter of the model, $V(\psi)$ is some function of ψ (acting as a potential for ψ) and S_m is the matter action. The term $\sqrt{-g}\xi\psi^2 R$ is a modification of

[1]This is not the most general possible scalar-tensor action, but contains all terms relevant to the models discussed in this thesis. For a more general form, see [59].

the standard Einstein-Hilbert action term[2] $\sqrt{-g}c^4R/16\pi G$, where the gravitational constant G is now given in terms of a non-constant field ψ. This term cannot be obtained by a minimal substitution of an expression in flat Minkowski space-time (replacing the Minkowski metric with a curved metric), so the inclusion of this term is called a *non-minimal substitution*.

A scalar-tensor theory could be one possible way to account for dark energy [61, 62] or even dark matter (see [63, 64] for recent ideas). Such a scalar is also predicted by some higher dimensional theories combining GR and quantum physics due to compactification of the extra dimensions, such as string theory [60, 65].

Unfortunately, the postulated existence of such scalars is generally in disagreement with experimental bounds. For example, many scalar-tensor theories with non-trivial scalar-matter coupling predict deviations from the inverse-square scaling of gravity or spontaneously break the equivalence principle, both of which have been strongly constrained (see [18, 66] and references therein for an overview of constraining experiments). Due to these experimental bounds, a simple scalar-tensor theory with a small scalar mass must couple to matter so weakly as to be cosmologically irrelevant, whereas a theory with a strong matter coupling must have a scalar mass high enough to be equally trivial in a cosmological setting [18].

Observations at both the solar system scale and the cosmological scale could however be brought into agreement for a scalar-tensor theory with a *screened scalar field*. A *screening mechanism* introduces non-linear dynamics to the model such that the properties of the scalar field vary in different environments. Examples of screening mechanisms will be presented in Chapter 3.4.

3.2 A phenomenological approach to physics beyond the Standard Model

This section will present screened scalar fields from a particle physics perspective.

Since its formulation, it has been clear that the Standard Model of particle physics does not form a complete description of the fundamental interactions of the Universe. The current fundamental physics research efforts include many approaches for resolving some of the shortcomings of the SM, such as supersymmetry, string theory and loop quantum gravity. Many of these theories predict that the Universe contains more types of particles than those found in the SM. However, no conclusive evidence of any of these extra particles has been found despite many concerted search efforts with dedicated experiments. If one of these theories is to be believed, then "why haven't we seen these extra particles?" is an obvious question to ask. *Screened scalar fields* can be constructed as a phenomenological approach to answering this question.

Consider a simple extension consisting of the SM plus an additional scalar field. This scalar field couples directly only to the Higgs field (a so-called *Higgs portal*). The theories mentioned above may include scalar fields of this type. It has been recently shown that this approach is equivalent to a conformally coupled scalar-tensor theory of gravity [67]. Therefore, experiments constraining screened scalar field models can add constraints to these theories beyond the SM.

[2] While the cosmological constant term is ignored here as it is irrelevant for Earth-bound experiments, it can of course be included in the model, e.g. in [60].

3.3 Conformal metric transformations and coupling

To introduce screening mechanisms, the coupling between matter and extra scalar fields must be explored. To that end, a *conformal transformation* can be defined as a metric transformation of the form

$$g_{\mu\nu} \rightarrow g'_{\mu\nu} = A\left(\boldsymbol{x}\right) g_{\mu\nu} \tag{3.2}$$

where $A\left(\boldsymbol{x}\right)$ is some arbitrary function of the space-time coordinate $\boldsymbol{x}$. Such a transformation can be said to move the coordinate system from one *conformal frame* to another.

Conformal transformations are entirely distinct from general coordinate transformations. For example, the line element $ds^2 = g_{\mu\nu}dx^\mu dx^\nu$ is invariant under general coordinate transformations but transforms as $ds'^2 = A\left(\boldsymbol{x}\right) ds^2$ under a conformal transformation. While this example would suggest that different conformal frames are physically inequivalent, it is simply an artefact of the rescaling of dimensionful quantities. Dimensionless quantities are conformally invariant and any action can be written in a dimensionless form, so the physical conclusions reached in different conformal frames are identical (see [68] for an example). The phenomenology of different frames (with appropriate care taken to rescale all dimensionful quantities) can be regarded as different interpretations of the same physical phenomena.[3,4]

A conformal transformation to simplify the action

The benefit of a conformal transformation for models in the form of Eq. (3.1) is that the non-minimal substitution term $\sqrt{-g}\xi\psi^2 R$ can be transformed into the conventional field independent Einstein-Hilbert term. The following derivation will largely follow [60].

Consider a conformal transformation of the form of Eq. (3.2) where $A\left(\boldsymbol{x}\right) = c^4\xi\psi^2\left(\boldsymbol{x}\right)/16\pi G$. With some straightforward but tedious algebra, it can be shown that the action transforms as

$$S' = \int\sqrt{-g'}\left(\frac{c^4}{16\pi G}R' - \frac{\Delta}{2}g'^{\mu\nu}\partial_\mu\psi\partial_\nu\psi - V\left(\psi\right)\right)d^4\boldsymbol{x} + S'_m \tag{3.3}$$

where

$$\Delta = \left[6 + \frac{1}{2\xi}\right]\frac{1}{\psi^2}. \tag{3.4}$$

If ψ is to be a normal field with positive energy, then ξ must be chosen such that $\Delta > 0$. With this choice made, the field ϕ can be introduced as the solution of the equation

$$\left(\frac{d\phi}{d\psi}\right)^2 = \Delta. \tag{3.5}$$

This redefinition allows the action in Eq. (3.3) to take the form

$$S' = \int\sqrt{-g'}\left(\frac{c^4}{16\pi G}R' - \frac{1}{2}g'^{\mu\nu}\partial_\mu\phi\partial_\nu\phi - V\left(\phi\right)\right)d^4\boldsymbol{x} + S'_m \tag{3.6}$$

[3] This statement is not without controversy; e.g. [60] dedicates an entire chapter to deciding which conformal frame represents the physically observed reality. However, no experiment can measure an absolute scale and all results must be stated in comparison with other experiments.

[4] It is not clear whether this equivalence still holds in quantised gravity models and this question is a topic of current research: see [69–71] and references therein for a discussion of this point.

which is exactly the form of Eq. (3.1) without a non-minimal coupling term. The field ψ in terms of ϕ is given by

$$\psi = \psi_0 e^{\chi\phi} \tag{3.7}$$

where ψ_0 is a constant and $\chi^2 = 1/\left(6 + 1/2\xi\right)$. It should be noted that the $\Delta > 0$ restriction implies $\chi \in \mathbb{R}$ but does not imply $\chi > 0$; this choice is usually made for other physical reasons depending on the particular scalar-tensor model.

The Einstein and Jordan frames

Due to the lack of non-minimal substitution, the frame defined in Eq. (3.6) is generally called the *Einstein frame*. The frame used in Eq. (3.1) is called the *Jordan frame* due to the pioneering work of Jordan in non-minimal substitution models [72].

In terms of the field ϕ used in Eq. (3.6), the components of the metrics in the Einstein and Jordan frames are related to each other by the conformal transformation

$$g^{(J)}_{\mu\nu} \propto e^{\phi/M} g^{(E)}_{\mu\nu} \tag{3.8}$$

where the proportionality is constant and $M^2 = 3/2 + 1/8\xi > 0$. If the field ψ is chosen such that $\psi_0^2 = 16\pi G/c^4\xi = 16\pi G\left(8M^2 - 12\right)/c^4$, then this constant of proportionality is 1 so

$$g^{(J)}_{\mu\nu} = e^{\phi/M} g^{(E)}_{\mu\nu}. \tag{3.9}$$

It is very important to note that the matter action S_m is modified by the conformal transformation. There is no direct coupling between the scalar field and matter in the Jordan frame and the matter action has the standard form. In the Einstein frame, the matter action is modified with an extra conformal term in front of the metric, i.e. direct coupling between matter and the scalar field ϕ. Scalar field models with this coupling to matter are called *conformally coupled*[5].

In the Einstein frame, the metric $\mathbf{g}^{(E)}$ is generated by all fields including the extra scalar field. Free particles follow the geodesics derived from this metric and also feel a gravity-like fifth force mediated by the extra scalar field. Conversely, there is no fifth force in the Jordan frame. However, the Einstein field equations are modified due to the non-minimal substitution in the Einstein-Hilbert action, so free particles follow paths different to those in the Einstein frame (namely the geodesics of $\mathbf{g}^{(J)}$). These paths depend locally on the scalar field. As discussed in the introduction to this section, the difference between these frames is a matter of interpreting any deviation from GR and SM predictions as either a fifth force or a modified metric.

Putting all of these concepts together, a scalar field which is conformally coupled to matter in the Einstein frame as described in this section and has some screening mechanism such as those described in Chapter 3.4 is a *conformally coupled screened scalar field*.

3.4 Screening mechanisms

There are many possible types of screening mechanisms for a scalar field. Three of the most commonly studied are presented here as an overview.

[5] A conformal transformation is not the most general type of metric transformation; a more general class of models can be constructed from the disformal transformation $g^{'}_{\mu\nu} = A^2\left(\phi\right) g_{\mu\nu} + B\left(\phi\right)\partial_\mu\phi\partial_\nu\phi$ [73]. For an overview of disformally coupled scalar field models, see [74]. It is interesting to note that disformally coupled models do not admit more types of screening mechanisms than conformally coupled models [74].

3.4.1 Minimal kinetic Lagrangian screening

Two commonly studied screening mechanisms can be derived from the action given in Eq. (3.6); the *chameleon* and *symmetron* mechanisms. These two mechanisms utilise alternative but complementary approaches to supressing the effects of a conformally coupled scalar field in the presence of matter. Both mechanisms can be derived from the same generic action, as will be done in this section.

Conformally coupled equations of motion

Consider a conformally coupled screened scalar field model with the Einstein frame action given by Eq. (3.6). The Jordan frame metric $\boldsymbol{g}^{(J)}$ is related to the Einstein frame metric $\boldsymbol{g}^{(E)}$ by the conformal transformation

$$g^{(J)}_{\mu\nu} = A^2(\phi)\, g^{(E)}_{\mu\nu}. \tag{3.10}$$

While the scalar field ϕ should couple to the full Einstein frame metric $\boldsymbol{g}$, the effect of the scalar as a deviation from GR must be at most a perturbation to match current experiments. Therefore, the effect of any deviation of the metric $\boldsymbol{g}$ from the flat Minkowski metric $\boldsymbol{\eta}$ in the kinetic term of Eq. (3.6) can be considered to be a perturbation of a perturbation and will be ignored here[6]. With this assumption, the Einstein frame action becomes

$$S = \int \sqrt{-g}\left(\frac{c^4}{16\pi G}R - \frac{1}{2}\eta^{\mu\nu}\partial_\mu\phi\partial_\nu\phi - V(\phi)\right)d^4\boldsymbol{x} + \int \mathcal{L}_m d^4x. \tag{3.11}$$

Varying the action with respect to the scalar field produces the equation of motion

$$\Box_\eta\phi - V_{,\phi} + \frac{A_{,\phi}}{A}g^{\mu\nu}T_{\mu\nu} = 0 \tag{3.12}$$

where

$$T_{\mu\nu} = -\frac{2}{\sqrt{-g}}\frac{\delta\mathcal{L}_m}{\delta g^{\mu\nu}} \tag{3.13}$$

is the stress-energy tensor for the matter Lagrangian.

The conserved Einstein frame equation of motion

Since the metric $\boldsymbol{g}$ is generated by both matter and the scalar field, the stress-energy tensor $\boldsymbol{T}$ (which includes matter but not the scalar field) is not conserved with respect to $\boldsymbol{g}$. However, the Jordan frame stress energy tensor defined as

$$T^{(J)}_{\mu\nu} = -\frac{2}{\sqrt{-g^{(J)}}}\frac{\delta\mathcal{L}_m}{\delta g^{\mu\nu}_{(J)}} \tag{3.14}$$

is conserved with respect to the Jordan frame metric, i.e.

$$\nabla^{(J)}_\mu T^{(J)\mu}{}_\nu = 0 \tag{3.15}$$

where $\boldsymbol{\nabla}^{(J)}$ is a covariant derivative with respect to $\boldsymbol{g}^{(J)}$. These two stress-energy tensors are related by $T_{\mu\nu} = A^2 T^{(J)}_{\mu\nu}$, so the equation of motion for ϕ can be written

[6] Although any full model must include these effects, this approximation is well satisfied within areas of high matter density but no extreme curvature e.g. within our solar system.

as

$$\Box\phi - V_{,\phi} + A^3 A_{,\phi} g^{\mu\nu}_{(J)} T^{(J)}_{\mu\nu} = 0. \tag{3.16}$$

For non-relativistic matter, the stress-energy tensor is approximately given by

$$g^{\mu\nu}_{(J)} T^{(J)}_{\mu\nu} \approx -\rho^{(J)} \tag{3.17}$$

where $\rho^{(J)}$ is the Jordan frame matter density. Since $T^{(J)}_{\mu\nu}$ is conserved with respect to $\boldsymbol{g}^{(J)}$, the density $\rho^{(J)}$ is conserved in the Jordan frame and not the Einstein frame. It is straightforward to show that the density[7] $\rho = A^3\rho^{(J)}$ is instead conserved in the Einstein frame when $g_{\mu 0} \approx 0$ for $\mu \neq 0$. Ignoring deviations of the metric $\boldsymbol{g}$ from the Minkowski metric $\boldsymbol{\eta}$ as done above fulfils this requirement. In terms of the density ρ, the equation of motion for the scalar field is

$$\Box\phi = V_{eff,\phi} \tag{3.18}$$

where the *effective potential* is given by

$$V_{eff}(\phi) = V(\phi) + A(\phi)\rho. \tag{3.19}$$

A solution of the equation of motion

To investigate the features of this model, it is instructive to consider an example scenario where a static object with some matter density ρ_{obj} is embedded in some homogeneous and isotropic background density ρ_0. If the effective potential has a minimum at some value of the field ϕ_{min}, then the field will assume the corresponding uniform value $\phi_0 = \phi_{\text{min}}(\rho_0)$ in the absence of the object. When the object is also present, the field will have some profile

$$\phi = \phi_0 + \delta\phi \tag{3.20}$$

where $\delta\phi$ is effectively the field sourced by the object. In the limit where $\delta\phi$ is a perturbation of ϕ_0, the equation of motion for $\delta\phi$ (expanded around ϕ_0 to first order) is given by

$$\nabla^2\delta\phi - m_0^2\delta\phi = A_{,\phi}(\phi_0)\,\rho_{\text{obj}} + \mathcal{O}\left(\delta\phi^2\right) \tag{3.21}$$

where the field perturbation $\delta\phi$ has an *effective mass* given by

$$m_0^2 = \left.\frac{d^2V_{eff}}{d\phi^2}\right|_{\phi=\phi_0}. \tag{3.22}$$

It is clear from Eq. (3.21) that $A_{,\phi}(\phi_0)$ acts as a coupling strength between the scalar field and matter. In the case where the object is a point mass of mass $\mathcal{M}$, its matter density becomes the distribution $\rho_{\text{obj}} = \mathcal{M}\delta(r)$ and Eq. (3.21) has the first order solution

$$\delta\phi(r) = A_{,\phi}(\phi_0)\frac{\mathcal{M}}{4\pi r}e^{-m_0 r} \tag{3.23}$$

where r parameterises the distance to the object.

There are several ways to supress the effect of a conformally coupled scalar field. When considering the profile in Eq. (3.23), the two obvious choices are either to increase the effective mass m_0 such that the resulting force has a very short range,

[7]Note that this is not the Einstein frame density $\rho^{(E)} = g^{\mu\nu}T_{\mu\nu}$, but differs by a factor of A.

or to decrease the coupling strength parameterised by $A_{,\phi}(\phi_0)$. If either of these parameters are fixed to experimental constraints, then the deviations from GR are trivial at all scales and the resulting models are uninteresting. Instead, these two methods will be applied dynamically in the following sections to construct two screening mechanisms.

3.4.1.1 Chameleon

The *chameleon mechanism* was proposed by Khoury and Weltman in 2004 [75]. In this model, a conformally coupled screened scalar field (*chameleon field* in this case) ϕ has a non-vanishing effective mass m_ϕ which depends on the environmental matter density. The chameleon field adapts in this way to its environment and becomes almost undetectable in regions of relatively high matter density, e.g. within our solar system.

The thin-shell effect

When a homogeneous object is large[8], then it can be shown that the interior of the object does not contribute to the profile of the chameleon field [75]. Only a thin shell of matter on the surface of the object contributes, so this is called the *thin-shell effect*. It is instructive for developing a physical intuition to consider the force due to the chameleon being mediated by off-shell chameleon particles travelling from the source mass to a test particle. If the effective chameleon mass is high then the chameleon particle cannot penetrate through much matter, so only the matter near the surface of the source mass can interact with the test mass[9].

Due to the thin-shell effect, a hollow object with a sufficiently thick barrier (e.g. a substantial wall of a vacuum chamber) can shield the chameleon field in the interior from the effects of the outside world and allow the chameleon field to reach a relatively unscreened regime. Using this effect, experiments on Earth can constrain chameleon field models that are otherwise consistent with solar system scale observations.

The chameleon model

To obtain a chameleon field model, the potential $V(\phi)$ in Eq. (3.6) is chosen such that the effective mass given in Eq. (3.22) increases with increasing ambient matter density. As pointed out in [75], many potentials arising from non-perturbative string theory effects and appearing in quintessence models satisfy this requirement. The most studied potential for chameleon models is

$$V(\phi) = \lambda^4 \exp\left[\lambda^n/\phi^n\right], \tag{3.24}$$

where λ is a constant and different choices of the integer n result in different models. The conformal coupling factor appearing in Eq. (3.10) is chosen to be

$$A(\phi) = e^{\phi/2M_C} \tag{3.25}$$

[8] In this case, "large" is defined as an object with a sufficiently strong effect on the effective chameleon mass such that it cannot be considered to be a perturbation on some background value. Note that this depends on both the spatial extent of the object and its density.

[9] Care must be taken that this analogy is not taken too literally; the chameleon model is a model of an explicitly classical scalar field and quantum effects such as tunnelling cannot be considered.

in line with the definition given in Eq. (3.9). The resulting effective potential to lowest order in ϕ is

$$V_{eff}\left(\phi\right) = \lambda^4 + \frac{\lambda^{4+n}}{\phi^n} + \frac{\rho}{2M_C}\phi. \tag{3.26}$$

This effective potential exhibits a minimum when n is positive or negative and even. However, when $n = -2$ then the effective mass does not scale with the matter density. Therefore, a chameleon field model is constructed when $n = \mathbb{Z}^+ \cup 2\mathbb{Z}^- \setminus \{-2\}$. The λ^4 term is a constant energy density that could contribute to dark energy; this motivates the simplest chameleon model where λ is set to the dark energy scale $\lambda_{\mathrm{DE}} \approx 2.4$ meV.

It is clear that the effective mass derived from this effective potential (and thus the strength of the force felt by matter due to the chameleon) is dependent on the ambient matter density ρ. This is the essence of the chameleon screening mechanism; the chameleon field has a high effective mass and thus a small force in areas of high ambient matter density, and a low effective mass and therefore a large force whenever the ambient matter density is low. For a visualisation of this effective potential and the associated effective mass, see [2, 3] reprinted below.

3.4.1.2 Symmetron

The *symmetron mechanism* was introduced with this name[10] by Hinterbichler and Khoury in 2010 [77]. While the chameleon mechanism has an effective mass adapting to its environment, the symmetron mechanism involves a $\mathbb{Z}_2$ symmetry in the coupling strength that is spontaneously broken in regions of low ambient matter density. This symmetry is restored above some threshold density and the coupling to matter (and thus any deviation from GR) vanishes.

The symmetron model

The potential and conformal coupling factor for the symmetron model are given by

$$V\left(\phi\right) = -\frac{1}{2}\mu^2\phi^2 + \frac{\lambda}{4}\phi^4\,,\; A\left(\phi\right) = e^{\phi^2/2M_S^2} = 1 + \frac{\phi^2}{2M_S^2} + \mathcal{O}\left(\frac{\phi^4}{M_S^4}\right). \tag{3.27}$$

A is chosen with this form to have the same $\mathbb{Z}_2$ symmetry ($\phi \to -\phi$) as V. The effective potential (where the conformal coupling factor is taken to first order) is

$$V_{eff} = \frac{1}{2}\left(\frac{\rho}{M_S^2} - \mu^2\right)\phi^2 + \frac{\lambda}{4}\phi^4 \tag{3.28}$$

where the irrelevant constant term has been removed. The ϕ^4/M_S^4 term in the conformal coupling factor is absorbed into a redefinition of λ.

The essence of the symmetron mechanism is as follows: there is a *critical density*

$$\rho_* = \mu^2 M_S^2 \tag{3.29}$$

at which the sign of the quadratic term of V_{eff} changes. At densities above ρ_*, V_{eff} reaches its minimum at $\phi = 0$ and there is no effect of the symmetron on matter. Below the critical density, the $\mathbb{Z}_2$ symmetry is spontaneously broken and

[10] A symmetron-like screening mechanism was first described in [76], but not in this form. See [2] for a brief review of the relevant literature.

the effective potential has two degenerate minima at

$$\phi^{\pm}_{\text{min}} = \pm \frac{\mu}{\sqrt{\lambda}} \sqrt{1 - \frac{\rho}{\rho_*}}. \tag{3.30}$$

In this case, the coupling to matter is non-trivial and can give rise to a force potentially stronger than gravity. The effective potentials for different density regimes are visualised in [2] and [3] which are reprinted below.

3.4.2 Non-minimal kinetic Lagrangian screening: the Vainshtein mechanism

The *Vainshtein mechanism* has a relatively long history in theories beyond GR. This screening mechanism was first proposed by Vainshtein in 1972 [78] in the context of massively quantised gravity models, but this model was found to suffer from some untenable pathologies [79]. The formulation of the Dvali-Gabadadze-Porrati brane-world model in 2000 [80] brought with it a re-introduction of the Vainshtein mechanism, and it is now used in models both with and without quantised massive gravity[11] [79].

Unlike the chameleon and symmetron mechanisms (where the effective mass or coupling strength respectively of a scalar are dynamic), the Vainshtein mechanism appears in models with Lagrangians of more than quadratic order in the field derivatives. The relative importance of the linear and non-linear kinetic terms in these Lagrangians depends on the distance from massive objects, and a properly constructed model will consequently have an interaction range between matter and the extra field that rapidly decreases at close proximity to these objects. The distance from an object at which the non-linear kinetic term becomes of equal importance to the linear kinetic term is the *Vainshtein radius*.

The cubic galileon model

The simplest scalar-tensor gravity model that displays the Vainshtein mechanism is the cubic galileon, which has the action [81]

$$S = \int \sqrt{-g} \left(\frac{c^4}{16\pi G} R - \frac{1}{2} g^{\mu\nu} \partial_\mu \phi \partial_\nu \phi - \frac{1}{2\Lambda^3} \Box_g \phi \left[g^{\mu\nu} \partial_\mu \phi \partial_\nu \phi \right] \right) d^4\boldsymbol{x} + S_m. \tag{3.31}$$

Note that this is not in the form of Eq. (3.6), but is instead a more general form comprising a subclass of Horndeski theory [59]. The constant parameter Λ determines the relative strengths of the linear and non-linear kinetic term. Around a spherical mass of density ρ and radius R, it can be shown that the non-linear kinetic term is dominant within the Vainshtein radius given by [82]

$$R_v = \left(\frac{8\rho R^3}{3M\Lambda^3} \right)^{1/3}. \tag{3.32}$$

[11] The recent almost simultaneous detection of gravitational waves and a range of electromagnetic signals from a neutron star merger [6] strongly constrains theories of massive gravity. For a review of the applicability of the Vainshtein mechanism in theories consistent with this measurement, see [53].

Far outside this radius, the ratio of the forces felt by matter due to the galileon and to gravity is given by

$$\left.\frac{F_\phi}{F_g}\right|_{r\gg R_v} = \frac{2M_{Pl}^2}{M^2} \tag{3.33}$$

where M_{Pl} is the reduced Planck mass. This type of force is strongly constrained by solar system experiments, and this model (without a screening mechanism) would require such a small coupling that the deviation from GR is irrelevant at all scales. However, the ratio of forces due to the galileon and to gravity within the Vainshtein radius are

$$\left.\frac{F_\phi}{F_g}\right|_{r\ll R_v} = \frac{4M_{Pl}^2}{M^2}\left(\frac{r}{R_v}\right)^{3/2} \tag{3.34}$$

due to the non-linear kinetic terms in Eq. (3.31). The galileon force is thus strongly supressed near the Earth and experimental predictions can be brought into agreement with observations.

3.5 Experimental constraints

Many models beyond GR and the SM have been strongly constrained by observations and experiments, and conformally coupled screened scalar fields are no exception. The screening mechanisms presented in this chapter are somewhat special in that they can be constrained simultaneously but complementarily from many directions in the parameter space. The screening of these models must be sufficiently strong that these models do not deviate from GR too much within our solar system, but the energy scale parameters must be sufficiently large to have a non-trivial effect on cosmological scales.

For example, experimental constraints on the chameleon and symmetron mechanisms can be found in [18]. When the energy scale of the simplest $n = 1$ chameleon model is set to the dark energy scale ($\Lambda = \Lambda_{DE} = 2.4$ meV), complementary Earth-bound experiments and astrophysical observations constrain the inverse coupling strength M from both directions to be [18, 83]

$$10^{-3}M_{Pl} < M < 10^{-1}M_{Pl}. \tag{3.35}$$

A single run of the Bose-Einstein condensate interferometer scheme proposed in [3] would constrain this coupling strength (with a null result) to be

$$M > M_{Pl}, \tag{3.36}$$

and so would either discover a chameleon field or completely rule out the simplest chameleon model.

Chapter 4

Quantum metrology with Gaussian states

This chapter serves as an introduction to enhancing measurement precision with the unique features of quantum mechanics, i.e. *quantum metrology*. It is clear from current technological development that the world is heading towards a second quantum revolution. From information theoretically secure cryptography and massively parallel resource optimisation to more mundane applications such as greatly increased global positioning accuracy, the utilisation of quantum effects and features is already driving technological advancement.

Among the advantages brought by quantum mechanics is a potential increase in measurement sensitivity for some applications. The most obviously commercially applied example is the enhanced sensitivity of quantum clocks, driving applications from the aforementioned global positioning systems to high precision gravimetry for mineral exploration, archaeological surveys, supporting large engineering projects etc. A prominent application of quantum metrology in fundamental physics is the implementation of squeezed states of light in the LIGO and VIRGO observatories [13, 14] and their astounding measurements of gravitational waves. Considering these clearly demonstrated benefits of quantum metrology, it seems only logical to apply the same techniques to searches for physics beyond general relativity and the standard model.

This chapter will introduce some basic[1] methods of quantum metrology with Gaussian states, which are relevant to deriving the results of [3].

The basics of metrological problems

A typical single parameter metrological problem can be described in the following way: suppose that some parameter λ must be determined. To determine it, a system is used which is initially in some state represented by an object ρ_0. This system may be classical or quantum, in which case the object ρ_0 may represent a set of well defined properties or probability distributions (such as a density matrix) respectively. The system is transformed by some process represented by a *channel* $\mathcal{E}(\lambda)$, where the action of the channel is dependent on the parameter λ; this process transforms the state of the system from ρ_0 to $\rho(\lambda)$. Finally a measurement $\hat{M}$ is taken of the system state $\rho(\lambda)$ which returns some outcome $x \in X$, where X is the set of possible measurement outcomes. Given the conditional probability distribution $p(x|\lambda)$ (which may either be previously known or measured with known values of

[1]While these methods are general, they are not all old well-established results. This is due to quantum metrology being a relatively young field, established only in the last few decades thanks to recent technological advances.

λ), a probability distribution for the possible values of λ can be constructed, and thus λ can be estimated.

Estimation problems may be divided into two broad categories of a priori knowledge of the parameter λ. If there is no significant knowledge of λ, then *global estimation theory* must be applied. Examples of such problems include generic quantum state tomography and volumetric rainfall measurement. If the value of λ is known to be localised around some approximate value, then *local estimation theory* can provide more accurate and sensitive methods for determining λ. Weight measurement with conventional balance scales and chemical indicator titration are examples of applications of local estimation theory. Since the parameters estimated in [3] are perturbative around some known value, only local estimation theory will be considered in this thesis.

The conditional probability distribution $p\left(x|\lambda\right)$ is (generally) dependent on the choice of measurement $\hat{M}$. When considering a problem suitable for local estimation theory, a good choice of $\hat{M}$ can lead to a precise estimate of λ. The initial state ρ_0 also influences the sensitivity of the estimate of λ in a slightly less obvious manner; the amount of information about λ contained in the final state $\rho\left(\lambda\right)$ (and thus the total amount of extractable information) can differ for different initial states. As an example, the success of a measurement of the birefringent properties of some transparent material depends on the choice of the polarisation of light used for the measurement. Determination of the optimal initial state ρ_0 and the optimal measurement $\hat{M}$ are the fundamental goals of local estimation theory.

4.1 Fisher information and the Cramer-Rao bound

Given N outcomes $x_1, \ldots, x_N$ of a measurement $\hat{M}$, an *estimator* $\bar{\lambda}$ for the parameter λ can be defined as a function mapping the measurement outcomes to the space of possible values of λ. This function must satisfy the property[2]

$$\lim_{N\to\infty} \bar{\lambda}\left(x_1, \cdots, x_N\right) = \lambda. \tag{4.1}$$

The *mean squared error* of an estimator is defined in the usual way as

$$\begin{aligned}\Delta\bar{\lambda}^2 &= \frac{1}{N}\left\langle \left(\bar{\lambda}-\lambda\right)^2\right\rangle \\ &= \frac{1}{N}\int_X \left[\bar{\lambda}\left(x_1, \cdots, x_N\right) - \lambda\right]^2 p\left(x_1|\lambda\right)\cdots p\left(x_N|\lambda\right) dx_1\cdots dx_N.\end{aligned} \tag{4.2}$$

A particularly important type of estimator is the *locally unbiased estimator*. This is defined as an estimator $\bar{\lambda}$ with an expectation value given by

$$\left\langle\bar{\lambda}\right\rangle = \int_X \bar{\lambda}\left(x_1, \cdots, x_N\right) p\left(x_1|\lambda\right)\cdots p\left(x_N|\lambda\right) dx_1\cdots dx_N = \lambda, \tag{4.3}$$

i.e. the values of x corresponding to over- and under-estimations balance each other.

4.1.1 Classical Fisher information

It can be shown that the mean squared error of a locally unbiased estimator is bounded from below. This bound is very useful in determining how optimal a

[2]When estimating a parameter with quantum states, it should be kept in mind that this procedure requires N initial copies of the state ρ_0 as each measurement of $\rho\left(\lambda\right)$ collapses the state.

particular input state and a particular measurement scheme are. The derivation of this bound will be briefly outlined in this section.

The Cramér-Rao bound

Given a normalised probability distribution $p(x|\lambda)$ (where $x \in X$) and a locally unbiased estimator $\bar{\lambda}$ for N estimates of λ, the defining property of $\bar{\lambda}$ (Eq. (4.3)) can be differentiated with respect to λ to read[3]

$$\int_X [\bar{\lambda} - \lambda]\, \partial_\lambda \left[\prod_{i=1}^{N} p(x_i|\lambda)\right] dx_1 \cdots dx_N = 1. \tag{4.4}$$

It is useful to define X' as the set of measurement outcomes $x \in X$ such that $p(x|\lambda) > 0$. For all outcomes x_0 outside this set ($x_0 \in X \backslash X'$), $p(x_0|\lambda) = 0$ as $p(x|\lambda) \geq 0 \forall x \in X$ so p attains a local minimum at $p(x_0|\lambda)$. Hence, X may be substituted for X' in Eq. (4.4). Since $p(x|\lambda) \neq 0 \forall x \in X'$, this can be rearranged to be

$$\int_{X'} \sqrt{[\bar{\lambda} - \lambda]^2 \prod_{i=1}^{N} p(x_i|\lambda)} \sqrt{\sum_{n=1}^{N} \left(\left[\frac{\partial_\lambda p(x_n|\lambda)}{p(x_n|\lambda)}\right]^2 \prod_{i=1}^{N} p(x_i|\lambda) \right)}\, dx_1 \cdots dx_N = 1. \tag{4.5}$$

Applying the Cauchy-Schwarz inequality and evaluating one of the integrals, this becomes

$$\sqrt{\int_{X'} [\bar{\lambda} - \lambda]^2 \left[\prod_{i=1}^{N} p(x_i|\lambda)\right] dx_1 \cdots dx_N} \sqrt{N \int_{X'} \frac{[\partial_\lambda p(x|\lambda)]^2}{p(x|\lambda)} dx} \geq 1 \tag{4.6}$$

which can be rearranged as (cf. Eq. (4.2))

$$\Delta \bar{\lambda}^2 \geq \frac{1}{N F(\lambda, \hat{M})}. \tag{4.7}$$

This is the *Cramér-Rao bound* (also derived in [84–86]), where

$$F(\lambda, \hat{M}) = \int_{X'} \frac{[\partial_\lambda p(x|\lambda)]^2}{p(x|\lambda)} dx \tag{4.8}$$

is the *Fisher information*.

The Fisher information

The Fisher information has a very straightforward interpretation: it measures how much information about λ can be extracted with the measurement $\hat{M}$. For example, if the measurement probability is uniform (no information about λ can be inferred) then its derivative is zero and the Fisher information vanishes. The Fisher information is clearly strongly dependent on the choice of measurement, and different choices may lead to different bounds on $\Delta\bar{\lambda}^2$ without changing the choice of $\bar{\lambda}$. It should be noted that the Fisher information depends also on the initial state

[3]Care must be taken here that the application of the Leibniz integration rule is valid for the form of the set X. This is satisfied in most normal cases (e.g. X is discrete and finite, X is a subset of $\mathbb{R}$, ...).

of the probe system ρ_0, as the probability distribution $p(x|\lambda)$ is dependent on the choice of both ρ_0 and $\hat{M}$.

It may be the case that λ is difficult and/or inconvenient to measure directly, but another parameter $\sigma(\lambda)$ can be more easily estimated. In this case, a basic application of the chain rule to Eq. (4.8) shows that

$$F\left(\lambda, \hat{M}\right) = \left(\frac{d\sigma}{d\lambda}\right)^2 F\left(\sigma, \hat{M}\right). \tag{4.9}$$

4.1.2 Quantum Fisher information

The Fisher information measures the amount of information that can be extracted from a final state $\rho(\lambda)$ with a particular measurement $\hat{M}$. It is however also interesting to ask how much information can be extracted from $\rho(\lambda)$ in general. To answer this question, the *quantum Fisher information* (QFI) can be defined as

$$H(\lambda) = \sup_{\hat{M}} F\left(\lambda, \hat{M}\right) \tag{4.10}$$

where $\sup_{\hat{M}}$ is the supremum over all possible measurements $\hat{M}$. This definition implies $H(\lambda) \geq F\left(\lambda, \hat{M}\right) \forall \hat{M}$ and thus immediately leads to the *quantum Cramér-Rao bound*

$$\Delta\bar{\lambda}^2 \geq \frac{1}{NH(\lambda)}. \tag{4.11}$$

This bound determines the best theoretically achievable[4] mean square error in estimating the parameter λ of a channel $\mathcal{E}(\lambda)$ with a particular initial state. While Eq. (4.10) is an intuitive and well motivated definition of the QFI, it is not a useful definition in terms of calculation.

Calculating the Fisher information for quantum states

A more useful expression for the QFI can be constructed for quantum states.

A quantum state is described by a density matrix $\hat{\boldsymbol{\rho}}$, with an initial state $\hat{\boldsymbol{\rho}}_0$ and a final state $\hat{\boldsymbol{\rho}}_\lambda$. A measurement of a quantum state is most generally described by a *positive operator valued measure* (POVM) written as $\hat{\boldsymbol{M}}$. When the POVM is evaluated for each possible measurement outcome x, the elements $\hat{\boldsymbol{M}}_x$ are self-adjoint operators. To be a POVM, $\hat{\boldsymbol{M}}$ must additionally satisfy the properties $\hat{\boldsymbol{M}}_x \geq 0 \forall x \in X$ and $\int_X \hat{\boldsymbol{M}}_x dx = \hat{I}$ where $\hat{I}$ is the identity operator.

The probability of measuring x given the parameter λ is then written as

$$p(x|\lambda) = \mathrm{tr}\left[\hat{\boldsymbol{M}}_x \hat{\boldsymbol{\rho}}_\lambda\right] \tag{4.12}$$

where $\mathrm{tr}[\cdot]$ is the trace.

The *symmetric logarithmic derivative* $\hat{\boldsymbol{L}}$ will be a key component in the expression for the QFI. $\hat{\boldsymbol{L}}$ is defined to be the solution of the operator equation

$$\frac{\hat{\boldsymbol{L}}(\lambda)\hat{\boldsymbol{\rho}}_\lambda + \hat{\boldsymbol{\rho}}_\lambda \hat{\boldsymbol{L}}(\lambda)}{2} = \partial_\lambda \hat{\boldsymbol{\rho}}_\lambda. \tag{4.13}$$

[4] It is also not immediately obvious that a particular choice of measurement saturates this maximum. While such a measurement always exists for single parameter estimation [86], it does not in general for estimating multiple parameters.

If a spectral decomposition of the quantum state into eigenvectors $|\psi_n\rangle$ is known, then the density matrix can be written in this basis as $\hat{\boldsymbol{\rho}}_\lambda = \sum_n p_n(\lambda) |\psi_n\rangle \langle\psi_n|$ and straightforward algebra shows that

$$\hat{\boldsymbol{L}}(\lambda) = 2\sum_{n,m} \frac{\langle\psi_n|\partial_\lambda \hat{\boldsymbol{\rho}}_\lambda|\psi_m\rangle}{p_n(\lambda) + p_m(\lambda)} |\psi_n\rangle \langle\psi_m| \tag{4.14}$$

is a solution of Eq. (4.13). From this expression, it is clear that the eigenvectors $|\psi_n\rangle$ are eigenvectors of the symmetric logarithmic derivative. With these definitions, a formula for explicitly calculating the QFI can now be constructed.

Consider a measurement scheme where the POVM $\hat{\boldsymbol{M}}$ is the set of projective measurements $\{\hat{\boldsymbol{P}}_n\}$, where each projection operator is given by $\hat{\boldsymbol{P}}_n = |\psi_n\rangle \langle\psi_n|$ in the same notation as above. The probability distribution for measuring the eigenvalue n is then

$$p(n|\lambda) = \mathrm{tr}\left[\hat{\boldsymbol{P}}_n \hat{\boldsymbol{\rho}}_\lambda\right], \tag{4.15}$$

which has the derivative[5]

$$\partial_\lambda p(n|\lambda) = \mathrm{tr}\left[\hat{\boldsymbol{P}}_n \partial_\lambda \hat{\boldsymbol{\rho}}_\lambda\right]. \tag{4.16}$$

The symmetric logarithmic derivative can be given the spectral decomposition

$$\hat{\boldsymbol{L}}(\lambda) = \sum_n l_n(\lambda) \hat{\boldsymbol{P}}_n. \tag{4.17}$$

Combining Eqs. (4.13)-(4.17) with Eq. (4.8), some straightforward algebra shows that the Fisher information for projective measurements is given by

$$F\left(\lambda, \hat{P}\right) = \mathrm{tr}\left[\hat{\boldsymbol{\rho}}_\lambda \hat{\boldsymbol{L}}^2(\lambda)\right]. \tag{4.18}$$

Calculating the quantum Fisher information

It can be shown that the Fisher information is bounded by $F\left(\lambda, \hat{M}\right) \leq \mathrm{tr}\left[\hat{\boldsymbol{\rho}}_\lambda \hat{\boldsymbol{L}}^2(\lambda)\right]$ [84, 86]. It is clear that the projective measurement scheme in Eq. (4.18) saturates this bound. Hence, it can be concluded that the quantum Fisher information for single parameter estimation is reached with projective measurements onto the eigenstates of the symmetric logarithmic derivative, and is given by

$$H(\lambda) = \mathrm{tr}\left[\hat{\boldsymbol{\rho}}_\lambda \hat{\boldsymbol{L}}^2(\lambda)\right]. \tag{4.19}$$

As for the Fisher information, is it obvious by inspection that

$$H(\lambda) = \left(\frac{d\sigma}{d\lambda}\right)^2 H(\sigma) \tag{4.20}$$

for some parameter $\sigma(\lambda)$. This expression is particularly useful for determining the maximum amount of information that can be retrieved from different intrinsic properties of a particular type of state, and using this information to optimise an input state.

[5]The spectral decomposition and thus the projectors $\hat{\boldsymbol{P}}_n$ should be dependent on λ. However, the approximate value of λ is known in local estimation theory and the projectors are constructed around this fixed approximate value in practice. Hence, the projectors are considered not to be dependent on the exact value of λ.

4.2 Optimal error scaling

The error $\Delta\bar{\lambda}$ in the estimation of a parameter λ can depend on the nature of the available resources utilised to make the estimation. For different types of initial states, limits on the possible attainable precision can be calculated from fundamental arguments, as well as determining how these limits scale with the number of available resources[6].

As will be shown, quantum states can in general achieve a better error scaling than classical states; this is the central advantage of quantum metrology. While this does not automatically mean that "quantum states are always better," there are many metrological applications where quantum states can outperform their classical counterparts.

The standard quantum limit

Consider a probe state used for estimating the parameter λ which is constructed of $\mathcal{N}$ uncorrelated copies of some initial state ρ_0. In the case where the channel $\mathcal{E}(\lambda)$ does not entangle the copies of ρ_0 (in the quantum sense), then the final state consists of $\mathcal{N}$ independent copies of a state $\rho(\lambda)$. A measurement of this final state can extract as much information as $\mathcal{N}$ individual measurements of the parameter λ. By the central limit theorem, the Fisher information will scale as $F\left(\lambda, \hat{M}\right) \sim \mathcal{N}$ and the error in estimating λ will scale as

$$\Delta\bar{\lambda} \sim \frac{1}{\sqrt{\mathcal{N}}}. \tag{4.21}$$

This is the *standard quantum limit* (SQL) or *shot-noise limit*. Note that the above description applies to all classical states, as entanglement and superposition are quantum features. Therefore, the SQL is the absolute scaling limit for classical parameter estimation.

Heisenberg scaling

If the $\mathcal{N}$ copies of a state ρ_0 comprising the initial probe state have some form of quantum entanglement, then a measurement of the final state is not equivalent to $\mathcal{N}$ independent measurements with the probe state ρ_0 and the central limit theorem no longer applies. In this case, it can be shown from fundamental quantum mechanics arguments that the error in estimating a parameter λ will at best scale as [85, 87]

$$\Delta\bar{\lambda} \sim \frac{1}{\mathcal{N}}. \tag{4.22}$$

This scaling is called the *Heisenberg limit* and is the fundamental limit for parameter estimation with quantum states. Some form of entanglement is crucial in achieving this Heisenberg limit, specifically in the operator generating the transformation that the parameter is encoded in [85]. For example, phase estimation at the Heisenberg limit requires probe states with energy entanglement. The question of exactly which quantum states can beat the SQL is subtle; for a discussion of this question see [87].

[6] It is important to note that the number of resources is not just as simple as e.g. counting the number of particles. When the input state consists of many copies of some initial state, then the relevant number of resources is given by the number of copies only when these copies do not become correlated with each other in the "parameter encoding" channel [87].

Although the definition of the Heisenberg limit in Eq. (4.22) is widely applicable, it cannot be used universally. When the encoding channel $\mathcal{E}(\lambda)$ creates entanglement between many copies of an initial probe state, then Eq. (4.22) is no longer sufficient. Instead, the Heisenberg limit must be defined in terms of the resources required to prepare the initial probe state [88].

4.3 Gaussian states

Gaussian states combine many attractive properties and are widely used, especially in the context of metrology [89]. Mathematically, Gaussian states are simple to handle in an elegant formalism that will be presented in Chapter 4.3.2. Experimentally, many Gaussian states are straightforward to prepare and manipulate (especially in optical systems [90]) and are resistant to decoherence [91]. These properties, combined with the ability to exhibit quantum properties such as entanglement, make Gaussian states an ideal tool for quantum metrology.

Defining Gaussian states

A Gaussian state is defined in the following way. Consider a quantum state with the density matrix $\hat{\boldsymbol{\rho}}$, for which the single particle Hilbert space can be decomposed in some discrete basis $\{|\psi_n\rangle\}$, e.g. momentum eigenstates. The annihilation operators $\hat{a}_n$ associated with these basis states can be combined to form a vector $\hat{\boldsymbol{A}} = (\hat{a}_1, \hat{a}_2, \cdots)$ which can be combined with the equivalent vector of creation operators to form the vector

$$\hat{\boldsymbol{X}} = \hat{\boldsymbol{A}} \otimes \hat{\boldsymbol{A}}^\dagger. \tag{4.23}$$

The commutation relations of the creation and annihilation operators comprising the components of the vector $\hat{\boldsymbol{X}}$ can be written in the form

$$\left[\hat{X}_i, \hat{X}_j^\dagger\right] = K_{ij}\hat{1} \tag{4.24}$$

where $\hat{1}$ is the identity operator, K_{ij} are elements of a matrix $\boldsymbol{K}$ which has the block form

$$\boldsymbol{K} = \begin{pmatrix} \mathbb{I}_N & 0 \\ 0 & -\mathbb{I}_N \end{pmatrix} \tag{4.25}$$

and N is the dimensionality of the basis $\{|\psi_n\rangle\}$[7].

The *Wigner characteristic function* of the state $\hat{\rho}$ is defined as

$$\chi(\boldsymbol{\xi}) = \mathrm{tr}\left[\hat{\boldsymbol{\rho}} e^{\hat{\boldsymbol{X}}^\dagger \boldsymbol{K} \boldsymbol{\xi}}\right]. \tag{4.26}$$

As suggested by the name, a *Gaussian state* is defined as a state whose characteristic function is Gaussian:

$$\chi(\boldsymbol{\xi}) = e^{-\frac{1}{4}\boldsymbol{\xi}^\dagger \boldsymbol{\Gamma} \boldsymbol{\xi} - i\boldsymbol{d}^\dagger \boldsymbol{K} \boldsymbol{\xi}}. \tag{4.27}$$

The components of the *displacement vector* $\boldsymbol{d}$ and *covariance matrix* $\boldsymbol{\Gamma}$ are defined as

$$\begin{aligned} d_i &= \langle \hat{X}_i \rangle = \mathrm{tr}\left[\hat{\boldsymbol{\rho}} \hat{X}_i\right], & (4.28) \\ \Gamma_{ij} &= \mathrm{tr}\left[\hat{\boldsymbol{\rho}}\left\{\hat{X}_i, \hat{X}_j^\dagger\right\}\right] - 2d_i d_j^\dagger, & (4.29) \end{aligned}$$

[7] N need not be finite, but is specified here for notational convenience.

where $\{\cdot,\cdot\}$ is the anti-commutator. Just like a Gaussian function, a Gaussian state is completely characterised by its first and second statistical moments $\boldsymbol{d}$ and $\boldsymbol{\Gamma}$. Comparison of Eq. (4.23) with Eqs. (4.28)-(4.29) suggests that $\boldsymbol{d}$ and $\boldsymbol{\Gamma}$ have the respective structures

$$\boldsymbol{d} = \left(\tilde{\boldsymbol{d}}, \tilde{\boldsymbol{d}}^*\right)^T, \boldsymbol{\Gamma} = \begin{pmatrix} \boldsymbol{A} & \boldsymbol{B} \\ \boldsymbol{B}^* & \boldsymbol{A}^* \end{pmatrix}. \tag{4.30}$$

The real and complex representations

Eqs. (4.28)-(4.29) define Gaussian states in a complex form. It is common in the literature to use the real form instead, in terms of position and momentum operators given by $\hat{x}_i = \frac{\hbar}{\sqrt{2}}\left(\hat{a}_i^\dagger + \hat{a}_i\right)$ and $\hat{p}_i = \frac{i\hbar}{\sqrt{2}}\left(\hat{a}_i^\dagger - \hat{a}_i\right)$ respectively [89, 92]. The vector $\hat{\boldsymbol{X}}$ is replaced in Eqs. (4.28)-(4.29) with the vector $\hat{\boldsymbol{Q}} = \left(\hat{x}_1, \cdots, \hat{x}_N, \hat{p}_1, \cdots, \hat{p}_N\right)^T$, and the matrix $\boldsymbol{K}$ is replaced by the matrix

$$\boldsymbol{\Omega} = \begin{pmatrix} 0 & \mathbb{I}_N \\ -\mathbb{I}_N & 0 \end{pmatrix}. \tag{4.31}$$

The complex form is generally easier to work with (e.g. $\boldsymbol{K}$ is diagonal, unitary and Hermitian whereas $\boldsymbol{\Omega}$ is not), and many expressions take a more elegant form. For these reasons, only the complex form is used in this thesis.

4.3.1 Common Gaussian states

Many of the most commonly experimentally used quantum states are Gaussian. To illustrate this point, a few examples of single mode non-thermal Gaussian states will now be given. These examples can be extended to multi-mode and thermal states in a straightforward manner.

The *vacuum state* is trivially a Gaussian state with a displacement vector and covariance matrix given by

$$\boldsymbol{d}^{vac} = \boldsymbol{0}, \boldsymbol{\Gamma}^{vac} = \mathbb{I}_2. \tag{4.32}$$

A *coherent state* is produced by applying the *Weyl displacement operator* $\hat{D}_k(\alpha) = \exp\left[\alpha\hat{a}_k^\dagger - \alpha^*\hat{a}_k\right]$ to a vacuum state, where $\alpha \in \mathbb{C}$ and k indexes the mode. In the Fock basis, it is given by

$$|\alpha\rangle_k = e^{-|\alpha|^2/2}\sum_{n=0}^{\infty}\frac{\alpha^n}{\sqrt{n!}}|n\rangle_k. \tag{4.33}$$

Applying the number operator $\hat{N}_k = \hat{a}_k^\dagger\hat{a}_k$, it is straightforward to show that the average number of particles in a coherent state is given by $N = |\alpha|^2$. The displacement vector and covariance matrix of this state are given by

$$\boldsymbol{d}^{coh} = \left(\alpha, \alpha^*\right)^T, \boldsymbol{\Gamma}^{coh} = \mathbb{I}_2. \tag{4.34}$$

A *real squeezed vacuum state* is produced by applying the *squeezing operator* $\hat{S}_k(r) = \exp\left[-\frac{r}{2}\left(\hat{a}_k^{\dagger 2} - \hat{a}_k^2\right)\right]$ (where $r \in \mathbb{R}$) to the vacuum state. In the Fock basis, it can be written as

$$|r\rangle_k = \frac{1}{\sqrt{\cosh(r)}}\sum_{n=0}^{\infty}\tanh^n(r)\frac{\sqrt{(2n)!}}{2^n n!}|2n\rangle_k. \tag{4.35}$$

As is clear from Eq. (4.35), a squeezing operation produces excitations in pairs. While the **product** of variances of non-commuting observables are fixed by the Heisenberg uncertainty principle, squeezed states have the property that the **ratio** of these variances is not 1 and grows with r. For a real squeezed vacuum state as given in Eq. (4.35), the variances in position x and momentum p are given by

$$\sigma_x^2 = \frac{\hbar}{2} e^{-r}, \sigma_p^2 = \frac{\hbar}{2} e^{r}. \tag{4.36}$$

For example when r is large and positive, the position of this squeezed state is much more tightly localised than an equivalent Fock state at the expense of broad momentum localisation. The displacement vector and covariance matrix of a real squeezed vacuum state are

$$\boldsymbol{d}^{sqz} = (0,0)^T, \boldsymbol{\Gamma}^{sqz} = \begin{pmatrix} \cosh(r) & -\sinh(r) \\ -\sinh(r) & \cosh(r) \end{pmatrix}. \tag{4.37}$$

4.3.2 The covariance matrix formalism

As mentioned above, a Gaussian state is completely characterised by its displacement vector $\boldsymbol{d}$ and its covariance matrix $\boldsymbol{\Gamma}$. The evolution of a Gaussian state can be described simply by deriving how $\boldsymbol{d}$ and $\boldsymbol{\Gamma}$ evolve.

A Gaussian transformation is one that maps Gaussian states onto Gaussian states. A Gaussian unitary is a Gaussian transformation represented by a unitary operator $\hat{U}$. Explicitly, a Gaussian state with the density matrix $\hat{\boldsymbol{\rho}}$ is transformed into the Gaussian state $\hat{\boldsymbol{\rho}}'$ with the transformation

$$\hat{\boldsymbol{\rho}}' = \hat{U}\hat{\boldsymbol{\rho}}\hat{U}^\dagger. \tag{4.38}$$

Under such a transformation, the characteristic function of the state $\hat{\boldsymbol{\rho}}'$ is Gaussian only if $\hat{U}$ has the form [93]

$$\hat{U} = e^{\frac{i}{2}\hat{\boldsymbol{X}}^\dagger \boldsymbol{W} \hat{\boldsymbol{X}} + \hat{\boldsymbol{X}}^\dagger \boldsymbol{K} \gamma}, \tag{4.39}$$

where $\hat{\boldsymbol{X}}$ and $\boldsymbol{K}$ are defined as they are in Eq. (4.26), γ is some vector of the form $\gamma = (\tilde{\gamma}, \tilde{\gamma}^*)^T$ and $\boldsymbol{W}$ is some Hermitian matrix with the same structure as the covariance matrix as outlined in Eq. (4.30).

For example, this unitary is exactly the Weyl displacement operator $\hat{D}(\gamma)$ in the case where $\boldsymbol{W} = 0$. If $\gamma = 0$ and $\boldsymbol{W} = ir\boldsymbol{\Omega}$ (see Eq. (4.31)) for a single mode state where $r \in \mathbb{R}$, then this unitary becomes the real single mode squeezing operator $\hat{S}(r)$.

Gaussian state transformations

Application of a unitary of the form of Eq. (4.39) to a Gaussian state will transform its displacement vector and covariance matrix. With the application of $\hat{U}$ to $\hat{\boldsymbol{X}}$ and the Baker-Campbell-Hausdorff formula, it can be shown that [94]

$$\hat{\boldsymbol{X}}' = \hat{U}\hat{\boldsymbol{X}}\hat{U}^\dagger = \boldsymbol{S}\hat{\boldsymbol{X}} + \boldsymbol{b} \tag{4.40}$$

where

$$\boldsymbol{S} = e^{i\boldsymbol{K}\boldsymbol{W}}, \boldsymbol{b} = \left(\int_0^1 e^{i\boldsymbol{K}\boldsymbol{W}t} dt\right)\gamma. \tag{4.41}$$

Combining the transformation of $\hat{X}$ in Eq. (4.40) with the definitions of the displacement vector and covariance matrix in Eqs. (4.28)-(4.29), it can be concluded that $\boldsymbol{d}$ and $\boldsymbol{\Gamma}$ transform as

$$\boldsymbol{d}' = \boldsymbol{S}\boldsymbol{d} + \boldsymbol{b}, \tag{4.42}$$
$$\boldsymbol{\Gamma}' = \boldsymbol{S}\boldsymbol{\Gamma}\boldsymbol{S}^{\dagger}. \tag{4.43}$$

These transformation relations are the central tool of the covariance matrix formalism and immensely simplify practical calculations. Since neither $\boldsymbol{S}$ nor $\boldsymbol{b}$ are operators or operator valued, they need only be evaluated once for each corresponding unitary operator to describe the evolution of **any** Gaussian state. This is to be contrasted with the infinite series of operators that must be evaluated for **each** Gaussian state in Eq. (4.38).

The symplectic group

It is straightforward to show that the $2N \times 2N$ matrix $\boldsymbol{S}$ has the same structure as the covariance matrix (see Eq. (4.30)) and satisfies the relation

$$\boldsymbol{S}\boldsymbol{K}\boldsymbol{S}^{\dagger} = \boldsymbol{K}. \tag{4.44}$$

These properties define the complex representation[8] of the real symplectic group of degree $2N$, $\mathrm{Sp}\left(2N, \mathbb{R}\right)$, where $\boldsymbol{K}$ assumes the role of the symplectic form[9]. While it is not the only possible type of matrix satisfying Eq. (4.44), $\boldsymbol{S}$ is the most important for the purposes of this thesis. Hence, $\boldsymbol{S}$ will be referred to as the *symplectic matrix* for the remainder of this thesis for notational convenience.

Examples of Gaussian unitaries

The (arguably) most simple unitary operation that can be applied to a quantum state is free phase evolution. This operation is represented by the operator $\hat{U}\left(\theta\right) = \exp\left(-\frac{i}{2}\hat{\boldsymbol{X}}^{\dagger}\boldsymbol{\Theta}\hat{\boldsymbol{X}}\right)$ where $\boldsymbol{\Theta} = \mathrm{diag}\left(\theta_1, \cdots, \theta_N, \theta_1, \cdots, \theta_N\right)$ and θ_k is the phase gained by the mode indexed by k. The covariance matrix formalism transformation under free phase evolution is parameterised by

$$\boldsymbol{S}^{ph} = \mathrm{diag}\left(e^{-i\theta_1}, \cdots, e^{-i\theta_N}, e^{i\theta_1}, \cdots, e^{i\theta_N}\right), \; \boldsymbol{b}^{ph} = 0. \tag{4.45}$$

Comparison of the Weyl displacement operator $\hat{D}\left(\gamma\right) = \exp\left[\hat{\boldsymbol{X}}^{\dagger}\boldsymbol{K}\gamma\right]$ with the generic unitary form in Eq. (4.39) suggests that the corresponding Gaussian state transformation has a particularly simple parameterisation as

$$\boldsymbol{S}^{dis} = \mathbb{I}_{2N}, \; \boldsymbol{b}^{dis} = \gamma. \tag{4.46}$$

Since setting $\gamma = 0$ and $\boldsymbol{W} = ir\boldsymbol{\Omega} : r \in \mathbb{R}$ for a single mode state in Eq. (4.39) produces a single mode real squeezing operator $\hat{S}\left(r\right)$, Gaussian state transformations under squeezing operations are parameterised as

$$\boldsymbol{S}^{sqz} = \begin{pmatrix} \cosh\left(r\right) & -\sinh\left(r\right) \\ -\sinh\left(r\right) & \cosh\left(r\right) \end{pmatrix}, \; \boldsymbol{b}^{sqz} = 0. \tag{4.47}$$

[8] The formalism presented here can of course be defined in the real representation, e.g. in [92].

[9] This is not an arbitrary choice; $\boldsymbol{K}$ is the complex representation equivalent of the standard non-singular skew-symmetric symplectic form in the real representation as defined in Eq. (4.31).

4.3.3 Quantum Fisher information for Gaussian states

Calculating the QFI for a Gaussian state has been a difficult task until recently. The density matrix of a Gaussian state is generally given by a relatively complicated infinite series, so the expression for the QFI in Eq. (4.19) is difficult to calculate. However, recent developments in expressing the QFI in the covariance matrix formalism make this calculation much more straightforward.

A short history

A formula for the QFI for multi-mode pure Gaussian states was derived from the Wigner function of these states by Pinel et. al. in 2012 [95]. In the same year, Marian and Marian found an expression for the fidelity between one- and two-mode Gaussian states [96], which allowed Pinel et. al. to construct a general formula for all single-mode Gaussian states [97].

By making a connection between the Stein equation and some components of the QFI, Monras derived a general expression for the QFI of multi-mode Gaussian states in 2013 [98]. This solution is given in terms of an infinite series (which is a solution of the Stein equation), and the infinite series is shown to converge for a particular generalisation of pure states.

To complete the generalisation of the results of [95], it was shown by Šafránek et. al. in 2015 [99] that the infinite series given in [98] converges as a geometric series. Moreover, an expression was given for the bound on the error produced by summing only a finite number of terms in the series.

A more detailed review of the QFI calculation techniques for Gaussian states can be found in [99].

The quantum Fisher information for pure Gaussian states

The results in this thesis (specifically in [3]) are obtained when considering metrology with pure Gaussian states. Given an initially pure Gaussian state with the displacement vector and covariance matrix $\boldsymbol{d}_0$ and $\boldsymbol{\Gamma}_0$ respectively, the action of a purity preserving channel $\mathcal{E}(\lambda)$ transforms this state to a final state characterised by $\boldsymbol{d}_0 \to \boldsymbol{d}_\lambda$ and $\boldsymbol{\Gamma}_0 \to \boldsymbol{\Gamma}_\lambda$. When measuring the final state, the QFI for estimating the parameter λ is given by [95, 98][10]

$$H(\lambda) = \frac{1}{4}\mathrm{tr}\left[\left(\boldsymbol{\Gamma}_\lambda^{-1}\partial_\lambda\boldsymbol{\Gamma}_\lambda\right)^2\right] + 2\left(\partial_\lambda \boldsymbol{d}_\lambda^\dagger\right)\boldsymbol{\Gamma}_\lambda^{-1}\partial_\lambda \boldsymbol{d}_\lambda. \tag{4.48}$$

Once the QFI can be calculated, then it can be optimised against different input states. Once the optimal input state has been found, then a measurement scheme can be found that saturates or comes close to saturating the QFI. This process is generally non-trivial but there exists a substantial body of literature for optimising measurements with Gaussian states (see e.g. [86, 89, 93, 100] and references therein).

Example: phase estimation with a coherent state

Phase estimation with an interferometer is one of the most common methods of measuring the optical properties of a material. The *Mach-Zehnder interferometer* (MZI, pictured schematically in Fig. (4.1)) is particularly experimentally straightforward to construct. When considering state evolution, this interferometer has two main

[10]The apparent factor of 2 discrepancy between Eq. (4.48) and [95] is due to a difference in the definition of $\hat{X}$ in terms of creation and annihilation operators.

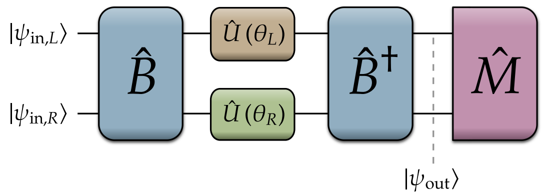

FIGURE 4.1: Schematic diagram of a MZI, comprising beam splitting operations $\hat{B}$, phase shifts $\hat{U}(\theta)$ and a measurement $\hat{M}$.

components; a beam splitter operation $\hat{B}$ and a free phase evolution $\hat{U}$ between the beam splitters. These operations are followed by a measurement $\hat{M}$.

The beam splitter is described by the operator[11]

$$\hat{B} = \exp\left[\frac{\pi}{4}\left(\hat{a}_L^\dagger \hat{a}_R - \hat{a}_R^\dagger \hat{a}_L\right)\right], \tag{4.49}$$

where L and R index the two arms of the interferometer. The symplectic matrix corresponding to the beam splitter operation is given by

$$\boldsymbol{S}_{\hat{B}} = \frac{1}{\sqrt{2}}\begin{pmatrix} 1 & -1 & 0 & 0 \\ 1 & 1 & 0 & 0 \\ 0 & 0 & 1 & -1 \\ 0 & 0 & 1 & 1 \end{pmatrix}. \tag{4.50}$$

The phase evolution between the beam splitters is given by the operator $\hat{U} = \exp\left(-i\hat{H}_{free}t\right)$, such that the action of $\hat{U}$ on $\hat{\boldsymbol{X}}$ (as defined in Eq. (4.23)) is given by

$$\hat{U}^\dagger \hat{\boldsymbol{X}} \hat{U} = \left(e^{i\theta_R}\hat{a}_R, e^{i\theta_L}\hat{a}_L, e^{-i\theta_R}\hat{a}_R^\dagger, e^{-i\theta_L}\hat{a}_L^\dagger\right)^T, \tag{4.51}$$

where θ_R and θ_L are the phases gained by the R and L arms of the interferometer respectively. The symplectic matrix representing the action of $\hat{U}$ is

$$\boldsymbol{S}_{\hat{U}} = \begin{pmatrix} e^{i\theta_R} & 0 & 0 & 0 \\ 0 & e^{i\theta_L} & 0 & 0 \\ 0 & 0 & e^{-i\theta_R} & 0 \\ 0 & 0 & 0 & e^{-i\theta_L} \end{pmatrix}. \tag{4.52}$$

When comparing Eqs. (4.50) and (4.52) with Eqs. (4.39) and (4.41), it is clear that the vector $\boldsymbol{b}$ is zero for both the beam splitter and phase evolution. The symplectic matrices hence form a complete description of the action of the MZI.

The parameter to be estimated in this interferometer is given by $\theta_- = \theta_R - \theta_L$. Therefore, it is convenient to express the phases in the basis (θ_+, θ_-) where $\theta_+ = \theta_R + \theta_L$.

Now that the operations of the interferometer have been defined, the input state must be considered. The state of light produced by a laser is generally given by a coherent state [85]. This state is one of the most common input states to a MZI, along with a vacuum state in the other arm. The displacement vector and covariance matrix of a single mode coherent state in one arm and a vacuum state in the other is

[11] This operator describes a balanced beam splitter, where the reflection and transmission probabilities are equal. Asymmetric beam splitters can of course be used here, but a balanced beam splitter is chosen for simplicity.

given by

$$\boldsymbol{d}_{\text{in}} = (\alpha, 0, \alpha^*, 0)^T \,, \, \boldsymbol{\Gamma}_{\text{in}} = \mathbb{I}_4. \tag{4.53}$$

The total effect of the MZI is parameterised by the symplectic matrix[12]

$$\boldsymbol{S}_{MZI} = \boldsymbol{S}^{\dagger}_{\hat{B}} \boldsymbol{S}_{\hat{U}} \boldsymbol{S}_{\hat{B}}, \tag{4.54}$$

under which the displacement vector and covariance matrix transform as

$$\begin{aligned} \boldsymbol{d}_{\text{out}} &= \boldsymbol{S}_{MZI} \boldsymbol{d}_{\text{in}} \\ &= \left(\alpha e^{\frac{i}{2}\theta_+} \cos\left(\frac{\theta_-}{2}\right), -i\alpha e^{\frac{i}{2}\theta_+} \sin\left(\frac{\theta_-}{2}\right), \right. \\ &\qquad \left. \alpha^* e^{-\frac{i}{2}\theta_+} \cos\left(\frac{\theta_-}{2}\right), i\alpha^* e^{-\frac{i}{2}\phi_+} \sin\left(\frac{\theta_-}{2}\right) \right)^T, \end{aligned} \tag{4.55}$$

$$\boldsymbol{\Gamma}_{\text{out}} = \boldsymbol{S}_{MZI} \boldsymbol{\Gamma}_{\text{in}} \boldsymbol{S}^{\dagger}_{MZI} = \mathbb{I}_4. \tag{4.56}$$

Evaluating the QFI for θ_- with Eq. (4.48) results in the simple expression

$$H(\theta_-) = |\alpha|^2 . \tag{4.57}$$

As explained in Chapter 4.3.1, the average number of particles in a coherent state is given by $\mathcal{N}_c = |\alpha|^2$. Hence, the QCRB for phase estimation with a coherent state in a MZI is given by

$$\Delta\theta_-^2 \geq \frac{1}{N\mathcal{N}_c}, \tag{4.58}$$

where $\mathcal{N}_c$ is the number of particles (photons) in the coherent state and N is the number of repeated measurements.

This QCRB scales with the SQL, while other initial states can produce better or worse scaling. For example, a repetition of the above process with two (mutually coherent) single mode squeezed states as inputs to the MZI results in a QCRB with Heisenberg scaling.

[12]The choice of $\hat{B}$ or $\hat{B}^\dagger$ for the second beam splitting operation is entirely arbitrary functionality-wise. However, some measurement schemes have an optimal phase shift difference to maximise the measurement sensitivity and the choice of $\hat{B}$ or $\hat{B}^\dagger$ can shift this optimal value.

Part II

Publications

Analogue simulation of gravitational waves in a 3+1-dimensional Bose-Einstein condensate

Own contribution: Tupac Bravo and Ivette Fuentes conceived of the idea of extending a previous $1+1$-dimensional result to $3+1$ dimensions. The acoustic metric derivation appearing in Appendix B was derived collaboratively by me, Tupac Bravo, Dennis Rätzel, Richard Howl and Joel Lindkvist. The main results were derived by me with input from Tupac Bravo and Dennis Rätzel, and I derived the explicit expressions for particular examples of gravitational wave sources. The publication draft was written by me with input from Tupac Bravo, and all other authors contributed to correcting this draft and responding to review comments.

PHYSICAL REVIEW D **98,** 025011 (2018)

Analogue simulation of gravitational waves in a 3 + 1-dimensional Bose-Einstein condensate

Daniel Hartley,[1,*] Tupac Bravo,[1] Dennis Rätzel,[1] Richard Howl,[1] and Ivette Fuentes[1,2]

[1]*Faculty of Physics, University of Vienna, Boltzmanngasse 5, 1090 Wien, Austria*
[2]*School of Mathematical Sciences, University of Nottingham, University Park, Nottingham NG7 2RD, United Kingdom*

(Received 27 December 2017; published 17 July 2018)

The recent detections of gravitational waves (GWs) by the LIGO and Virgo collaborations have opened the field of GW astronomy, intensifying interest in GWs and other possible detectors sensitive in different frequency ranges. Although strong GW producing events are rare and currently unpredictable, GWs can in principle be simulated in analogue systems at will in the lab. Simulation of GWs in a manifestly quantum system would allow for the study of the interaction of quantum phenomena with GWs. Such predicted interaction is exploited in a recently proposed Bose-Einstein condensate (BEC) based GW detector. In this paper, we show how to manipulate a BEC to mimic the effect of a passing GW. By simultaneously varying the external potential applied to the BEC, and an external magnetic field near a Feshbach resonance, we show that the resulting change in speed of sound can directly reproduce a GW metric. We also show how to simulate a metric used in the recently proposed BEC based GW detector, to provide an environment for testing the proposed metrology scheme of the detector. Explicit expressions for simulations of various GW sources are given. This result is also useful to generally test the interaction of quantum phenomena with GWs in a curved spacetime analogue experiment.

DOI: 10.1103/PhysRevD.98.025011

I. INTRODUCTION

In the 36 years since the seminal proposal of Unruh to measure an acoustic analogue to Hawking radiation from a "sonic horizon" in a fluid [1], interest in analogue simulation of gravitational fields has grown from theoretical proposals to experiments in numerous systems. These include Bose-Einstein condensates (BECs) [2–4], water waves [5,6] and optical fibers [7] among others. Particular interest has been shown in using the phonon field in a BEC, since this is a quantum system and so allows for the study of how nonclassical properties, such as entanglement, are modified or generated by simulated gravitational fields. This has recently culminated in the first observation of the entanglement of acoustic Hawking radiation [8], potentially providing clues to fundamental questions for quantum gravity, such as the information paradox. In addition to Hawking radiation from a waterfall horizon, other proposed simulations using BECs have included conformal Schwarzschild black holes [9,10], rotating black holes [11], Friedmann-Robertson-Walker geometries [12,13], inflation [14,15] and extensions to Einstein's general relativity, such as aether fields [9]. In past work [16], two of us have considered the simulation of gravitational waves (GWs) in $1 + 1$ dimensions. These are perturbations of spacetime generated by a changing quadrupole moment of a mass distribution, and have recently been detected in a milestone moment in science [17–21]. This has led to a new field of GW astronomy, enabling the exploration of the Universe through gravitational as well as electromagnetic radiation. Simulating GWs in fluid systems could be of astronomical interest, for example, in studying GWs in numerically challenging, strong-field regimes. Furthermore, since BECs are quantum systems, this could enable the study of predicted effects such as particle creation in GW backgrounds [22], and quantum decoherence due to GWs [23]. While we are interested in simulating the effect of GWs, simulating the evolution of a GW itself on a curved background has also been proposed in [24], where a metamaterial emulates a curved background spacetime and two-photon states model the evolution of a GW on that background.

Simulating GWs with BECs could also be used in studies of a proposed BEC GW detector [25–27]. This detector consists of a BEC constrained to a rigid trap with a prepared quantum state of phonons, such as a two-mode squeezed state. The transformation induced by the GW produces mode-mixing and phonon creation in a phenomenon resembling the dynamical Casimir effect [28,29], making the final state distinguishable from the probe state, i.e., decreasing the fidelity between the initial and final states.

*Corresponding author: daniel.hartley@univie.ac.at.

The lower the fidelity between the probe and final state, the better the estimation. Nonclassical squeezed states allow for quantum metrology techniques resulting in better estimation than a classical device. At resonance, mode-mixing or phonon creation are maximized, giving rise to optimal parameter estimation. Such a quantum resonance process is absent in laser interferometers since the frequencies of the GWs are far from the optical regime. However, using resonance to detect GWs was the concept behind the first GW detector proposals, Weber bars, which are metal objects measuring meters in length. The GW resonance in the BEC detector is similar since the much smaller size, $\mathcal{O}(\mu m)$, is compensated for by a much smaller speed of sound, $\mathcal{O}(mm/s)$ compared to $\mathcal{O}(km/s)$ [30]. However, the BEC detector can be cooled to considerably lower temperatures, $\mathcal{O}(nK)$, and is a strictly quantum device. This allows for the use of quantum metrology and, therefore, sensitivities that are inaccessible to classical devices [31]. A discussion of the viability of such a detector and further details can be found in [25]. Further studies of the viability of such a detector are in progress and this article is part of this effort. Simulating the effect of a GW derived in [25] could be useful for testing the metrological scheme proposed in [25,26].

Here we extend the work on $1+1$ GWs to the simulation of $3+1$ GWs in BECs in a covariant formalism [16]. With this extension, all properties of a GW can be simulated, such as its polarization and propagation vector, and the conformal factor in front of the analogue metric no longer diverges. The paper is outlined as follows. In Sec. II we present the spacetime metric of a GW and the acoustic metric in a BEC. In Sec. III we derive and demonstrate the simulation of a GW metric in $3+1$ dimensions, as well as the metric derived in [25]. Examples of GWs are presented in Sec. IV, giving explicit forms of the flow velocities needed to simulate the effect of commonly investigated GW sources, including compact binary inspirals and neutron star spin down. In Sec. V we reduce the metric derived in Sec. III to $1+1$ dimensions and compare this to previously published work in [16], and we conclude in Sec. VI.

A. Definitions and conventions

Throughout this paper, we use the metric signature $(-,+,+,+)$; the coordinates used are Minkowski coordinates given by (ct,x,y,z) unless otherwise stated; and the Minkowski metric in these coordinates is given by

$$\eta_{\mu\nu} = \mathrm{diag}(-1,1,1,1). \tag{1}$$

II. GRAVITATIONAL WAVES AND THE ACOUSTIC METRIC

A. GW spacetime metric

We first consider the general form of the metric tensor perturbed by a GW. For a single source GW far from the source, the metric tensor can be expressed as [32,33]

$$g^{(gw)}_{\mu\nu} = \eta_{\mu\nu} + \epsilon h_{\mu\nu}, \tag{2}$$

where $\eta_{\mu\nu}$ is the flat Minkowski metric defined in Sec. I A, and $h_{\mu\nu}$ is some perturbation corresponding to the passing GW, parametrized by ϵ, where $|\epsilon| \ll 1$. Standard notation omits this ϵ and applies the condition $|h_{\mu\nu}| \ll 1$, but we use ϵ here as a global perturbation scale factor for consistency and clarity.

1. Transverse traceless gauge

This perturbation $h_{\mu\nu}$ can be expressed in the transverse traceless (TT) gauge, in coordinates x^μ_{TT}, for a GW traveling in the $\hat{z}$ direction as [33]

$$h^{\mathrm{TT}}_{\mu\nu} = \begin{pmatrix} 0 & 0 & 0 & 0 \\ 0 & h_+(t) & h_\times(t) & 0 \\ 0 & h_\times(t) & -h_+(t) & 0 \\ 0 & 0 & 0 & 0 \end{pmatrix}, \tag{3}$$

where h_+ and $h_\times$ are time-dependent functions corresponding to two "polarizations" of the GW. These h_+ and $h_\times$ functions are typically called "strain" functions. We ignore the z dependence of the strain functions, as the wavelength of a GW is typically much longer than the width of a BEC (for example, the GWs detected by the LIGO and Virgo collaborations have wavelengths exceeding 10^6 m). Outside the source of the GWs, these strain functions obey the simple wave equation

$$\eta^{\rho\sigma}\partial_\rho\partial_\sigma h^{TT}_{\mu\nu} = 0. \tag{4}$$

We introduce the GW metric in this gauge, as it is the clearest and most widely known, despite not necessarily being the most physically useful.

2. Fermi normal coordinates

Any metric in linearized gravity of the form of Eq. (2) has a "gauge freedom," namely a choice of small coordinate transformation in any arbitrary direction. Consider a linearized coordinate transformation with some function ζ, such that

$$x^\mu \to x^\mu + \epsilon\zeta^\mu(x^\mu). \tag{5}$$

Under such a coordinate transformation, the metric in Eq. (2) transforms as

$$\eta_{\mu\nu} + \epsilon h_{\mu\nu} \to \eta_{\mu\nu} + \epsilon[h_{\mu\nu} - \partial_\nu\zeta_\mu - \partial_\mu\zeta_\nu] + \mathcal{O}(\epsilon^2). \tag{6}$$

Hence, making a coordinate transformation $x^\mu_{TT} \to x^\mu = x^\mu_{TT} + \epsilon\zeta^\mu$ from the TT gauge with the function

$$\zeta^\mu = \left(\frac{1}{4c}(2xy\partial_t h_\times + (x^2 - y^2)\partial_t h_+),\right.$$
$$\left.\frac{1}{2}(xh_+ + yh_\times), \frac{1}{2}(xh_\times - yh_+), 0\right), \tag{7}$$

the metric perturbation in Eq. (3) in these new coordinates is

$$h^{\mathrm{TT}}_{\mu\nu} \to h_{\mu\nu} = \begin{pmatrix} -h_{00} & \mathbf{0}^{\mathrm{T}} \\ \mathbf{0} & \mathbb{I}_3 \end{pmatrix} + \mathcal{O}(\epsilon^2) \tag{8}$$

where $\mathbb{I}_n$ is the n-dimensional identity matrix, and

$$h_{00} = -\frac{1}{2c^2}(2xy\partial_t^2 h_\times + (x^2 - y^2)\partial_t^2 h_+). \tag{9}$$

These coordinates are Fermi normal coordinates, and are the inertial frame limit of the "proper detector frame." This metric perturbation can also be derived by considering coordinates matching proper length and time, then linearizing the metric with respect to $R = \sqrt{\eta_{ij}x^i x^j}$ (derived for example in [33], Sec. I.3.3). One of the most useful features of these coordinates is that they match the laboratory coordinates of an experiment in free fall, e.g., a drag free satellite orbiting the Earth. It is also a good approximation for the suspended mirrors of the LIGO experiments. For notational convenience, we also define

$$H_{00}(t, x, y) = \int_0^t h_{00}(t', x, y) c dt'$$
$$= -\frac{1}{c}\left(xy\partial_t h_\times + \frac{1}{2}(x^2 - y^2)\partial_t h_+\right). \tag{10}$$

B. Acoustic metric

To simulate a GW metric in a BEC, we will follow the description of a BEC on a general background metric given in [13,34,35]. This description models the BEC as a barotropic, irrotational and inviscid fluid, in a covariant formalism. We are interested in (i) simulating a spacetime metric using a quantum system and (ii) simulating the effects of spacetime dynamics on a phononic field. In both cases we require a covariant formalism that enables us to properly describe a general relativistic spacetime and its effects on quantum fields. The formalism developed in [13,34,35] enables us to do so. We point out that the system that we consider here is a regular BEC, as those currently demonstrated in the laboratory. This system is usually described with nonrelativistic quantum mechanics. However, in (ii) we are taking into account the underlying spacetime background on which the BEC sits on, which requires the covariant treatment mentioned above. We point out that we are not considering a system that is moving with relativistic speeds or has excitations with relativistic energies. Such a relativistic system would also need to be described by the same formalism since covariance is also necessary.

Any BEC which can be described as a superfluid is automatically barotropic and inviscid. In the superfluid regime, the BEC is described by a classical mean field ϕ expressed as

$$\phi = \sqrt{\rho} e^{i\theta}, \tag{11}$$

with quantum fluctuations $\hat{\psi}$, defined in terms of the total field $\hat{\Phi}$ as

$$\hat{\Phi} = \phi(1 + \hat{\psi}). \tag{12}$$

We are interested in the behavior of these fluctuations in the "phononic" regime. The relativistic phononic regime condition can be written explicitly as [13]

$$|k| \ll \frac{\sqrt{2}}{\xi}\left(1 + \frac{\hbar^2}{2m^2\xi^2 u_0^2}\right) \min\left[1, \frac{m u_0 \xi}{\sqrt{2}\hbar}\right], \tag{13}$$

where k is the spatial frequency of a phononic excitation of the BEC, u is the flow velocity of the BEC defined as

$$u_\mu = \frac{\hbar}{m}\partial_\mu \theta \tag{14}$$

and ξ is the "healing length" defined as

$$\xi = \frac{1}{\sqrt{\lambda\rho}}. \tag{15}$$

λ encodes the strength of the interaction, defined in terms of the interaction potential U as

$$U(\phi^\dagger \phi, \lambda) = \frac{1}{2}\lambda|\phi^\dagger\phi|^2 + \cdots \tag{16}$$

where extra terms are ϕ^6 interactions and higher, which we ignore here. The interaction strength λ is related to the scattering length a by

$$\lambda = 8\pi a. \tag{17}$$

Taking the nonrelativistic limit of this condition, we find that the phonons should have wavelengths far longer than the healing length ξ. In this regime, and with certain additional assumptions about the mean-field properties, the fluctuations obey a relativistic Klein-Gordon-like equation

$$\frac{1}{\sqrt{-G}}\partial_\mu(\sqrt{-G}G^{\mu\nu}\partial_\nu\hat{\psi}) = 0 \tag{18}$$

for a tensor $G_{\mu\nu}$ with determinant G, called the "acoustic metric." The general acoustic metric is given by (see Appendix B)

$$G_{\mu\nu} = \frac{\rho c}{c_s}\left(g_{\mu\nu} + r\frac{v_\mu v_\nu}{c^2}\right), \tag{19}$$

where $g_{\mu\nu}$ is the background spacetime metric, ρ is the bulk density defined as $\rho = \phi^*\phi$, r is related to the speed of sound c_s as

$$r = 1 - \frac{c_s^2}{c^2} \tag{20}$$

and v is the normalized flow velocity defined as

$$v_\mu = \frac{cu_\mu}{|u|}. \tag{21}$$

The speed of sound c_s is defined as

$$c_s^2 = \frac{c^2 c_0^2/|u|^2}{1 + c_0^2/|u|^2}, \tag{22}$$

where

$$c_0^2 = \frac{\hbar^2}{2m^2}\rho\partial_\rho^2 U(\rho,\lambda) = \frac{\hbar^2}{2m^2}\lambda\rho. \tag{23}$$

The flow velocity v is normalized as

$$g^{\mu\nu}v_\mu v_\nu = -c^2. \tag{24}$$

Note that the definition of the flow velocity imposes irrotationality, i.e.,

$$\partial_\mu u_\nu = \partial_\nu u_\mu. \tag{25}$$

Due to the global phase symmetry of the Lagrangian that Eq. (18) is derived from, there is a conserved current. The conservation of this current can be expressed as

$$\nabla_\mu(\rho u^\mu) = 0, \tag{26}$$

also called the continuity equation, where ∇_μ is the covariant derivative with respect to $g_{\mu\nu}$. The velocity normalization $|u|$ and density ρ can also be directly related to the internal and external potentials U and V as

$$|u|^2 = c^2 + \frac{\hbar^2}{m^2}\left\{V + \frac{\partial U(\rho,\lambda)}{\partial\rho} - \frac{\nabla_\mu\nabla^\mu\sqrt{\rho}}{\sqrt{\rho}}\right\}. \tag{27}$$

III. GRAVITATIONAL WAVE SIMULATION

In this paper, we present two results corresponding to different types of simulation. The first in Sec. III A is a direct simulation of the GW metric in Eq. (2). The second result in Sec. III B is a simulation of the acoustic metric derived in [25], to test the proposed metrological scheme.

A. GW metric simulation

The goal of this section is to directly simulate a GW spacetime, such that the acoustic metric $G_{\mu\nu}$ has the form

$$G_{\mu\nu}^{(\mathrm{GW})} = \eta_{\mu\nu} + h_{\mu\nu}. \tag{28}$$

We start with the GW metric in Fermi normal coordinates, as introduced in Sec. II A 2. If we consider a BEC at rest in these coordinates, i.e., $v_\mu = -c\delta_\mu^0$, where the background metric is the flat Minkowski metric, then the acoustic metric has the form

$$G_{\mu\nu}^{(\mathrm{SIM})} = \frac{\rho c}{c_s}\begin{pmatrix} -c_s^2/c^2 & \mathbf{0}^{\mathrm{T}} \\ \mathbf{0} & \mathbb{I}_3 \end{pmatrix}. \tag{29}$$

It should be noted that the density is not completely unrestricted; the choice of flow velocity restricts the density through the continuity equation. From the definition of the flow velocity in Eq. (14) and the choice of normalized velocity above,

$$\frac{\hbar}{m}\partial_\mu\theta = -|u|c\delta_\mu^0 \tag{30}$$

which implies that $|u|$ can only be a function of time. Hence, with the continuity equation [Eq. (B16)], for this particular choice of normalized velocity, we must have

$$\frac{\partial_t\rho}{\rho} = -\frac{\partial_t|u|}{|u|}. \tag{31}$$

1. Bulk properties

Comparison of Eqs. (8) and (29) suggests that, to simulate the GW metric, we must modulate the speed of sound as

$$c_s^2 = c_{s0}^2(1 + \epsilon h_{00}), \tag{32}$$

where c_{s0} is the speed of sound in the absence of a simulated GW. If we rescale the time coordinate as

$$c_{s0}\tau = \left(\frac{c_{s0}^2}{c^2}\right)ct, \tag{33}$$

then the acoustic metric has the form

$$G_{\mu'\nu'}^{(\mathrm{SIM})} = \frac{\rho c}{c_s}\begin{pmatrix} -1 - \epsilon h_{00} & \mathbf{0}^{\mathrm{T}} \\ \mathbf{0} & \mathbb{I}_3 \end{pmatrix} \tag{34}$$

which matches the desired metric in Eq. (28) up to a conformal factor. The conformal factor will be discussed further later in this subsection, as well as in Sec. III C.

2. Implementation

As mentioned earlier in Sec. III A, we must have $|u|$ dependent on time only. Furthermore, having a density that is changing in time in the absence of flows implies changing the local atom number density in the BEC in a uniform and precisely controlled way, which seems experimentally unfeasible. If it is possible to control the density independently of the flows, then modulating the density to match the speed of sound sets the conformal factor in Eq. (34) to be constant, and thus physically irrelevant. If it is not feasible to control the density without inducing flows, then we must conclude that the density must be constant in time, and thus

$$\partial_t |u| = -\frac{|u|\partial_t \rho}{\rho} = 0, \tag{35}$$

so $|u|$ is constant in both space and time. This conclusion can also be drawn from the chemical potential μ of the BEC. If the BEC is stationary, then μ is constant. Since

$$\mu = \frac{i\hbar\partial_t \phi}{\phi} = mc|u|, \tag{36}$$

we can conclude that $|u|$ is constant. Using Eq. (27), we can see that all of these restrictions on the density, speed of sound and flows are only achievable by balancing the external potential V and internal interaction strength λ to modulate the speed of sound while leaving the density constant in time. Specifically, we must have

$$V = -\lambda\rho - \frac{m^2}{\hbar^2}(c^2 - |u|^2) + \frac{\nabla^2\sqrt{\rho}}{\sqrt{\rho}}. \tag{37}$$

It is well known that the interaction strength in a BEC can be modulated with an external magnetic field around a Feshbach resonance (see for example [36]). Defining

$$\lambda = \lambda_0 + \epsilon\lambda_1 \tag{38}$$

and

$$V = V_0 + \epsilon V_1 \tag{39}$$

for "unperturbed" interaction strength λ_0 and external potential V_0, we must have

$$V_1 = -\lambda_1 \rho. \tag{40}$$

From the definitions of c_s and c_0 in Eqs. (22) and (23) it is straightforward to show that the interaction strength perturbation must have the form

$$\lambda_1 = \frac{\lambda_0}{r_0} h_{00} \tag{41}$$

and thus

$$V_1 = -\frac{\lambda_0 \rho}{r_0} h_{00}, \tag{42}$$

where

$$r_0 = 1 - \frac{c_{s0}^2}{c^2}. \tag{43}$$

The density may still vary over space, with a shape determined by the "unperturbed" external potential V_0 as usual. Physically, this would result in a BEC cloud "not moving" in time (no flows, fixed density distribution), but with a carefully balanced trapping potential and applied magnetic field changing the speed of sound. This is somewhat analogous to modulating the refractive index in a dielectric, a scheme which has also been explored for its applications in analogue gravity (for example, in [7,37]). It should be noted that implementing the conditions presented in this section does not necessarily result in an exact simulation, as the effective metrics in Eqs. (34) and (28), with the above speed of sound perturbation, differ by a conformal factor, as in the simulation of various black hole geometries in [10,13,38]. Explicitly, in our case,

$$\begin{aligned} G_{\mu\nu}^{(\mathrm{SIM})} &= \frac{\rho c}{c_s} G_{\mu\nu}^{(\mathrm{GW})} \\ &= \frac{\rho c}{c_{s0}}\left(1 - \frac{\epsilon}{2}h_{00} + \mathcal{O}(\epsilon^2)\right) G_{\mu\nu}^{(\mathrm{GW})}. \end{aligned} \tag{44}$$

The conformal factor will be discussed further in Sec. III C. While a GW is a coordinate-independent physical effect, the simulation presented here reproduces elements of a metric in a particular coordinate system, and is thus not a coordinate-independent solution.

3. Nonrelativistic limit

In the explicitly nonrelativistic limit, the spatial flows are much slower than the speed of light, so $u^0 \to c$. The interaction strength must also be weak, so $c_0 \ll c$. From the definition of c_s in Eq. (22), it is clear that we must have $c_s \ll c$. In this regime, the phononic regime dispersion relation condition in Eq. (13) reduces to

$$|k| \ll \frac{\sqrt{2}}{\xi}. \tag{45}$$

We also assume that the term $\hbar^2 \partial_t^2 \phi / mc^2$ can be neglected; i.e., the excitation energy of each boson is much smaller than its mass energy. The equation governing the evolution of the field ϕ becomes the Gross-Pitaevskii equation,

$$i\hbar\partial_t \phi = \left(-\frac{\hbar^2}{2m}\nabla^2 + V^{\mathrm{NR}} + \lambda^{\mathrm{NR}}|\phi|^2\right)\phi \tag{46}$$

where the external potential and interaction strength are related to those defined in Sec. II B by

$$V^{\mathrm{NR}} = \frac{\hbar^2}{2m} V, \tag{47}$$

$$\lambda^{\mathrm{NR}} = \frac{\hbar^2}{2m} \lambda. \tag{48}$$

In the nonrelativistic limit, these are given by

$$V_1^{\mathrm{NR}} = \epsilon \frac{mc_{s0}^2}{2c^2} (2xy\partial_t^2 h_\times + (x^2 - y^2)\partial_t^2 h_+), \tag{49}$$

$$\lambda_1^{\mathrm{NR}} = -\epsilon \frac{mc_{s0}^2}{2\rho c^2} (2xy\partial_t^2 h_\times + (x^2 - y^2)\partial_t^2 h_+). \tag{50}$$

B. GW effect simulation

The goal of this section is to simulate the acoustic metric given in [25], to test the metrological scheme proposed in [25,26]. This metric has the form

$$G_{\mu\nu}^{(gw)} = \frac{\rho_0 c}{c_{s0}} \left(\eta_{\mu\nu} + h_{\mu\nu} + r_0 \frac{v_{0\mu} v_{0\nu}}{c^2} \right), \tag{51}$$

where ρ_0, c_{s0} and v_0 are the properties of the mean field ϕ "unperturbed" by a simulated GW. In [25], the BEC is considered to be at rest ($v_{0\mu} = -c\delta_\mu^0$) in the TT frame, so this is the condition that we will simulate with. Such a simulation can also be done with a BEC at rest in Fermi normal coordinates, which is not the initial condition considered in [25], and this solution is presented in the Appendix A.

1. Acoustic metric with background GW

The metric perturbation h in Fermi normal coordinates is given in Eq. (8). Going from the TT frame to Fermi normal coordinates, the flow velocity transforms as

$$v_{TT}^\mu = c\delta_0^\mu$$
$$\rightarrow v^\mu = c\left(1 - \frac{\epsilon}{2} h_{00}, -\frac{\epsilon}{2}\partial_x H_{00}, -\frac{\epsilon}{2}\partial_y H_{00}, 0\right). \tag{52}$$

Hence, the acoustic metric has the form

$$G_{\mu\nu}^{(gw)} = \frac{\rho_0 c}{c_{s0}} \begin{pmatrix} -c_{s0}^2/c^2 - \epsilon(1+r_0)h_{00} & \frac{r_0\epsilon}{2}\partial_x H_{00} & \frac{r_0\epsilon}{2}\partial_y H_{00} & 0 \\ \frac{r_0\epsilon}{2}\partial_x H_{00} & & & \\ \frac{r_0\epsilon}{2}\partial_y H_{00} & & \mathbb{I}_3 & \\ 0 & & & \end{pmatrix}. \tag{53}$$

This is the form of the acoustic metric that we will simulate.

2. Acoustic metric with simulated GW

To simulate the metric in Eq. (53), we perturb the bulk properties of the BEC in Fermi normal coordinates (i.e., lab frame). When constructing the simulation, we consider the background metric to be the flat Minkowski metric in Eq. (1), with no GW. Let the density, speed of sound and flow velocity be respectively described as

$$\rho = \rho_0 + \epsilon\rho_1, \tag{54}$$

$$c_s^2 = c_{s0}^2 + \epsilon c_{s1}^2, \tag{55}$$

and

$$v = (v_0, \epsilon v_1, \epsilon v_2, 0), \tag{56}$$

with normalization

$$|u| = |u|_0 + \epsilon |u|_1. \tag{57}$$

ρ_0, c_{s0}, $|u|_0$ and v_0 are bulk properties of the BEC in the absence of a simulated gravitational wave, as above. It should be noted that these bulk properties are not necessarily constant in space or time; they are just the natural evolution of the BEC with no simulated gravitational wave disturbing them. Checking the normalization in Eq. (24), we see that

$$v_0 = \sqrt{c^2 - \epsilon^2(v_1^2 + v_2^2)} = c + \mathcal{O}(\epsilon^2) \tag{58}$$

so, to first order, $v_0 = c$. With this flow velocity, the acoustic metric is

$$G_{\mu\nu}^{(\mathrm{sim})} = \frac{\rho c}{c_s} \begin{pmatrix} -c_s^2/c^2 & \epsilon r v_1/c & \epsilon r v_2/c & 0 \\ \epsilon r v_1/c & & & \\ \epsilon r v_2/c & & \mathbb{I}_3 & \\ 0 & & & \end{pmatrix} \tag{59}$$

to first order in ϵ. Comparison of Eqs. (53) and (59) suggests that the velocity perturbation functions should take the form

$$v_1 = \frac{1}{2}\partial_x H_{00}, \tag{60}$$

$$v_2 = \frac{1}{2}\partial_y H_{00}. \tag{61}$$

and the speed of sound perturbation must be

$$c_{s1}^2 = c^2(1 + r_0)h_{00}. \tag{62}$$

As in Sec. III A, these conditions result in a conformal simulation, with the conformal factor

$$G_{\mu\nu}^{(\mathrm{sim})} = \left(1 + \epsilon\frac{\rho_1}{\rho_0}\right)G_{\mu\nu}^{(gw)}. \tag{63}$$

If all components of both effective metrics are to match, there is no way to avoid this conformal factor. The form of the density perturbation ρ_1 required to implements Eqs. (60) and (61) will be calculated in Sec. III B 3. The conformal factor will be discussed further in Sec. III C.

3. Bulk properties for simulation

To implement the normalized velocity profile given above, we must calculate the restrictions placed on the other bulk properties of the condensate. From Eq. (25), we can derive the velocity normalization required for irrotational flow. We find that

$$|u|(t,\boldsymbol{x}) = |u|_0 - \frac{\epsilon}{2c}\partial_t(|u|_0 H_{00}), \tag{64}$$

where $\boldsymbol{x}$ represents all spatial dimensions (x, y and z). As in Sec. III A, in the limit of $\epsilon \to 0$, the BEC is stationary. Hence, the chemical potential is constant, so $|u|_0$ is constant in both space and time. Similarly, from these results and the continuity equation, Eq. (B16), we can derive the form of the density and its perturbation. We find that the density and its perturbation have the form

$$\rho_0(t,\boldsymbol{x}) = \frac{\alpha(\boldsymbol{x})}{|u|_0} \tag{65}$$

and

$$\rho_1 = -\rho_0\left(\frac{|u|_1}{|u|_0} + \frac{c}{2}\left[(xh_+ + yh_\times)\frac{\partial_x\rho_0}{\rho_0} + (xh_\times - yh_+)\frac{\partial_y\rho_0}{\rho_0}\right]\right), \tag{66}$$

where $\alpha(\boldsymbol{x})$ is some arbitrary function of integration, encoding the spatial shape of the BEC cloud. It should be noted that the results of this section are not fundamental restrictions on the bulk properties on the BEC; rather, they are conditions that must be imposed in an experiment to facilitate the implementation of the desired flow velocities and speed of sound. As in Sec. III A, all of these conditions cannot be satisfied with an arbitrary interaction strength λ. Taking the same approach as above, we define a "perturbed" interaction strength

$$\lambda = \lambda_0 + \epsilon\lambda_1. \tag{67}$$

In general from Eqs. (22) and (23), we must have

$$\lambda_1 = \lambda_0\left(2\frac{|u|_1}{|u|_0} - \frac{\rho_1}{\rho_0} + \frac{c_{s1}^2}{r_0 c_{s0}^2}\right). \tag{68}$$

With the results of this section, this expression becomes

$$\lambda_1 = \lambda_0\left[\left(\frac{c^2}{c_{s0}^2}\left[1 + \frac{1}{r_0}\right] - \frac{3}{2}\right)h_{00} - \frac{1}{2}\left((xh_+ + yh_\times)\frac{\partial_x\rho_0}{\rho_0} + (xh_\times - yh_+)\frac{\partial_y\rho_0}{\rho_0}\right)\right]. \tag{69}$$

Using Eq. (27), this corresponds to an external potential

$$V = V_0 + \epsilon\left\{-\lambda_0\rho_1 - \lambda_1\rho_0 + \frac{2m^2}{\hbar^2}|u|_0|u|_1 + \frac{1}{\sqrt{\rho_0}}\left[\frac{\Box\sqrt{\rho_0}}{\sqrt{\rho_0}} + \Box\right]\frac{\rho_1}{2\sqrt{\rho_0}}\right\}. \tag{70}$$

4. Static bulk solution

Consider a BEC trapped in a uniform box potential with infinite potential walls. In such a case, the density of the BEC is approximately constant in space everywhere inside the box, apart from a region close to the boundaries of the trap, where the density goes to zero. The width of this boundary region is given by the healing length defined above in Eq. (15). However, as stated in the motivation for the definition of Eq. (15), we are interested in perturbations whose wavelength far exceeds the healing length. Hence, for the perturbations we are considering, in a uniform box potential, we can assume constant density everywhere. This is also assumed in the detector proposal [25]. As in Sec. III A, it seems most reasonable to require that ρ_0 be constant in time, and thus $|u|_0$ is also. In this case, the perturbed bulk properties required to simulate a gravitational wave derived above can be simplified somewhat. Applying these conditions, we find

$$|u| = |u|_0\left(1 - \frac{\epsilon}{2}h_{00}\right), \tag{71}$$

$$\rho = \rho_0\left(1 + \frac{\epsilon}{2}h_{00}\right), \tag{72}$$

implemented with

$$\lambda_1 = \lambda_0\left(\frac{c^2}{c_{s0}^2}\left[1 + \frac{1}{r_0}\right] - \frac{3}{2}\right)h_{00}, \tag{73}$$

$$V_1 = -\left[\lambda_0\rho_0\left(\frac{c^2}{c_{s0}^2}\left[\frac{3}{2} + \frac{1}{r_0}\right] - \frac{3}{2}\right) + \frac{1}{4c^2}\partial_t^2\right]h_{00}. \tag{74}$$

Using the definitions and conditions presented in Sec. III A 3, the nonrelativistic limit of these potential and interaction strength perturbations are

$$\lambda_1^{\mathrm{NR}} = -\frac{\lambda_0^{\mathrm{NR}}}{c_{s0}^2}(2xy\partial_t^2 h_\times + (x^2-y^2)\partial_t^2 h_+), \quad (75)$$

$$V_1^{\mathrm{NR}} = \frac{5\lambda_0^{\mathrm{NR}}\rho_0}{2c_{s0}^2}(2xy\partial_t^2 h_\times + (x^2-y^2)\partial_t^2 h_+). \quad (76)$$

C. Conformal factor

While the evolution of the phonon field is not generally conformally invariant in $3+1$ dimensions, there are conformally invariant properties that may be usefully measured and compared against theoretical predictions. The Weyl tensor is one of the standard examples of conformally invariant objects in the framework of general relativity, and for a GW spacetime has the form

$$C_{\alpha\mu\beta\nu} = -k_{[\alpha}\bar{h}_{\mu][\nu}k_{\beta]}, \quad (77)$$

where k_μ is the wave vector of the GW, and $\bar{h}_{\mu\nu}$ is the trace reversed perturbation defined as

$$\bar{h}_{\mu\nu} = h_{\mu\nu} - \frac{1}{2}\eta_{\mu\nu}h^\sigma{}_\sigma \quad (78)$$

for metric perturbation $h_{\mu\nu}$ and Minkowski metric $\eta_{\mu\nu}$ as defined above. This follows simply from the Riemann tensor for a GW spacetime [32],

$$R_{\alpha\mu\beta\nu} = \frac{1}{2}(h_{\alpha\nu,\mu\beta} + h_{\mu\beta,\nu\alpha} - h_{\mu\nu,\alpha\beta} - h_{\alpha\beta,\mu\nu}). \quad (79)$$

In the TT gauge, the elements of the Weyl tensor have simple forms such as

$$C_{0101} = -k_z^2 h_+, \qquad C_{0102} = -k_z^2 h_\times, \quad (80)$$

which can be measured by the detector and compared against experimental parameters of the simulation.

IV. EXAMPLES OF GW SOURCES

A. Nonaxisymmetric neutron star

Rotating neutron stars are one of the strongest predicted sources of continuous GWs [39]. Any imperfections in the symmetry of the mass distribution of a neutron star generate gravitational radiation as the star spins. The simplest case of a nonaxisymmetric neutron star spinning down has strain functions of the form [40]

$$\epsilon h_+(t) = h_0\left(\frac{1+\cos^2\iota}{2}\right)\cos\Phi(t), \quad (81)$$

$$\epsilon h_\times(t) = h_0\cos\iota\sin\Phi(t), \quad (82)$$

where ι is the inclination of the neutron star's rotation axis to the line of sight, the phase evolution is

$$\Phi(t) = \Phi_0 + 2\pi f(t-t_0) \quad (83)$$

for rotation frequency $f/2$ and reference time t_0, and the amplitude h_0 is

$$h_0 = \frac{4\pi^2 G}{c^4}\frac{I_{zz}\epsilon_{xy}f^2}{d} \quad (84)$$

with ellipticity

$$\epsilon_{xy} = \frac{I_{xx} - I_{yy}}{I_{zz}} \quad (85)$$

where I_{ii} is the moment of inertia of the neutron star about some i axis, d is the distance to the neutron star and G is Newton's gravitational constant. This coordinate system is defined such that the axis of rotation is parallel to the z axis. On the timescale of a detection event, the frequency is constant to very good approximation, so terms in $\partial_t f$ in the phase are ignored [40]. The signal emitted by such a neutron star can be directly simulated with the interaction and external potential perturbations

$$\lambda_1 = \frac{\lambda_0 f^2 h_0}{2r_0c^2}\left(2xy\cos\iota\sin\Phi + (x^2-y^2)\left(\frac{1+\cos^2\iota}{2}\right)\cos\Phi\right), \quad (86)$$

$$V_1 = -\lambda_1\rho. \quad (87)$$

B. Compact binary coalescence

The first direct experimental proof of the existence of GWs was recently reported by the LIGO Collaboration in [17], with the measurement of the GW signature of the final moments of a compact binary inspiral involving two black holes. These black holes were approximately 29 and 36 times the mass of the sun respectively, and 3 solar masses in energy were radiated in the form of GWs in the inspiral and collision. The form of the emitted gravitational radiation during the collision in the "strong gravity regime" must be calculated numerically, but the radiation emitted during the well-separated inspiral phase, and the ringdown after coalescence, has well-known solutions.

1. Inspiral

During the inspiral of a compact binary system, while the two compact objects are still well separated, the gravitational radiation far from the binary system has the form [32]

$$\epsilon h_+(t) = 2(1+\cos^2\iota)\frac{\mu}{d}[\pi M f(t)]^{2/3}\cos[2\pi F(t)], \quad (88)$$

$$\epsilon h_\times(t) = 4\cos\iota\frac{\mu}{d}[\pi M f(t)]^{2/3}\sin[2\pi F(t)], \quad (89)$$

where ι is the inclination axis of inspiral axis to detector, $M = M_1 + M_2$ and $\mu = M_1 M_2/M^2$ for the two masses M_1 and M_2, d is the distance from the inspiral barycenter to the detector,

$$F(t) = \int^t f(t')dt', \quad (90)$$

and

$$f(t) = \frac{1}{\pi}\left[\frac{5}{256}\frac{1}{\mu M^{2/3}}\frac{1}{(t_0 - t)}\right]^{3/8} \quad (91)$$

with some reference time t_0. This is a sinusoidal signal whose amplitude and frequency increase as the time t reaches the reference time t_0, i.e., the time of collision. This is the characteristic "chirp" observed by the LIGO Collaboration in [17–19]. To directly simulate this metric, the corresponding interaction and external potential perturbations are

$$\begin{aligned}\lambda_1 = -\frac{\lambda_0}{r_0 c^2}\frac{\mu}{d}(\pi M f)^{2/3}\Bigg\{&4xy\cos\iota\left[\left(\frac{7\pi f}{4(t_0-t)}\right)\cos(2\pi F) + \left(\frac{5}{16(t_0-t)^2} - (2\pi f)^2\right)\sin(2\pi F)\right] \\ &+ (x^2-y^2)(1+\cos^2\iota)\left[\left(\frac{5}{16(t_0-t)^2} - (2\pi f)^2\right)\cos(2\pi F) - \left(\frac{7\pi f}{4(t_0-t)}\right)\sin(2\pi F)\right]\Bigg\},\end{aligned} \quad (92)$$

$$V_1 = -\lambda_1\rho. \quad (93)$$

2. Ringdown

After a binary system with sufficient mass to form a black hole has collided and coalesced, the resulting black hole rotates due to conservation of angular momentum. The ringdown of the coalesced object into a stable rotating black hole can thus be modeled as a perturbed Kerr black hole. The simplest single-mode ringdown of a Kerr black hole has strain functions of the form [41]

$$\epsilon h_+(t) = \frac{\mathcal{A}}{d}(1+\cos^2\iota)e^{(\Phi_0-\Phi(t))/2Q}\cos\Phi(t), \quad (94)$$

$$\epsilon h_\times(t) = \frac{\mathcal{A}}{d}(2\cos\iota)e^{(\Phi_0-\Phi(t))/2Q}\sin\Phi(t), \quad (95)$$

where

$$\Phi(t) = \Phi_0 + 2\pi f(t - t_0) \quad (96)$$

as above, ι is still the inclination angle of rotation axis to the detector, d is the distance from the source to the detector, and Q is the "quality factor" fitted numerically with

$$Q = 0.7000 + 1.4187(1-\hat{a})^{-0.4990} \quad (97)$$

for spin parameter $\hat{a} = cS/GM^2$, with spin angular momentum S. The GW amplitude $\mathcal{A}$ is given by

$$\mathcal{A} = \frac{GM}{c^2}\sqrt{\frac{5\varepsilon}{2}}Q^{-1/2}F(Q)^{-1/2}g(\hat{a})^{-1/2} \quad (98)$$

where $F(Q)=1+1/4Q^2$, $g(\hat{a})=1.5251-1.1568(1-\hat{a})^{0.1292}$ and ε is the fraction of the black hole mass radiated away. Functionally, this is a decaying sinusoid of constant frequency. The corresponding interaction and external potential perturbations for simulation are

$$\begin{aligned}\lambda_1 = -\frac{\lambda_0}{r_0 c^2}\Bigg\{&2xy\cos\iota\left(\left[\frac{1}{4Q^2}-1\right]\sin\Phi - \frac{1}{Q}\cos\Phi\right) \\ &+\frac{1}{2}(x^2-y^2)(1+\cos^2\iota)\left[\frac{1}{Q}\sin\Phi + \left(\frac{1}{4Q^2}-1\right)\cos\Phi\right]\Bigg\} \\ &\times\frac{\mathcal{A}}{d}(2\pi f)^2 e^{(\Phi_0-\Phi)/2Q},\end{aligned} \quad (99)$$

$$V_1 = -\lambda_1\rho. \quad (100)$$

V. REDUCTION TO 1+1

In this section, we restrict ourselves to an effective 1-dimensional field to compare to earlier work in [16]. In an effective $1+1$-dimensional spacetime, the GW metric reduces to

$$g_{\mu\nu} = \begin{pmatrix} -1 - \epsilon x^2\partial_t^2 h_+/2c^2 & 0 \\ 0 & 1 \end{pmatrix}. \quad (101)$$

To simulate this, the speed of sound is chosen as

$$c_s^2 = c_{s0}^2\left(1 - \epsilon\frac{x^2}{2}\partial_t^2 h_+\right) \quad (102)$$

and a time scaling of

$$c_{s0}\tau = \left(\frac{c_{s0}^2}{c^2}\right)ct \quad (103)$$

results in a simulation

$$G^{(\mathrm{SIM})}_{\mu'\nu'} = \frac{\rho c}{c_s}\begin{pmatrix} -1 - \epsilon x^2 \partial_t^2 h_+/2c^2 & 0 \\ 0 & 1 \end{pmatrix}. \tag{104}$$

In $1+1$ dimensions, the equations of motion are conformally independent, so this is an exact simulation. Following the same procedure as in Sec. III A, we require that the flow velocity normalization be completely constant and conclude that the density is constant in time. The interaction strength and external potential perturbations required to implement this are then

$$\lambda_1 = -\frac{\lambda_0}{r_0 c^2}\left(\frac{x^2}{2}\partial_t^2 h_+\right), \tag{105}$$

$$V_1 = \frac{\lambda_0 \rho}{r_0 c^2}\left(\frac{x^2}{2}\partial_t^2 h_+\right). \tag{106}$$

We must stress that this is an effective $1+1$-dimensional theory, and care must be taken when dealing with the actual field dynamics. Although this seems to work at the level of the metric, a naive suppression of the remaining spatial dimensions cannot be done due to the fact that the conformal factor is dimensionally dependent, and diverges when the number of spatial dimensions is exactly 1 [42]. Nevertheless, as long as the system is sufficiently constrained in the extra dimensions, e.g., in a highly elongated trap, a well-behaved effective $1+1$-dimensional system can always be constructed.

VI. CONCLUSION

We have shown how to simulate a GW spacetime in $3+1$ dimensions for quantum excitations of a BEC, up to a conformal factor, as well as simulating the acoustic metric used in [25] to propose a GW detector. By making use of the "gauge freedom" of the GW metric corresponding to a linearized coordinate transformation, we chose a frame in which the metric perturbation could be simulated by perturbing the speed of sound in the BEC. We then examined the restrictions this places on other bulk properties through the continuity equation and experimental limitations, and calculated the external and interaction potential perturbations needed to implement such a simulation in the lab. Although the simulated metric is related to the target metric by a nonconstant conformal factor, we show that there are still useful properties that can be measured and tested in an experiment. We also give explicit expressions for the simulation of GWs from various sources. This work generalizes the results of [16] and presents a complementary approach to simulation in effectively $1+1$-dimensional BECs.

The results presented here can also be derived in the context of an explicitly nonrelativistic treatment of a BEC, such as that derived in [42]. In a nonrelativistic BEC, phonons on the BEC still propagate on a Lorentzian effective spacetime described by an acoustic metric, but this metric is necessarily spatially conformally flat. We consider a BEC in a covariant formalism in this paper to match the approach of [25–27] for the simulation in Sec. III B, and to express the interaction of a BEC with GWs in a natural way. As explained in Sec. II B, the simulation of GWs presented in this paper does not rely on the relativistic nature of the BEC or any relativistic effects, nor do the perturbations to the external and interaction potentials disappear in the nonrelativistic limit.

We have studied GWs in the context of perturbations around a flat spacetime metric and assuming GWs to be far outside the source. Other interesting simulations could involve GWs propagating on curved backgrounds, such as black holes [9,10] or during inflation [43], or in strong-field regimes. Furthermore, since phonons are quantum quasiparticles, this opens up the possibility of studying predicted effects of quantum field theory in curved spacetime, such as how a GW may affect the entanglement of quantum systems, a phenomena that is utilized in the BEC GW detector proposed in [25]. This, therefore, also presents a potential, and fully configurable, testing environment for this GW detector metrological scheme. To obtain a full simulation of the GW detector, we need a better understanding of the effect of the GW on the bulk of the BEC. As mentioned in the conclusion of [16], an experimental simulation of the effect of a large amplitude GW and subsequent detection of phonons would also be a proof-of-concept demonstration of the generation of phonons by GWs as predicted in [25].

ACKNOWLEDGMENTS

The authors thank Joel Lindkvist and David Edward Bruschi for helpful discussion and comments. D. H. acknowledges funding from the Vienna Doctoral Program on Complex Quantum Systems (CoQuS) under the Austrian Science Fund (FWF) project code W 1210-N25. T. B. acknowledges funding from CONACYT under project code 261699/359033. D. R. thanks the Alexander von Humboldt Foundation for supporting his research with their Feodor Lynen Fellowship. R. H. and I. F. would like to acknowledge that this project was made possible through the support of the grant "Leaps in cosmology: gravitational wave detection with quantum systems" (Grant No. 58745) from the John Templeton Foundation. The opinions expressed in this publication are those of the authors and do not necessarily reflect the views of the John Templeton Foundation.

APPENDIX A: SIMULATION IN ALTERNATIVE COORDINATES

As explained in Sec. III B, it is possible to simulate the effect of a GW starting with no flows in Fermi normal coordinates. This solution is presented here. As above, let the density, speed of sound and flow velocity normalization be respectively described as

$$\rho = \rho_0 + \epsilon\rho_1, \tag{A1}$$

$$c_s^2 = c_{s0}^2 + \epsilon c_{s1}^2, \tag{A2}$$

and

$$|u| = |u|_0 + \epsilon|u|_1, \tag{A3}$$

where ϵ is the small parameter defined above. ρ_0, c_{s0}, and $|u|_0$ are bulk properties of the BEC in the absence of a simulated GW.

1. Effective metric with background gravitational wave

In Fermi normal coordinates, we consider the flows in the BEC to be $v_\mu = -v_0\delta^0_\mu$. With the normalization equation [Eq. (24)], we can determine the function v_0 as

$$\begin{aligned} g^{\mu\nu}v_\mu v_\nu &= -c^2 \\ g^{\mu\nu}v_\mu v_\nu &= (\eta^{\mu\nu} - \epsilon h^{\mu\nu})v_0\delta^0_\mu v_0\delta^0_\nu \\ &= (-1+\epsilon h_{00})v_0^2 \\ &= -c^2 \end{aligned} \tag{A4}$$

$$\Rightarrow v_0^2 = c^2(1+\epsilon h_{00}). \tag{A5}$$

Then, with a background GW, the acoustic metric has the form

$$G^{(gw)}_{\mu\nu} = \frac{\rho_0 c}{c_{s0}}\begin{pmatrix} -c_{s0}^2/c^2(1+\epsilon h_{00}) & \mathbf{0}^\mathrm{T} \\ \mathbf{0} & \mathbb{I}_3 \end{pmatrix} + \mathcal{O}(\epsilon^2). \tag{A6}$$

2. Effective metric with simulated gravitational wave

Consider the background metric $g_{\mu\nu}$ in Fermi normal coordinates to be the flat Minkowski metric $\eta_{\mu\nu}$ defined as in Eq. (1), with no background GW ($h_{\mu\nu} = 0$). In these coordinates, consider the case where there are no flows on the BEC, so the flow velocity is

$$v|_{h\to 0} = (c, 0, 0, 0). \tag{A7}$$

To simulate the effect of a GW, we perturb the bulk properties of the BEC. The acoustic metric is

$$G^{(\mathrm{sim})}_{\mu\nu} = \frac{\rho c}{c_s}\begin{pmatrix} -c_s^2/c^2 & \mathbf{0}^\mathrm{T} \\ \mathbf{0} & \mathbb{I}_3 \end{pmatrix} + \mathcal{O}(\epsilon^2). \tag{A8}$$

3. Simulation

Comparison of Eqs. (A6) and (A8) suggests that, to simulate a background GW in these coordinates, the speed of sound should be modulated as

$$c_s^2 = c_{s0}^2(1+\epsilon h_{00}). \tag{A9}$$

As with the simulation presented in the main body of the paper, this simulation differs from an exact simulation by a conformal factor:

$$G^{(\mathrm{sim})}_{\mu\nu} = \left(1 + \epsilon\left[\frac{\rho_1}{\rho_0} - \frac{h_{00}}{2}\right]\right)G^{(gw)}_{\mu\nu}. \tag{A10}$$

a. Bulk properties for simulation

To implement the normalized velocity profile given above, we must calculate the restrictions placed on the other bulk properties of the condensate. From Eq. (25),

$$|u| = |u|_0(t), \tag{A11}$$

and from Eq. (B16),

$$\rho_0(t, \boldsymbol{x}) = \frac{\alpha(\boldsymbol{x})}{|u|_0(t)}. \tag{A12}$$

As in Sec. III A, it seems most reasonable to require that $\partial_t\rho_0 = 0$ and so $|u|_0$ is completely constant. Defining a "perturbed" interaction strength as

$$\lambda = \lambda_0 + \epsilon\lambda_1, \tag{A13}$$

the results of this section and Eqs. (22) and (23) are simultaneously satisfied if

$$\lambda_1 = \frac{\lambda_0}{r_0}h_{00}. \tag{A14}$$

This can be implemented together with the external potential

$$V_1 = -\frac{\lambda_0\rho}{r_0}h_{00}. \tag{A15}$$

APPENDIX B: ACOUSTIC METRIC WITH GENERAL BACKGROUND METRIC

In [13,34], the acoustic metric is derived for a flat Minkowski background metric. Since we require the same for a general background metric, in this Appendix we extend the acoustic metric to the case where the background metric is not necessarily flat.

1. Equations of motion and basic approximations

a. Lagrangian

The Lagrangian density for an interacting massive complex scalar field $\hat{\Phi}$ on a (in general curved) background with metric $g_{\mu\nu}$ may be written as

$$\mathcal{L} = -\sqrt{-g}\left\{ g^{\mu\nu}\partial_\mu \hat{\Phi}^\dagger \partial_\nu \hat{\Phi} + \left(\frac{m^2c^2}{\hbar^2} + V\right)\hat{\Phi}^\dagger\hat{\Phi} + U(\hat{\Phi}^\dagger\hat{\Phi}, \lambda_i)\right\} \tag{B1}$$

where m is the mass, the external potential V is generally a function of space and time, and the interaction potential U depends on coupling constants λ_i which are also in principle functions of space and time. The background metric $g_{\mu\nu}$ cannot be completely general; we restrict ourselves to spacetimes with sufficiently weak curvature such that Bose-Einstein condensation can still be well defined. Further restrictions on the metric will be given in Appendix B 2 b. The interaction potential U can be expanded as

$$U(\hat{\Phi}^\dagger\hat{\Phi}, \lambda_i) = \frac{1}{2!}\lambda_2 \hat{\Phi}^\dagger\hat{\Phi}^\dagger\hat{\Phi}\,\hat{\Phi} + \frac{1}{3!}\lambda_3\hat{\Phi}^\dagger\hat{\Phi}^\dagger\hat{\Phi}^\dagger\hat{\Phi}\,\hat{\Phi}\,\hat{\Phi} + \cdots. \tag{B2}$$

We will consider only the first term of U corresponding to two-particle interactions, and ignore further terms corresponding to interactions with three or more particles. For notational convenience, we will drop the label on λ_2 so

$$U(\hat{\Phi}^\dagger\hat{\Phi}, \lambda_i) \approx \frac{1}{2}\lambda\hat{\Phi}^\dagger\hat{\Phi}^\dagger\hat{\Phi}\,\hat{\Phi}. \tag{B3}$$

The Euler-Lagrange equation for $\hat{\Phi}^\dagger$ is

$$\left[\Box_g - \left(\frac{m^2c^2}{\hbar^2} + V\right) - \lambda\hat{\Phi}^\dagger\hat{\Phi}\right]\hat{\Phi} = 0 \tag{B4}$$

where

$$\Box_g\hat{\Phi} = \frac{1}{\sqrt{-g}}\partial_\mu(\sqrt{-g}g^{\mu\nu}\partial_\nu\hat{\Phi}) \tag{B5}$$

and g is the determinant of $g_{\mu\nu}$.

b. Approximations

We now let this field $\hat{\Phi}$ represent a Bose-Einstein condensate and make the Bogoliubov approximation to separate the "condensed fraction" of the field ϕ from a small "uncondensed fraction" $\hat{\psi}$. This is done multiplicatively as

$$\hat{\Phi} = \phi(1 + \hat{\psi}) \tag{B6}$$

to simplify the equation for $\hat{\psi}$ later. As part of the Bogoliubov approximation, we say that

$$\langle\hat{\Phi}\rangle = \phi \Rightarrow \langle\hat{\psi}\rangle = 0 \tag{B7}$$

where $\langle\cdot\rangle$ is a nonequilibrium average. Taking the average of Eq. (B4),

$$\left[\Box_g - \left(\frac{m^2c^2}{\hbar^2} + V\right) - \lambda|\phi|^2\right]\phi - \lambda|\phi|^2\phi[\langle\hat{\psi}\,\hat{\psi}\rangle + 2\langle\hat{\psi}^\dagger\hat{\psi}\rangle + \langle\hat{\psi}^\dagger\hat{\psi}\,\hat{\psi}\rangle] = 0. \tag{B8}$$

We now take the Popov approximation

$$\langle\hat{\psi}\,\hat{\psi}\rangle = 0 = \langle\hat{\psi}\,\hat{\psi}\,\hat{\psi}\rangle \tag{B9}$$

and require that the density of excited atoms be much smaller than the density of mean-field atoms, i.e.,

$$\langle\hat{\psi}^\dagger\hat{\psi}\rangle \ll 1. \tag{B10}$$

This results in a nonlinear Klein-Gordon-like equation for the mean field ϕ:

$$\left[\Box_g - \left(\frac{m^2c^2}{\hbar^2} + V\right) - \lambda|\phi|^2\right]\phi = 0. \tag{B11}$$

This is a curved spacetime generalization of the Gross-Pitaevskii equation. In flat spacetime [where the metric is the Minkowski metric $\eta_{\mu\nu}$ defined in Eq. (1)] and in the nonrelativistic limit, we can replace ϕ with a lower energy field

$$\phi = \varphi e^{imc^2t/\hbar} \tag{B12}$$

and take the limit of $c \to \infty$. Assuming that the energy of excitations in φ is sufficiently low such that we can ignore terms of order $\partial_t^2\varphi$, the remaining terms of Eq. (B11) have the form

$$i\hbar\partial_t\varphi = \left[-\frac{\hbar^2}{2m}\nabla^2 + V_{\mathrm{NR}} + g_{\mathrm{NR}}|\varphi|^2\right]\varphi \tag{B13}$$

where

$$g_{\mathrm{NR}} = \frac{\hbar^2}{2m}\lambda, \qquad V_{\mathrm{NR}} = \frac{\hbar^2}{2m}V, \tag{B14}$$

which is the usual time-dependent Gross-Pitaevskii equation.

c. Continuity and velocity normalization equations

If the mean field ϕ is written in the Madelung representation $\phi = \sqrt{\rho}e^{i\theta}$ and defining a flow velocity

$$u^\mu = \frac{\hbar}{m}g^{\mu\nu}\partial_\nu\theta, \tag{B15}$$

then separating the real and imaginary components of Eq. (B11) results in two equations:

$$\nabla_\mu(\rho u^\mu) = 0, \tag{B16}$$

$$-g_{\mu\nu}u^\mu u^\nu = c^2 + \frac{\hbar^2}{m^2}\left\{V + \lambda\rho - \frac{\Box_g\sqrt{\rho}}{\sqrt{\rho}}\right\}. \tag{B17}$$

Equation (B16) is a continuity equation, and can also be derived from the global phase $U(1)$ symmetry of the Lagrangian density in Eq. (B1). Equation (B17) allows us to directly relate the external and interaction potentials with the mean-field properties of the BEC without necessarily solving the full dynamics with Eq. (B11).

2. Phonon equations

a. Equations for $\hat{\psi}$

Combining Eqs. (B4), (B6) and (B11), we find

$$[i\hbar u^\mu\partial_\mu - \hat{T}_\rho - mc_0^2]\hat{\psi} = mc_0^2\hat{\psi}^\dagger \tag{B18}$$

where

$$c_0^2 = \frac{\hbar^2}{2m^2}\lambda\rho, \tag{B19}$$

and

$$\hat{T}_\rho\hat{\psi} = -\frac{\hbar^2}{2m\rho\sqrt{-g}}\partial_\mu(\rho\sqrt{-g}g^{\mu\nu}\partial_\nu\hat{\psi}) \tag{B20}$$

is a generalized kinetic operator, which reduces to the standard kinetic energy operator $T = -(\hbar^2/2m)\nabla^2$ for constant ρ in the nonrelativistic flat spacetime limit. Note that we require the solution to Eq. (B11) to solve Eq. (B18) but not vice versa, as we are neglecting the backreaction of $\hat{\psi}$ on ϕ. Taking the equivalent equation to Eq. (B18) for $\hat{\psi}^\dagger$ and combining these to eliminate $\hat{\psi}^\dagger$, we find

$$\left([i\hbar u^\mu\partial_\mu + \hat{T}_\rho]\frac{1}{c_0^2}[-i\hbar u^\mu\partial_\mu + \hat{T}_\rho] + 2m\hat{T}_\rho\right)\hat{\psi} = 0. \tag{B21}$$

It is important to note that although Eq. (B18) implies Eq. (B21), the converse is not true.

b. Relative term strength

The phonon equation Eq. (B21) can be expanded into four terms as

$$\hat{T}_1 + \hat{T}_2 + \hat{T}_3 + \hat{T}_4 = 0 \tag{B22}$$

where

$$\hat{T}_1 = i\hbar u^\mu\partial_\mu\frac{1}{c_0^2}[-i\hbar u^\nu\partial_\nu]\hat{\psi}, \tag{B23}$$

$$\hat{T}_2 = i\hbar\left[u^\mu\partial_\mu\frac{1}{c_0^2}\hat{T}_\rho - \hat{T}_\rho\frac{1}{c_0^2}u^\mu\partial_\mu\right]\hat{\psi}, \tag{B24}$$

$$\hat{T}_3 = \hat{T}_\rho\frac{1}{c_0^2}\hat{T}_\rho\hat{\psi} \tag{B25}$$

and

$$\hat{T}_4 = 2m\hat{T}_\rho\hat{\psi}. \tag{B26}$$

We make an eikonal approximation, where

$$\left|\frac{\partial_t\rho}{\rho}\right| \ll \omega, \qquad \left|\frac{\partial_t c_0}{c_0}\right| \ll \omega, \qquad \left|\frac{\partial_t u^\mu}{u^\mu}\right| \ll \omega \tag{B27}$$

and the corresponding relations for variations in space as in the flat space case, but also

$$\left|\frac{\partial_t g_{\mu\nu}}{g_{\mu\nu}}\right| \ll \omega, \qquad \left|\frac{\partial_t g}{2g}\right| \ll \omega \tag{B28}$$

with the corresponding relations for variations in space. Note that Eq. (B28) restricts the curvature of the metric with respect to the phonon mode frequencies. For linearized gravity and realistic phonon frequencies, this will always hold. Additionally, following [13,35] we consider small momenta in the phononic regime, such that the dispersion relation is linear and terms quartic in k can be neglected. With these approximations, $\hat{T}_2$ and $\hat{T}_3$ are negligible in comparison to $\hat{T}_1$ and $\hat{T}_4$, so we are left with

$$\left[u^\mu\partial_\mu\frac{1}{c_0^2}u^\nu\partial_\nu + \frac{2m}{\hbar^2}\hat{T}_\rho\right]\hat{\psi} = 0. \tag{B29}$$

Expanding Eq. (B29), we find an equation of the form

$$\partial_\mu(f^{\mu\nu}\partial_\nu\hat{\psi}) = 0 \tag{B30}$$

where

$$f^{\mu\nu} = \rho\sqrt{-g}\left[g^{\mu\nu} - \frac{u^\mu u^\nu}{c_0^2}\right]. \tag{B31}$$

c. Acoustic metric

Equation (B30) has a form similar to a Klein-Gordon equation for a massless noninteracting scalar field $\hat{\psi}$ in a spacetime with an effective metric given by

$$f^{\mu\nu} = \sqrt{-G}G^{\mu\nu}. \tag{B32}$$

Taking the determinant of this equation, we have

$$G = -(-f)^{\frac{2}{n-2}} \tag{B33}$$

where n is the total number of dimensions, noting that f is the determinant of $f^{\mu\nu}$, but G is the determinant of $G_{\mu\nu}$. Taking the determinant of $f^{\mu\nu}$, we find that

$$\sqrt{-G} = \sqrt{-g}\rho^{\frac{n}{n-2}}\left(\frac{c}{c_s}\right)^{\frac{2}{n-2}} \tag{B34}$$

where the scalar speed of sound c_s is defined as

$$c_s^2 = \frac{c^2 c_0^2}{|u|^2 + c_0^2}. \tag{B35}$$

Hence, defining normalized flow velocity as

$$v^\mu = \frac{c}{|u|} u^\mu, \tag{B36}$$

the inverse general acoustic metric is

$$G^{\mu\nu} = \left(\frac{\rho c}{c_s}\right)^{-\frac{2}{n-2}} \left[g^{\mu\nu} + \left(1 - \frac{c^2}{c_s^2}\right) \frac{v^\mu v^\nu}{c^2}\right] \tag{B37}$$

which can be inverted to define the general acoustic metric

$$G_{\mu\nu} = \left(\frac{\rho c}{c_s}\right)^{\frac{2}{n-2}} \left[g_{\mu\nu} + \left(1 - \frac{c_s^2}{c^2}\right) \frac{v_\mu v_\nu}{c^2}\right]. \tag{B38}$$

[1] W. G. Unruh, Phys. Rev. Lett. **46**, 1351 (1981).
[2] O. Lahav, A. Itah, A. Blumkin, C. Gordon, S. Rinott, A. Zayats, and J. Steinhauer, Phys. Rev. Lett. **105**, 240401 (2010).
[3] C.-L. Hung, V. Gurarie, and C. Chin, Science **341**, 1213 (2013).
[4] J. Steinhauer, Nat. Phys. **10**, 864 (2014).
[5] S. Weinfurtner, E. W. Tedford, M. C. J. Penrice, W. G. Unruh, and G. A. Lawrence, Phys. Rev. Lett. **106**, 021302 (2011).
[6] L.-P. Euvé, F. Michel, R. Parentani, and G. Rousseaux, Phys. Rev. D **91**, 024020 (2015).
[7] T. G. Philbin, C. Kuklewicz, S. Robertson, S. Hill, F. König, and U. Leonhardt, Science **319**, 1367 (2008).
[8] J. Steinhauer, Nat. Phys. **12**, 959 (2016).
[9] B. Cropp, S. Liberati, and R. Turcati, Phys. Rev. D **94**, 063003 (2016).
[10] R. Dey, S. Liberati, and R. Turcati, Phys. Rev. D **94**, 104068 (2016).
[11] L. Giacomelli and S. Liberati, Phys. Rev. D **96**, 064014 (2017).
[12] C. Barceló, S. Liberati, and M. Visser, Int. J. Mod. Phys. D **12**, 1641 (2003).
[13] S. Fagnocchi, S. Finazzi, S. Liberati, M. Kormos, and A. Trombettoni, New J. Phys. **12**, 095012 (2010).
[14] U. R. Fischer and R. Schützhold, Phys. Rev. A **70**, 063615 (2004).
[15] S.-Y. Chä and U. R. Fischer, Phys. Rev. Lett. **118**, 130404 (2017).
[16] T. Bravo, C. Sabín, and I. Fuentes, EPJ Quantum Techno. **2**, 3 (2015).
[17] B. P. Abbott, R. Abbott, T. D. Abbott, M. R. Abernathy, F. Acernese, K. Ackley, C. Adams, T. Adams, P. Addesso, R. X. Adhikari, V. B. Adya, C. Affeldt, M. Agathos, K. Agatsuma, N. Aggarwal *et al.* (LIGO Scientific Collaboration and Virgo Collaboration), Phys. Rev. Lett. **116**, 061102 (2016).
[18] B. P. Abbott, R. Abbott, T. D. Abbott, M. R. Abernathy, F. Acernese, K. Ackley, C. Adams, T. Adams, P. Addesso, R. X. Adhikari, V. B. Adya, C. Affeldt, M. Agathos, K. Agatsuma, N. Aggarwal *et al.* (LIGO Scientific Collaboration and Virgo Collaboration), Phys. Rev. Lett. **116**, 241103 (2016).
[19] B. P. Abbott, R. Abbott, T. D. Abbott, F. Acernese, K. Ackley, C. Adams, T. Adams, P. Addesso, R. X. Adhikari, V. B. Adya, C. Affeldt, M. Afrough, B. Agarwal, M. Agathos, K. Agatsuma *et al.* (LIGO Scientific and Virgo Collaboration), Phys. Rev. Lett. **118**, 221101 (2017).
[20] B. P. Abbott, R. Abbott, T. D. Abbott, F. Acernese, K. Ackley, C. Adams, T. Adams, P. Addesso, R. X. Adhikari, V. B. Adya, C. Affeldt, M. Afrough, B. Agarwal, M. Agathos, K. Agatsuma *et al.* (LIGO Scientific Collaboration and Virgo Collaboration), Phys. Rev. Lett. **119**, 141101 (2017).
[21] B. P. Abbott, R. Abbott, T. D. Abbott, F. Acernese, K. Ackley, C. Adams, T. Adams, P. Addesso, R. X. Adhikari, V. B. Adya, C. Affeldt, M. Afrough, B. Agarwal, M. Agathos, K. Agatsuma *et al.* (LIGO Scientific Collaboration and Virgo Collaboration), Phys. Rev. Lett. **119**, 161101 (2017).
[22] P. Jones, P. McDougall, and D. Singleton, Phys. Rev. D **95**, 065010 (2017).
[23] M.-T. Jaekel, B. Lamine, A. Lambrecht, S. Reynaud, and P. M. Neto, in *Proceedings Leiden 2006* (World Scientific, Leiden, Netherlands, 2006), p. 125.
[24] I. Fernandez-Corbaton, M. Cirio, A. Bse, L. Lamata, E. Solano, and G. Molina-Terriza, Sci. Rep. **5**, 11538 (2015).
[25] C. Sabín, D. E. Bruschi, M. Ahmadi, and I. Fuentes, New J. Phys. **16**, 085003 (2014).
[26] C. Sabín, J. Kohlrus, D. E. Bruschi, and I. Fuentes, EPJ Quantum Techno. **3**, 8 (2016).
[27] R. Howl, L. Hackermüller, D. E. Bruschi, and I. Fuentes, arXiv:1607.06666v2.
[28] G. T. Moore, J. Math. Phys. (N.Y.) **11**, 2679 (1970).
[29] S. A. Fulling and P. C. W. Davies, Proc. R. Soc. A **348**, 393 (1976).
[30] R. Howl, C. Sabín, L. Hackermüller, and I. Fuentes, J. Phys. B **51**, 015303 (2018).
[31] S. L. Braunstein and C. M. Caves, Phys. Rev. Lett. **72**, 3439 (1994).
[32] C. W. Misner, K. S. Thorne, and J. A. Wheeler, *Gravitation* (W. H. Freeman and Company, San Francisco, 1973).

[33] M. Maggiore, *Gravitational Waves* (Oxford University Press, Oxford, 2007).
[34] M. Visser and C. Molina-Paris, New J. Phys. **12**, 095014 (2010).
[35] D. E. Bruschi, C. Sabín, A. White, V. Baccetti, D. K. L. Oi, and I. Fuentes, New J. Phys. **16**, 053041 (2014).
[36] U. Schneider, L. Hackermüller, J. P. Ronzheimer, S. Will, S. Braun, T. Best, I. Bloch, E. Demler, S. Mandt, D. Rasch, and A. Rosch, Nat. Phys. **8**, 213 (2012).
[37] U. Leonhardt, Nature (London) **415**, 406 (2002).
[38] M. G. Richarte, I. G. Salako, J. P. M. Graça, H. Moradpour, and A. Övgün, Phys. Rev. D **96**, 084022 (2017).
[39] J. Aasi, B. P. Abbott, R. Abbott, T. Abbott, M. R. Abernathy, T. Accadia, F. Acernese, K. Ackley, C. Adams, T. Adams, P. Addesso, R. X. Adhikari, C. Affeldt, M. Agathos, N. Aggarwal *et al.* (LIGO Scientific Collaboration and Virgo Collaboration), Phys. Rev. D **90**, 062010 (2014).
[40] C. Palomba, arXiv:1201.3176.
[41] J. Aasi, B. P. Abbott, R. Abbott, T. Abbott, M. R. Abernathy, F. Acernese, K. Ackley, C. Adams, T. Adams, P. Addesso, R. X. Adhikari, C. Affeldt, M. Agathos, N. Aggarwal, O. D. Aguiar *et al.* (LIGO Scientific Collaboration and Virgo Collaboration), Phys. Rev. D **89**, 102006 (2014).
[42] C. Barceló, S. Liberati, and M. Visser, Living Rev. Relativity **8**, 12 (2005).
[43] P. O. Fedichev and U. R. Fischer, Phys. Rev. Lett. **91**, 240407 (2003).

Quantum simulation of dark energy candidates

Own contribution: The idea of investigating the simulation of conformally coupled screened scalar field models was conceived in discussions between Ivette Fuentes and myself after discussions between Christian Käding and Ivette Fuentes. I derived the main results and the publication draft was written by me and Christian Käding. All authors contributed to correcting the draft and responding to review comments.

PHYSICAL REVIEW D **99,** 105002 (2019)

Quantum simulation of dark energy candidates

Daniel Hartley,[1,*] Christian Käding,[2] Richard Howl,[3] and Ivette Fuentes[3]
[1]*Faculty of Physics, University of Vienna, Boltzmanngasse 5, 1090 Wien, Austria*
[2]*School of Physics & Astronomy, University of Nottingham, University Park, Nottingham NG7 2RD, United Kingdom*
[3]*School of Mathematical Sciences, University of Nottingham, University Park, Nottingham NG7 2RD, United Kingdom*

(Received 8 January 2019; published 10 May 2019)

Additional scalar fields from scalar-tensor, modified gravity or higher dimensional theories beyond general relativity may account for dark energy and the accelerating expansion of the Universe. These theories have led to proposed models of screening mechanisms, such as chameleon and symmetron fields, to account for the tight experimental bounds on fifth-force searches. Cold atom systems have been very successfully used to constrain the parameters of these screening models, and may in the future eliminate the interesting parameter space of some models entirely. In this paper, we show how to manipulate a Bose-Einstein condensate to simulate the effect of any scalar field model coupled conformally to the metric. We give explicit expressions for the simulation of various common models. This result may be useful for investigating the computationally challenging evolution of particles on a screened scalar field background, as well as for testing the metrology scheme of an upcoming detector proposal.

DOI: 10.1103/PhysRevD.99.105002

I. INTRODUCTION

General relativity (GR) is a tremendously successful theory and has made many accurate physical predictions. Nevertheless, often motivated by attempts to unify gravity with other forces of Nature (e.g., Kaluza-Klein theory [1,2]), modifications to Einstein's theory of gravity have been proposed and investigated since its formulation. Amongst these modified theories of gravity, scalar-tensor theories (e.g., Brans-Dicke theory [3]) are some of the most studied. This is partly due to the fact that coupling an additional scalar field to the metric tensor is one of the simplest ways to extend general relativity. Modified theories of gravity like $f(R)$-gravity (see [4] for a review) can additionally be shown to be equivalent to scalar-tensor theories, and higher dimensional theories (e.g., string theory) predict the existence of effective scalar field modes in 4-dimensional spacetime due to compactifications of the extra dimensions (see e.g., [5]).

Modifications of gravity gained even greater attention after the accelerated expansion of the Universe was discovered [6,7] and the puzzle of dark energy—the energy that supposedly drives this expansion—arose. Consequently, there have been several proposed explanations for the nature of dark energy based on scalar-tensor theories (see e.g., [8,9] for an overview of models). Some of these models have already been ruled out by observations but others are still viable theories (see e.g., [10] for an overview of allowed and excluded models). The theories that are still candidates for explaining dark energy (and potentially other phenomena like dark matter—see e.g., [11,12] for recent ideas) must be studied further and tested experimentally (e.g., as was done in 2017 with the observation of gravitational waves from a binary neutron star merger [13,14]). In particular, understanding the properties and effects of the involved scalar fields is of utmost importance and finding hints of their existence would be a scientific breakthrough.

Many scalar-tensor theories assume the coupling between the metric tensor and these scalar fields to be via a conformal factor, as will be elaborated on in Sec. II A. Cold atom systems (e.g., atom interferometers [15,16]) are great tools for studying the effects of scalar fields with this particular type of coupling in experiments, and constraining these models. As we will show in this article, Bose-Einstein condensates (BECs) are an excellent means to simulate the behavior of matter in spacetimes with a conformally coupling scalar field. In particular, such analogue simulations will be very useful for better understanding the behavior of matter under the influence of scalar fields with nonlinear behavior since their nonlinearities can make computer simulations challenging.

A good analogy can be an invaluable tool in studying a complex or inaccessible system. From the first theoretical proposal to model a "sonic horizon" with fluid flow in 1981 [17] to experiments ranging from water waves [18–20] to BECs [21–23], nonlinear optical media [24,25] and more,

*Corresponding author.
daniel.hartley@univie.ac.at

analogue gravity has become a widely varied approach for probing aspects of the physics of curved spacetime. BECs in particular have generated a rich catalogue of analogue models, as they are both relatively simple and manifestly quantum systems. This allows for the study of how non-classical properties, such as entanglement, are modified or generated by simulated gravitational fields. In a manifestly quantum system, we also have access to the powerful tools of quantum metrology.

Excerpts from this catalogue of analogue models include conformal Schwarzschild black holes [26,27], rotating black holes [28], Bañados-Teitelboim-Zanelli (BTZ) black holes [29], Friedmann-Robertson-Walker geometries [30,31], inflation [32,33] and extensions to general relativity such as aether fields [26]. Three of us have extended this catalogue to include gravitational wave space-times [34,35]. As an example, there has recently been an experimental implementation of a waterfall horizon leading to observation of density correlations across the horizon [36,37], and controversy over their interpretation as entangled acoustic Hawking radiation [38].

In our particular case, simulating the effect of conformally coupled screened scalar field models on matter in a covariant formalism will inform potential future work on the effect of screened scalar fields on particle creation, decoherence or other interesting quantum effects, as well as allowing us to test the metrological scheme of an upcoming proposal for a detector [39] constraining these models. The approach we take towards modeling our BEC and its phonons comes from quantum field theory in curved spacetime. It is manifestly covariant and thus allows us to introduce the background spacetime in a clear and natural way.

While much can be learned from the study of analogue systems, it should be stressed that analogue is of course not identity. Thus, no analogue can be used to falsify a theory or truly discover new effects and features. If some new or unexpected result presents itself in an analogue model, great care must be taken to distinguish real physical features of the system being modeled from artefacts of the analogue system. What analogue systems can teach us is how and where to look for features and effects of a theory or real system, as well as performing important self-consistency checks and demonstrating effects that are not reliant on precise and complete accuracy of the analogy. Testing the metrological scheme of a detector as mentioned above is an example of one such effect.

In Sec. II A, we introduce conformally coupled screened scalar field models. In Sec. II B, we introduce the "acoustic metric," a description of the evolution of phonons on a BEC as a scalar field on some curved background which depends both on the real background spacetime as well as the mean-field properties of the BEC.

In Sec. III, we derive both the direct simulation of a conformally coupled screened scalar field model metric, as well as the simulation of the effect of such a metric on phonons on the BEC. For clarity, the first of these simulations (direct simulation) is a manipulation of the experimental parameters of the BEC to produce a situation in which the phonons on the BEC act as if they were a massless noninteracting boson field in a spacetime governed by the conformal metric introduced in Sec. II A. The second of these simulations (effect simulation) involves deriving and then artificially reproducing the effect of a conformally coupled screened scalar field as if it were in the real background metric. As it turns out (and as will be shown in Sec. III), these scenarios happen to be mathematically equivalent in this case. These two scenarios are not always equivalent, e.g., for gravitational waves in [35]. Note that neither of these scenarios is equivalent to simulating the evolution of the screened scalar field itself.

In Sec. IV, we present some of the major conformally coupled screened scalar field models, comprising chameleons, symmetrons, dilatons, Galileons and D-BIons, and give explicit examples for simulating these particular models. We conclude in Sec. V.

II. BACKGROUND

A. Conformally coupled screened scalar fields

Theories like string theory or f(R)-gravity naturally predict the existence of additional scalar fields coupled to the metric tensor. Some of these fields can be part of possible explanations for the nature of dark energy in the form of models like quintessence (see e.g., [40]), or simply by having a nonvanishing vacuum expectation value which leads to a cosmological constant term. For example, a scalar field φ with potential $V(\varphi) = \lambda\varphi^4 - \Lambda^3\varphi$ has a vacuum expectation value $\varphi_0 \neq 0$ and leads to a cosmological constant $\lambda\varphi_0^4 - \Lambda^3\varphi_0$ after splitting $\varphi = \varphi_0 + \delta\varphi$ into a constant background and a fluctuation term.

The resulting modifications of general relativity (GR) are investigated in scalar-tensor theories of gravity [41]. Since an additional scalar field is coupled to the metric tensor in these theories, the Einstein-Hilbert action is modified correspondingly. For example, f(R)-gravity leads to a gravitational action

$$S_G = \frac{M_P^2}{2}\int d^4x\sqrt{-\tilde{g}}\Phi\tilde{R}, \tag{1}$$

where M_P is the reduced Planck mass and Φ is an additional scalar field. With $\sim$ we denote a quantity in the Jordan frame which is one of infinitely many possible conformal frames [42] in which a theory of gravity can be formulated in. There are no explicit interactions between the scalar and the matter fields in this particular frame.

Besides the Jordan frame, it is common practice to make use of a second specific frame called the Einstein frame. In this particular frame the gravitational action takes on the canonical form of the Einstein-Hilbert action but is accompanied by some additional scalar field terms. For example, the f(R)-gravitational action (1) is given in the Einstein frame by

$$S_G = \frac{M_P^2}{2}\int d^4x\sqrt{-g}\left(R + 3\frac{\Box\Phi}{\Phi} - \frac{9}{2}(\nabla\ln\Phi)^2\right), \quad (2)$$

and a redefinition of $\Phi =: \exp[2\varphi/\sqrt{6}M_P]$ leads to a canonical kinetic term for the scalar field φ.

Besides serving as different mathematical formulations of the same theory, Jordan and Einstein frames also lead to different but ultimately equivalent interpretations of the same physical phenomenon. In the Jordan frame formulation, Einstein's theory of gravity is modified in such a way that test particles follow different geodesics from those predicted in GR, while in the Einstein frame formulation, test particles still follow GR's geodesics but are also subject to a gravity-like fifth force of Nature carried by the additional scalar field φ. This hypothetical fifth force will be further discussed later in this subsection.

In order to go from one frame to another, a conformal transformation is applied such that Jordan frame metric $\tilde{g}_{\mu\nu}$ and Einstein frame metric $g_{\mu\nu}$ are related by

$$\tilde{g}_{\mu\nu} = A(\varphi)g_{\mu\nu}. \quad (3)$$

Using the frequently applied definition $A(\varphi) =: \exp[\zeta^2(\varphi)]$ and assuming $|\zeta|^2 \ll 1$, Eq. (3) can be reduced to

$$\tilde{g}_{\mu\nu} = (1 + \zeta^2 + \mathcal{O}(\zeta^4))g_{\mu\nu}. \quad (4)$$

All experiments and observations performed so far within our solar system have been in agreement with the predictions of GR (e.g., lunar laser ranging [43] and gravitational lensing measurements [44]). To be consistent with these experiments, any theory beyond GR must modify these predictions at most perturbatively, which is why we may assume $|\zeta|^2 \ll 1$.

In this article we will refer to scalar fields coupling to the Einstein frame metric in this way as "conformally coupling scalar fields." This particular way of coupling a scalar field φ to the gravitational metric can give rise to a coupling between φ and ordinary matter fields via the trace of the energy momentum tensor $T^{\mu\nu}$. Such a coupling gives rise to a fifth force whose existence has not yet been confirmed by local observations [45]. It should be stressed that this fifth force is generally not considered to be an explanation for the accelerated expansion of the Universe, but rather is a byproduct of some scalar field models used to explain dark energy. Assuming the existence of additional scalar fields, this apparent absence of a fifth force poses a conundrum as the scalar fields' coupling to matter requires it to be there. A simple solution would be to assume this coupling to be extremely weak, such that the force is universally unmeasurably weak. However, such a scenario would be a result of fine-tuning and of little to no observational interest.

A much more interesting solution is to assume that the scalar field is subject to a screening mechanism—a mechanism that suppresses the scalar field and its force in environments of high mass density but allows them to act with their full strength in vacuum. There are several models for such screened scalar fields with different types of screening mechanisms, some of which we will present in more detail in Sec. IV. Screened scalar fields have been the subject of many different types of experiments in recent years and there are still ongoing efforts to constrain and detect them. An overview of experiments for some popular models can be found in [46,47].

B. Acoustic metric

A BEC is formed when many bosons are all collectively brought into the same state so that quantum features (such as long range order and wave function interference) determine the macroscopic behavior of the boson collective. Practically, this is done by cooling a dilute gas of bosons such that the vast majority of the boson population is in the ground state. To simulate the effect of a screened scalar field on a BEC, we will describe the BEC as a barotropic, irrotational and inviscid fluid in a covariant formalism, following the approach of [35,48]. As in [35], we emphasize that we are considering a regular BEC as those currently demonstrated in experiments so there are no "relativistic" features such as high speeds, large energies or strong coupling.

Following the above references, we describe the evolution of the total field operator $\hat{\Phi}$ of the BEC with the Lagrangian density

$$\mathcal{L} = -\sqrt{-g}\left\{g^{\mu\nu}\partial_\mu\hat{\Phi}^\dagger\partial_\nu\hat{\Phi} + \left(\frac{m^2c^2}{\hbar^2} + V\right)\hat{\Phi}^\dagger\hat{\Phi} + U(\hat{\Phi}^\dagger\hat{\Phi}, \lambda_i)\right\}, \quad (5)$$

where $g_{\mu\nu}$ is the metric of the (in general curved) background spacetime, V is the applied external potential and U is the interaction potential defined as

$$U(\hat{\Phi}^\dagger\hat{\Phi}, \lambda_i) = \frac{\lambda_2}{2!}\hat{\Phi}^\dagger\hat{\Phi}^\dagger\hat{\Phi}\hat{\Phi} + \frac{\lambda_3}{3!}\hat{\Phi}^\dagger\hat{\Phi}^\dagger\hat{\Phi}^\dagger\hat{\Phi}\hat{\Phi}\hat{\Phi} + \cdots. \quad (6)$$

As usual, the nth term of this expansion of U corresponds to n-particle interactions. We will only consider the first order two-particle contact interaction term and neglect higher order terms, as is standard when describing simple BEC systems [49]. For notational convenience, we drop the index on λ and write

$$U(\hat{\Phi}^\dagger\hat{\Phi}, \lambda_i) \approx \frac{\lambda}{2}\hat{\Phi}^\dagger\hat{\Phi}^\dagger\hat{\Phi}\hat{\Phi}. \tag{7}$$

This interaction strength λ can be related to first order to the s-wave scattering length a by

$$\lambda = 8\pi a. \tag{8}$$

We then separate the total field $\hat{\Phi}$ into the "classical" mean field $\phi = \sqrt{\rho}e^{i\theta}$ and the quantum fluctuations $\hat{\psi}$ as

$$\hat{\Phi} = \phi(1 + \hat{\psi}), \tag{9}$$

where we have made the Bogoliubov approximation so $\langle\hat{\Phi}\rangle \approx \phi$ and $\langle\hat{\psi}^\dagger\hat{\psi}\rangle \ll |\phi|^2$. In the long wavelength limit, these fluctuations $\hat{\psi}$ take the form of massless noninteracting phonons. We can write the long wavelength limit explicitly as

$$|k| \ll \frac{\sqrt{2}}{\xi}\left(1 + \frac{\hbar^2}{2m^2\xi^2u_0^2}\right) \min\left(1, \frac{mu_0\xi}{\sqrt{2}\hbar}\right) \tag{10}$$

where k is the spatial frequency of a phononic excitation, u is the flow velocity of the BEC defined as

$$u_\mu = \frac{\hbar}{m}\partial_\mu\theta, \tag{11}$$

and ξ is the "healing length" defined as

$$\xi = \frac{1}{\sqrt{\lambda\bar{\rho}}} \tag{12}$$

where $\bar{\rho}$ is the average density.

The healing length can be physically motivated as follows: consider our field $\hat{\Phi}$ in a 1-D box trap of length L with infinitely high walls. If the interaction strength vanishes (i.e., $\lambda = 0$), then the ground state wave function has the familiar harmonic oscillator ground state shape [49]

$$|\phi|^2 = \frac{2\bar{\rho}}{L}\sin^2\left[k\left(x + \frac{L}{2}\right)\right], \tag{13}$$

where $k = \pi/L$. However, if $\lambda \neq 0$ then the ground state wave function is approximately constant in space far from the boundaries. Close to the boundary $x = -L/2$, we have [49]

$$|\phi|^2 \propto \tanh^2\left[\frac{x + L/2}{\sqrt{2}\xi}\right] \tag{14}$$

so ϕ is approximately constant in space everywhere except an interval of the order ξ near the boundaries. In the long wavelength limit of Eq. (10), we consider phonon wavelengths much longer than the healing length ξ so for a box trap, the mean field density is approximately constant everywhere.

Taking the equations of motion of Eq. (5) and splitting the mean field ϕ and perturbations $\hat{\psi}$ as in [35] in $3+1$ dimensions, we arrive at a Klein-Gordon-like equation of the form

$$\frac{1}{\sqrt{-G}}\partial_\mu\sqrt{-G}G^{\mu\nu}\partial_\nu\hat{\psi} = 0 \tag{15}$$

where $G_{\mu\nu}$ is a tensor acting like an effective "acoustic metric" with the form

$$G_{\mu\nu} = \frac{\rho c}{c_s}\left[g_{\mu\nu} + \left(1 - \frac{c_s^2}{c^2}\right)\frac{v_\mu v_\nu}{c^2}\right]. \tag{16}$$

In Eq. (16), we have defined the normalized flow velocity as

$$v^\mu = \frac{c}{|u|}u^\mu \tag{17}$$

and the scalar speed of sound as

$$c_s^2 = \frac{c^2c_0^2}{c_0^2 + |u|^2} \tag{18}$$

where

$$c_0^2 = \frac{\hbar^2}{2m^2}\rho\partial_\rho^2U(\rho,\lambda) = \frac{\hbar^2}{2m^2}\lambda\rho. \tag{19}$$

Note that the definition of the flow velocity as the gradient of the phase imposes irrotationality, i.e.,

$$\partial_\mu u_\nu = \partial_\nu u_\mu. \tag{20}$$

The equations of motion of the mean field ϕ can be split into real and imaginary components resulting in a continuity equation

$$\nabla_\mu(\rho u^\mu) = 0 \tag{21}$$

and an equation directly relating bulk field properties with potentials:

$$|u|^2 = c^2 + \frac{\hbar^2}{m^2}\left\{V + \partial_\rho U(\rho,\lambda) - \frac{\nabla_\mu\nabla^\mu\sqrt{\rho}}{\sqrt{\rho}}\right\}. \tag{22}$$

The continuity equation can also be derived directly from the Lagrangian as the conserved current associated to the global $U(1)$ phase symmetry of the total field.

It should be noted that this approach is more general and includes the effects of the background space-time in a more natural way than standard approaches in BEC analogue gravity. Starting from nonrelativistic fluid equations or the Gross-Pitaevskii equation, an acoustic metric with the form

$$G_{\mu\nu} \propto \begin{pmatrix} -(c_s^2 - v^2)/c^2 & -v_i/c \\ -v_j/c & \delta_{ij} \end{pmatrix} \tag{23}$$

can be derived, where c_s is the speed of sound as above but v is the 3-flow velocity (see [50] and references therein). This model has been used for analogue gravity with both water waves and BECs, but is not a complete picture and notably omits any effects of the background space-time.

Equation (23) can be recovered from Eq. (16) in the completely nonrelativistic flat spacetime limit. A more complete model similar to that in Eq. (16) has been derived in a relativistic field theory context in [31] and from relativistic fluid equations in [51], but these both consider the background metric to be the flat Minkowski metric. Equation (16) has been derived in [35,48] and includes the effect of a (in general) curved background space-time metric in a natural way through a covariant formalism. This allows us to include any effects of the background metric arising at low (nonrelativistic) energies when taking the nonrelativistic limit to model real experiments.

1. Nonrelativistic limits

As previously mentioned, we are not considering a BEC with relativistic energies, speeds or coupling strength. Hence, it is worth considering approximations that can be made with the definitions and results of Sec. II B in the low energy limit.

Replacing the total field $\hat{\Phi}$ with a lower energy field

$$\hat{\Phi} = \hat{\Phi}_{\mathrm{NR}} e^{imc^2 t/\hbar} \tag{24}$$

and considering the background spacetime to be flat results in the standard time dependent Gross-Pitaevskii equation (see e.g., [49])

$$i\hbar\partial_t \hat{\Phi}_{\mathrm{NR}} = \left[-\frac{\hbar^2}{2m}\nabla^2 + V_{\mathrm{NR}} + g_{\mathrm{NR}}\hat{\Phi}^\dagger_{\mathrm{NR}}\hat{\Phi}_{\mathrm{NR}} \right]\hat{\Phi}_{\mathrm{NR}} \tag{25}$$

where the external potential and coupling strength are defined as

$$V_{\mathrm{NR}} = \frac{\hbar^2}{2m}V, \qquad g_{\mathrm{NR}} = \frac{\hbar^2}{2m}\lambda. \tag{26}$$

When the external potential V and interaction strength λ are constant in time, the temporal frequency of the solutions to the Gross-Pitaevskii equation is the ground state energy, generally referred to as the normalized chemical potential $\mu/\hbar$. Thus, we can write the normalization of the flow velocity $|u|$ as

$$|u| = c + \frac{\mu}{mc}. \tag{27}$$

Estimating a typical chemical potential as $\mu/\hbar \sim 10^3$ Hz in a rubidium BEC (see e.g., [52] for typical experimental parameters in BEC analogue gravity), we have

$$|u|^2 - c^2 \sim 10^{-6}\ \mathrm{m^2\,s^{-2}}. \tag{28}$$

In a harmonic trap where

$$V_{\mathrm{NR}} \sim \frac{1}{2}m\omega_i^2 x_i^2 \tag{29}$$

with a trapping frequency of $\omega \sim 10^2$ Hz, a 100 μm wide cloud has a maximum potential of

$$\frac{\hbar^2}{m^2}V \sim \omega^2 x^2 \sim 10^{-4}\ \mathrm{m^2\,s^{-2}}. \tag{30}$$

Hence, the contribution of the chemical potential in Eq. (22) through Eq. (27) is two orders of magnitude below that of the applied potentials and thus can be neglected in this equation.

We can make similar approximations in the definition of c_s in Eq. (18). Estimating the scattering length of rubidium as $a \sim 100a_0$ [52] where a_0 is the Bohr radius in our approximately Gaussian cloud of width 100 μm with 10^6 atoms, $c_0 \sim 10^{-3}$ m/s so we can say $c_0^2 \ll c^2$ with confidence. Thus, with the approximations $\mu \ll mc^2$ and $c_0^2 \ll c^2$ we can say

$$c_s^2 \approx c_0^2 - \frac{c_0^2}{c^2}\left(c_0^2 + \frac{\mu}{mc^2}\right) \approx c_0^2. \tag{31}$$

2. Defining flat space

We define a "flat" acoustic metric for the phonons in the absence of any simulated fields as the acoustic metric in coordinates with the following conditions:

(1) The background spacetime is flat, i.e., $g_{\mu\nu} = \eta_{\mu\nu} = \mathrm{diag}(-1,1,1,1)$,
(2) No flows, i.e., $v_i = 0$,
(3) Static density, i.e., $\rho_0 = \rho_0(\boldsymbol{x}) \Leftrightarrow \partial_t\rho_0 = 0$, and
(4) Unperturbed interaction strength λ, so $\partial_t\lambda = \partial_x\lambda = 0$.

Note that $\partial_t\rho = \partial_t\lambda = 0$ and the approximation $c_s^2 \approx c_0^2$ imply that $\partial_t c_s = 0$. We assume in every case that the "unperturbed" bulk properties can be described in this way. The density ρ_0 is in general a function of space, but can also be constant by careful choice of trapping potentials as explained above in Sec. II B.

The acoustic metric in $n+1$ dimensions then has the form

$$G^0_{\mu\nu} = \frac{\rho_0 c}{c_{s0}}\begin{pmatrix} -c_{s0}^2/c^2 & \\ & \mathbb{I}_n \end{pmatrix} \tag{32}$$

where $\mathbb{I}_n$ is the $n \times n$ identity matrix. If the speed of sound is also constant in space, then a simple time rescaling results in a metric trivially conformal to the $n+1$-dimensional Minkowski metric. Note that the "no flows" restriction implies that the phase of the mean field is a function of time only.

III. GENERAL SIMULATION

In this section, we present two results; the first in Sec. III A is a direct simulation of the Jordan frame metric in Eq. (4) and the second in Sec. III B is a simulation of the effect of a conformally coupled screened scalar field.

As explained in the Introduction, the direct simulation has the phonon field behaving as a massless noninteracting boson field on a background with a conformally coupled screened scalar field, whereas the effect simulation recreates the equations of motion for the phonons with a real conformally coupled screened scalar field in the background metric affecting the atoms of the BEC, with scalar field parameters chosen by an experimentalist for the simulation. It bears repeating that neither of these simulations is a simulation of the evolution of the conformally coupled screened scalar field.

A. Direct simulation

We first wish to directly simulate a Jordan frame metric, so

$$G^{(\mathrm{sim})}_{\mu\nu} = (1+\zeta^2)G^0_{\mu\nu}. \tag{33}$$

Explicitly, this is

$$\frac{\rho c}{c_s}\begin{pmatrix} -c_s^2/c^2 & \\ & \mathbb{I}_n \end{pmatrix} = (1+\zeta^2)\frac{\rho_0 c}{c_{s0}}\begin{pmatrix} -c_{s0}^2/c^2 & \\ & \mathbb{I}_n \end{pmatrix}. \tag{34}$$

To preserve the structure of the metric, we must have $c_s = c_{s0}$. It is then clear that we must also have

$$\rho = \rho_0(1+\zeta^2). \tag{35}$$

It is not possible to simultaneously satisfy all of the equations and conditions given above and in Sec. II B in $3+1$ dimensions if $\zeta^2(\varphi)$ is a completely general function of time and space: if we write the bulk phase as

$$\theta(t) = \frac{mc^2}{\hbar}t + \vartheta(t) \tag{36}$$

and require $\hbar\partial_t\vartheta \ll mc^2$ (nonrelativistic limit) then Eq. (21) becomes

$$\partial_t\left(\rho(t,\boldsymbol{x})\left[1+\frac{\hbar}{mc^2}\partial_t\vartheta(t)\right]\right) = 0. \tag{37}$$

This does not have a general solution for $\vartheta(t)$ given some arbitrary $\rho(t,\boldsymbol{x})$. As an example, consider

$$\rho(t,\boldsymbol{x}) = \rho_0(y,z)\exp\left[-\frac{x^2}{(\sigma+\varsigma t)^2}\right], \tag{38}$$

i.e., a Gaussian expanding linearly in x at a constant rate ς. Substituting this into Eq. (37) and rearranging terms, we find

$$2\varsigma x^2 = -(\sigma+\varsigma t)^3\left[\frac{\hbar\partial_t^2\vartheta}{mc^2+\hbar\partial_t\vartheta}\right]. \tag{39}$$

This clearly has no solution for nonzero ς if ϑ is to be a function of time only. Note also that Eq. (37) in the nonrelativistic limit (which is representative of all real experiments) requires the density to be a function of space only. Equation (37) has a general solution if the density is only a function of space; namely $\vartheta = \mu t$ where μ is the chemical potential.

In the case where $\partial_t\zeta^2 = 0$ i.e., ζ^2 is only a function of space or is constant, we can fulfill the continuity equation [Eq. (21)] to first order without modifying the chemical potential. From the definition of c_s, we can see that all of the above requirements can only be simultaneously fulfilled if the interaction strength is not fixed. It is well known that the interaction strength in a BEC can be modulated with an external magnetic field around a Feshbach resonance (see for example [53]).

To implement the density profile $\rho = \rho_0(1+\zeta^2)$ with an unchanged speed of sound, with Eqs. (21) and (22) we conclude that the external and interaction potentials should be modulated as

$$\lambda = \lambda_0(1-\zeta^2), \tag{40}$$

$$\begin{aligned} V &= V_0 + \left[\frac{\Box\sqrt{\rho}}{\sqrt{\rho}} - \frac{\Box\sqrt{\rho_0}}{\sqrt{\rho_0}}\right] \\ &= V_0 + \left[\frac{\partial^i\sqrt{\rho_0}}{\sqrt{\rho_0}}(\partial_i\zeta^2) + \frac{1}{2}\nabla^2\zeta^2\right] \end{aligned} \tag{41}$$

in Cartesian coordinates, where i runs over spatial indices and ∇^2 is the Laplacian, which can be easily calculated for any specific form of the initial density ρ_0. The perturbation to V captures the change in the shape of ρ induced by the perturbation ζ^2; if ζ^2 does not vary in space, then the change in the interaction strength expands or contracts the BEC without modifying c_s so no extra change in V is necessary.

B. Effect simulation

We now want to simulate the acoustic metric as seen by the phonons in the influence of some scalar field model. The conformal factor in the Jordan metric in Eq. (4) enters the acoustic metric both directly and indirectly. The normalized flow velocity is normalized to c^2, so

$$-\tilde{g}^{\mu\nu} v_\mu v_\nu = -\tilde{g}^{00} v_0^2 = c^2 \Rightarrow v_0 = c\left(1+\frac{1}{2}\zeta^2\right). \quad (42)$$

Hence, we want

$$G_{\mu\nu}^{(\mathrm{sim})} \to G_{\mu\nu}^{(\phi)} = \frac{\rho_0 c}{c_{s0}}\left(\tilde{g}_{\mu\nu} + \left(1-\frac{c_{s0}^2}{c^2}\right)(1+\zeta^2)\delta_{\mu\nu}^{00}\right). \quad (43)$$

Expanding this expression, we have

$$(1+\zeta^2)\frac{\rho_0 c}{c_{s0}}\begin{pmatrix} -c_{s0}^2/c^2 & \\ & \mathbb{I}_3 \end{pmatrix} = \frac{\rho c}{c_s}\begin{pmatrix} -c_s^2/c^2 & \\ & \mathbb{I}_3 \end{pmatrix}. \quad (44)$$

As this is identical to Eq. (34), the results of Sec. III A apply to this case as well. Note that this is not a given result for any metric to be simulated; e.g., the two types of simulation differ for a gravitational wave metric [35].

C. 1+1 dimensions

The reduction of these results to an effective $1+1$ dimensional condensate is not experimentally interesting as the phonons, in the low wavelength limit, behave as massless noninteracting Klein-Gordon bosons and thus their evolution is conformally invariant. Effects of any conformally coupled screened scalar field can only be seen here in the full $3+1$ dimensional analysis.

However, introducing an additional disformal coupling, such that the Jordan frame metric in Eq. (4) takes on the form [54]

$$\tilde{g}_{\mu\nu} = (1+\zeta^2(\varphi))g_{\mu\nu} + B(\varphi, \partial\varphi)\partial_\mu\varphi\partial_\nu\varphi, \quad (45)$$

allows the scalar field to also couple to massless particles. B is the disformal coupling parameter and can be chosen to be constant or a function of φ, $\partial\varphi$ depending on the model. Consequently, disformally coupling scalar fields could be treated when only considering an effective $1+1$ dimensional condensate, but this goes beyond the scope of this article.

IV. MODELS AND EXAMPLES

We will now give examples of conformally coupling scalar fields that are commonly used in modified theories of gravity and whose effects could be simulated as described in Sec. III (see [8,9,55,56] for overviews of modern modified gravity theories and screened scalar fields). To give a simple but commonly used example, we consider a situation in which the screening for each field is sourced by a static homogeneous sphere of radius R and give the resulting field profile outside the source. Every type of scalar field presented below has some individual type of screening mechanism. A screening mechanism allows a fifth force carried by a field to generally be strong (e.g., relative to gravity) but heavily suppressed in special circumstances (e.g., in the relatively dense environment within our solar system and, crucially, experimentally accessible space on and near the Earth).

For each presented scalar field (denoted by φ) we will give the Lagrangian density $\mathcal{L}_\varphi$ which specifies the model. With this we can define an action $S_\varphi \coloneqq \int d^4x\mathcal{L}_\varphi$, such that the effective action of our four-dimensional Universe is schematically given in the Einstein frame by

$$S_{\mathrm{4DUniverse}} = S_{\mathrm{SM}} + S_{\mathrm{Gravity}} + S_\varphi \quad (46)$$

with S_{SM} denoting the action of the Standard Model of particle physics [57] and S_{Gravity} the gravitational action. A more concrete description of how the gravitational action and the scalar field action are connected can be found in the form of Horndeski theory [58], which is the most general scalar tensor theory that gives rise to second order equations of motion.

The metric used in defining these models is the flat Minkowski metric. While any deviation of the real background metric from the Minkowski metric will have an effect on the form of these conformally coupled screened scalar field models, these deviations are observationally irrelevant. As pointed out in Sec. II A, the effect of these scalar field models must be a perturbation on GR to fit current experiments. Any deviation of the background metric from the Minkowski metric is therefore a perturbation of a perturbation and thus unmeasurable practically and unimportant to first order.

A. Chameleon

The chameleon scalar field model was first introduced in [59,60] and deals with a screened scalar field φ whose nonvanishing effective mass m_φ is dependent on the environmental density. As its animal counterpart is adaptive to the color of its surrounding, the chameleon field adapts its mass to the environment—a denser environment leads to a heavier chameleon mass.

Since the chameleon force $F_\varphi(r)$ depends on the radius r away from a chameleon source in the same way as a Yukawa potential [61] (see also e.g., [62])

$$F_\varphi(r) \sim \exp\left[-m_\varphi rc/\hbar\right]/r, \quad (47)$$

a heavy chameleon carries a shorter ranged force than a light one (the force is "Yukawa suppressed"). This gives rise to the thin-shell effect which allows only the thin outermost layer of mass of an object to effectively contribute to the chameleon force (see Fig. 1). Consequently, the chameleon fifth force coming from objects in our solar system is screened.

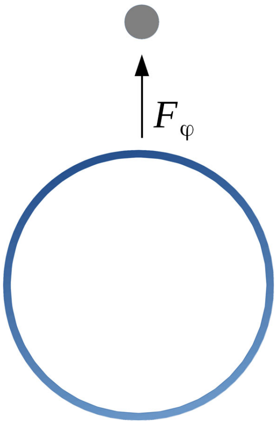

FIG. 1. Thin-shell effect: Only a thin shell of mass contributes to the chameleon force F_φ sourced by a homogeneous massive object.

Nevertheless, there have been successful attempts to constrain the chameleon parameter space with Earth-based experiments since it is possible to create situations in which the field reaches its unscreened regime in the vacuum of a vacuum chamber (see [46,47] for an overview). This is also made possible by the thin-shell effect. More precisely, if the wall of a vacuum chamber is thick enough, the outside world will not contribute to the fifth force which allows it to be relatively unscreened.

The chameleon model is described by the Lagrangian density [60]

$$\mathcal{L}_\varphi = -\frac{1}{2}(\partial\varphi)^2 - \frac{\Lambda^{4+n}}{\varphi^n} - \frac{\varphi}{M}\rho. \tag{48}$$

where $n \in \mathbb{Z}^+ \cup \{x : -1 < x < 0\} \cup 2\mathbb{Z}^- \setminus \{-2\}$ distinguishes between different chameleon models and ρ is the density of matter. This matter coupling term arises from the coupling between φ and $T^\mu{}_\mu$ discussed in Sec. II A, under the assumption that matter can be approximated as a perfect fluid with negligible pressure. Λ and M determine the strength of the self-interaction and the chameleon-matter coupling, respectively.

The sum of the two final terms in Eq. (48) results in an effective potential with a local minimum (see Fig. 2) and therefore in a nonvanishing, ρ-dependent chameleon mass. The exact value of this resulting mass is also controlled by n, Λ and M.

Here ζ^2 appearing in Eq. (4) is given by $\zeta^2(\varphi) = \varphi/M$ and the field profile outside a static spherically symmetric source is given by [60]

$$\varphi(r) = -(\varphi_\infty - \varphi_{\mathrm{obj}})\frac{R}{r}e^{-m_{\varphi,\infty}rc/\hbar} + \varphi_\infty, \tag{49}$$

with φ_{obj} being the value of the chameleon inside the source. If the source is screened, φ_{obj} is actually the minimum of the chameleon within the source. A quantity which is labeled with ∞ is given in terms of ρ_∞ which describes the mass density of the environment surrounding the object sourcing the chameleon (e.g., it would represent the density of the vacuum around a massive sphere in a vacuum chamber). The use of the label ∞ stems from the idealistic case of having an infinitely extended environment in which $\varphi(r) \to \varphi_\infty$ for $r \to \infty$.

To simulate a chameleon field Jordan frame metric, the external and interaction potentials as defined in Eqs. (5) and (7) must be

$$V(r) = V_0 + \left[\frac{\partial_r\sqrt{\rho_0}}{\sqrt{\rho_0}}\left(\frac{1}{r} + \frac{m_{\varphi,\infty}c}{\hbar}\right) - \frac{m^2_{\varphi,\infty}c^2}{2\hbar^2}\right]\frac{\varphi_\infty - \varphi(r)}{M}, \tag{50}$$

$$\lambda(r) = \lambda_0\left(1 - \frac{\varphi(r)}{M}\right). \tag{51}$$

B. Symmetron

The symmetron is another commonly studied screened scalar field model and was first described in [63–68] and introduced with its current name in [69,70]. As in the

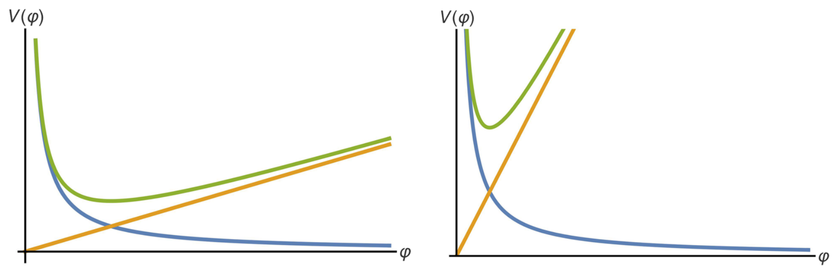

FIG. 2. The blue line represents the self-interaction potential of the chameleon (for $n > 0$), the orange line depicts the interaction potential of the chameleon with matter and the green line is the effective potential given by the sum of those two. In contrast to the two potentials alone, the effective potential has a minimum which allows the chameleon to have a nonvanishing mass. The left (right) figure represents the case of a low (high) environmental mass density.

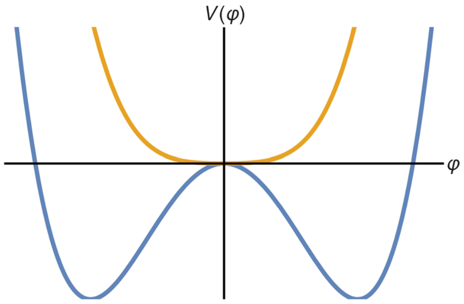

FIG. 3. At low values of the density ρ, the potential allows for spontaneous breaking of the $\mathbb{Z}_2$ symmetry and therefore gives a nonvanishing vacuum expectation value to the symmetron (blue line). However, for $\rho \gg \mu^2 M^2$, the symmetron can only have a vanishing vacuum expectation value and is therefore screened (orange line).

chameleon case, its screening mechanism is based on a coupling to matter which is dependent on the environmental density ρ. However, instead of being screened by having a heavy mass, the symmetron decouples from matter in dense environments.

The Lagrangian of the symmetron φ is given by

$$\mathcal{L}_\varphi = -\frac{1}{2}(\partial\varphi)^2 - \frac{1}{2}\left(\frac{\rho}{M^2} - \mu^2\right)\varphi^2 - \frac{\lambda}{4}\varphi^4, \tag{52}$$

where λ and M determine the strength of self-interaction and symmetron-matter coupling respectively. μ is a mass that, together with M and the mass density ρ, controls the decoupling from matter. The effective potential in this Lagrangian has a $\mathbb{Z}_2$ symmetry (see Fig. 3) which can be spontaneously broken in environments of low mass density, such that the symmetron obtains a nonvanishing vacuum expectation value φ_0. However, in regions of high density, i.e., where $\rho \gg \mu^2 M^2$, the symmetry is restored and φ can only take on a vanishing vacuum expectation value.

It is common practice to split a scalar field into a background value φ_0 and a small fluctuation $\delta\varphi$, such that $\varphi = \varphi_0 + \delta\varphi.\delta\varphi$ is the actual carrier of the fifth force and its interaction to matter is approximately proportional to $\rho\varphi_0\delta\varphi$ (at first order in $\delta\varphi$) which produces a force $F_\varphi \sim \varphi_0 \nabla\delta\varphi$. Consequently, the interaction to matter is turned off and the force is suppressed when the $\mathbb{Z}_2$ symmetry is restored in environments of large mass density since $\varphi_0 \equiv 0$ there.

For symmetrons we have ζ^2 appearing in Eq. (4) given by $\zeta^2(\varphi) = \varphi^2/2M^2$ and a field profile around a static spherically symmetric source given by [71]

$$\varphi(r) = \varphi_{0,\mathrm{out}} - (\varphi_{0,\mathrm{out}} - \varphi_{0,\mathrm{in}})\frac{R}{r}e^{m_{\mathrm{out}}(R-r)c/\hbar} \times \frac{Rm_{\mathrm{in}} - \tanh(m_{\mathrm{in}}Rc/\hbar)}{Rm_{\mathrm{in}} + Rm_{\mathrm{out}}\tanh(m_{\mathrm{in}}Rc/\hbar)}, \tag{53}$$

where "in" and "out" denote quantities depending on the density in- and outside the sphere, respectively.

To simulate a symmetron field Jordan frame metric, the external and interaction potentials as defined in Eqs. (5) and (7) must be

$$V(r) = V_0 + \left[\frac{\partial_r\sqrt{\rho_0}}{\sqrt{\rho_0}}\left(\frac{1}{r} + \frac{m_{\mathrm{out}}c}{\hbar}\right) - \frac{m_{\mathrm{out}}^2c^2}{2\hbar^2}\right]\frac{\varphi(\varphi_{0,\mathrm{out}} - \varphi)}{M^2} + \frac{1}{2}\left(\frac{1}{r} + \frac{m_{\mathrm{out}}c}{\hbar}\right)^2\left(\frac{\varphi_{0,\mathrm{out}} - \varphi}{M}\right)^2, \tag{54}$$

$$\lambda = \lambda_0\left(1 - \frac{\varphi^2}{2M^2}\right). \tag{55}$$

C. Dilaton

Dilatons are scalar fields commonly appearing in discussions of string theory compactifications. Similar to symmetrons, their force is screened by a decoupling to matter in regions of large environmental density. In the string context their screening behavior was first elaborated on in [65]. A more modern discussion with implications for cosmology can be found in [72].

Following [9], we write the dilaton Lagrangian as

$$\mathcal{L}_\varphi = -(\partial\varphi)^2 - V_0 e^{-\varphi/M_P} - \frac{(\varphi - \varphi_*)^2}{2M^2}\rho, \tag{56}$$

where V_0 is a constant of mass dimension 4, M_P is the reduced Planck mass, M controls the dilaton-matter coupling and φ_* is a critical constant field value for which the dilaton decouples. This decoupling at $\varphi \approx \varphi_*$ is the essence of the dilaton screening mechanism since the value of φ_* is chosen such that it occurs in environments of high mass density.

Here ζ^2 appearing in Eq. (4) is given by $\zeta^2(\varphi) = (\varphi - \varphi_*)^2/2M^2$ and if we expand the exponential potential in Eq. (56) up to second order in φ/M_P, then the dilaton field profile is of the same form as the symmetron profile in Eq. (53).

To simulate a dilaton field Jordan frame metric, the external and interaction potentials as defined in Eqs. (5) and (7) must be

$$V = V_0 + \frac{1}{M^2}\left[\frac{1}{2}\left(\frac{1}{r} + \frac{m_{\mathrm{out}}c}{\hbar}\right)^2(\varphi_{0,\mathrm{out}} - \varphi) + \left[\frac{\partial_r\sqrt{\rho_0}}{\sqrt{\rho_0}}\left(\frac{1}{r} + \frac{m_{\mathrm{out}}c}{\hbar}\right) - \frac{m_{\mathrm{out}}^2c^2}{2\hbar^2}\right](\varphi - \varphi_*)\right](\varphi_{0,\mathrm{out}} - \varphi), \tag{57}$$

$$\lambda = \lambda_0\left(1 - \frac{(\varphi - \varphi_*)^2}{2M^2}\right). \tag{58}$$

D. Galileon

Galileons were first introduced in the context of Dvali-Gabadadze-Porrati (DGP) braneworld models [73]. As described in more detail in [9], Galileons are higher derivative field theories with second order equations of motion. In (nearly) flat space the cubic Galileon Lagrangian is [74]

$$\mathcal{L}_\varphi = -\frac{1}{2}(\nabla\varphi)^2 - \frac{1}{2\Lambda^3}\Box\varphi(\nabla\varphi)^2 - \frac{\varphi}{M}\rho, \tag{59}$$

where $\Box \coloneqq \partial^\mu\partial_\mu$, Λ controls the impact of the nonlinear kinetic terms and M determines the Galileon-matter coupling. In principle, there are also quartic and quintic Galileon terms (see e.g., [74]) which are not included in this example. The free Lagrangian (including potential quartic and quintic terms) is symmetric under the Galilean shift

$$\varphi(x) \mapsto \varphi(x) + c + b_\mu x^\mu. \tag{60}$$

While the matter coupling term breaks this symmetry, $M \gg \Lambda$ so the symmetry breaking is mild (and discussed further in [9]).

The Galileon force is screened close to a massive object by the Vainshtein mechanism [75]. In short, within a certain radius—the Vainshtein radius R_v—around a massive object, the nonlinear terms of Eq. (59) dominate over and consequently suppress the kinetic term. This shortens the interaction range of the Galileon and therefore weakens the resulting force. More details on this can inter alia be found in [9].

Here we have ζ^2 appearing in Eq. (4) given by $\zeta^2(\varphi) = \varphi/M$ as in the chameleon case and the field profile around a static spherically symmetric source is given by [76]

$$\begin{aligned}\varphi(r) = \frac{\Lambda^3}{8}\Bigg(&r^2\left[\sqrt{1+\frac{R_v^3}{r^3}}-1\right] \\ &+3\sqrt{R_v^3 R}\left[\sqrt{\frac{r}{R^2}}\,{}_2F_1\left(\frac{1}{6},\frac{1}{2};\frac{7}{6};-\frac{r^3}{R_v^3}\right)\right. \\ &\left.\left.-\,{}_2F_1\left(\frac{1}{6},\frac{1}{2};\frac{7}{6};-\frac{R^3}{R_v^3}\right)\right]\right),\end{aligned} \tag{61}$$

where ${}_2F_1$ denotes a Gaussian hypergeometric function and the Vainshtein radius R_v is given by

$$R_v = \left(\frac{8\rho R^3}{3M\Lambda^3}\right)^{1/3}. \tag{62}$$

Analytic solutions for field profiles around planar and cylindrical sources can be found in [76].

To simulate a Galileon field Jordan frame metric, the external and interaction potentials as defined in Eqs. (5) and (7) must be

$$\begin{aligned}V = V_0 &+ \frac{\partial_r\sqrt{\rho_0}}{\sqrt{\rho_0}}\frac{\partial_r\varphi}{M} + \frac{\Lambda^3}{8M}\Bigg\{3\left(\sqrt{1+\frac{R_\nu^3}{r^3}}-1\right) \\ &+\frac{1}{4}\sqrt{\frac{R_\nu^3}{r}}\frac{1}{\sqrt{1+\frac{r^3}{R_\nu^3}}}\left[-3+\frac{3r}{4}-\frac{21}{2r}-\frac{R_\nu^6}{6r^5}+\frac{3(3-r)}{4(1+\frac{R_\nu^3}{r^3})}\right] \\ &+\frac{1}{4}\sqrt{\frac{R_\nu^3}{r}}\left[3+\frac{9}{2r}+\frac{R_\nu^6}{6r^5}\right]{}_2F_1\left(\frac{1}{6},\frac{1}{2};\frac{7}{6};-\frac{r^3}{R_\nu^3}\right)\Bigg\},\end{aligned} \tag{63}$$

$$\lambda = \lambda_0\left(1-\frac{\varphi}{M}\right). \tag{64}$$

E. D-BIon

D-BIons are a type of screened scalar fields based on braneworld related Dirac-Born-Infeld (DBI) theories and, similarly to Galileons, are screened by the Vainshtein mechanism [77]. However, instead of relying on nonlinear terms in second derivatives, they are screened via nonlinearities in first derivatives. Their matter-coupled Lagrangian is given by

$$\mathcal{L}_\varphi = \Lambda^4\sqrt{1-\frac{(\nabla\varphi)^2}{\Lambda^4}} - \frac{\varphi}{M}\rho \tag{65}$$

and leads to the following field profile around a static spherically symmetric source [76]:

$$\begin{aligned}\varphi(r) = &\frac{\Lambda^2 R^3}{R_v^2}\left(\sqrt{1+\frac{R_v^4}{R^4}}-1\right) \\ &-\frac{\Lambda^2 R_v^2}{R}\left[\frac{R}{r}\,{}_2F_1\left(\frac{1}{4},\frac{1}{2};\frac{5}{4};-\frac{R_v^4}{r^4}\right)\right. \\ &\left.-\,{}_2F_1\left(\frac{1}{4},\frac{1}{2};\frac{5}{4};-\frac{R_v^4}{R^4}\right)\right]\end{aligned} \tag{66}$$

with Vainshtein radius

$$R_v = \sqrt{\frac{\rho R^3}{3M\Lambda^2}}. \tag{67}$$

As in the Galileon case, Λ controls the impact of the nonlinear kinetic terms and M determines the Galileon-matter coupling. Analytic solutions for field profiles around planar and cylindrical sources can be found in [76]. Again, we have ζ^2 appearing in Eq. (4) given by $\zeta^2(\varphi) = \varphi/M$.

To simulate a D-BIon field Jordan frame metric, the external and interaction potentials as defined in Eqs. (5) and (7) must be

$$V = V_0 + \frac{\partial_r \sqrt{\rho_0}}{\sqrt{\rho_0}} \frac{\partial_r \varphi}{M} + \frac{\Lambda^2}{8M} \left\{ \left(\frac{r^2}{R_\nu^2} \left[\frac{5}{R^2} - 1 \right] + \frac{r^7}{4R^2 R_\nu^6} + \frac{2R_\nu^2}{R^2 r^2 (1 + \frac{R_\nu^4}{r^4})} \right) \frac{1}{\sqrt{1 + \frac{R_\nu^4}{r^4}}} - \left(\frac{r^2}{R_\nu^2} \left[\frac{5}{R^2} - 1 \right] + \frac{r^7}{4R^2 R_\nu^6} \right) F_{21} \left(\frac{1}{4}, \frac{1}{2}; \frac{5}{4}; -\frac{R_\nu^4}{r^4} \right) \right\}, \quad (68)$$

$$\lambda = \lambda_0 \left(1 - \frac{\varphi}{M} \right). \quad (69)$$

V. CONCLUSION

We have shown how to simulate a conformally coupled screened scalar field spacetime for quantum excitations of a BEC. By modulating the applied external potential V and a magnetic field near a Feshbach resonance to modulate the interatomic interaction strength, the density can be varied in space without modifying the speed of sound, thus reproducing the desired metric. This simulation is applicable to any conformally coupled screened scalar field model when the scalar field is constant in time.

We find in this particular case that directly simulating a Jordan frame metric and simulating the effect of a conformally coupled screened scalar field are functionally equivalent. We also find that the reduction of this problem to $1 + 1$ dimensions results in any effect vanishing, so a full $3 + 1$ dimensional analysis is required. Finally, we give specific examples of chameleon, symmetron, dilaton, Galileon and D-BIon fields and explicit implementations of these particular models for the field around a spherical mass in a vacuum chamber.

Constructing such a simulation will be useful in several applications. First, computer simulation of the behavior of matter under the influence of screened scalar fields is challenging due to the nonlinearities of the models. Second, simulating conformally coupled screened scalar field models in a covariant formalism will allow us to test the metrological scheme of an upcoming proposal for a detector [39] constraining these models, as well as informing future work on the effect of screened scalar fields on particle creation, decoherence or other interesting quantum effects.

ACKNOWLEDGMENTS

The authors thank Clare Burrage and Ben Thrussell for helpful comments. D. H. acknowledges funding from the Vienna Doctoral Program on Complex Quantum Systems (CoQuS) under the Austrian Science Fund (FWF) Project No. W 1210-N25. C. K. is supported by the School of Physics & Astronomy of the University of Nottingham and via a Vice-Chancellor's Scholarship for Research Excellence. R. H. and I. F. would like to acknowledge that this project was made possible through the support of the Penrose Institute and the grant "Leaps in cosmology: Gravitational wave detection with quantum systems" (No. 58745) from the John Templeton Foundation. The opinions expressed in this publication are those of the authors and do not necessarily reflect the views of the John Templeton Foundation.

[1] T. Kaluza, Sitzungsber. Preuss. Akad. Wiss. Phys. Math. Kl. **1921**, 966 (1921).
[2] O. Klein, Z. Phys. **37**, 895 (1926).
[3] C. Brans and R. H. Dicke, Phys. Rev. **124**, 925 (1961).
[4] T. P. Sotiriou and V. Faraoni, Rev. Mod. Phys. **82**, 451 (2010).
[5] I. K. Wehus and F. Ravndal, Int. J. Mod. Phys. A **19**, 4671 (2004).
[6] S. Perlmutter *et al.*, Astrophys. J. **517**, 565 (1999).
[7] A. G. Riess *et al.*, Astron. J. **116**, 1009 (1998).
[8] T. Clifton, P. G. Ferreira, A. Padilla, and C. Skordis, Phys. Rep. **513**, 1 (2012).
[9] A. Joyce, B. Jain, J. Khoury, and M. Trodden, Phys. Rep. **568**, 1 (2015).
[10] M. Ishak, Living Rev. Relativity **22**, 1 (2019).
[11] J. Khoury, Phys. Rev. D **91**, 024022 (2015).
[12] C. Burrage, E. J. Copeland, and P. Millington, Phys. Rev. D **95**, 064050 (2017).
[13] B. P. Abbott *et al.*, Phys. Rev. Lett. **119**, 161101 (2017).
[14] D. Langlois, R. Saito, D. Yamauchi, and K. Noui, Phys. Rev. D **97**, 061501(R) (2018).
[15] C. Burrage, E. J. Copeland, and E. A. Hinds, J. Cosmol. Astropart. Phys. 03 (2015) 042.
[16] M. Jaffe, P. Haslinger, V. Xu, P. Hamilton, A. Upadhye, B. Elder, J. Khoury, and H. Müller, Nat. Phys. **13**, 938 (2017).
[17] W. G. Unruh, Phys. Rev. Lett. **46**, 1351 (1981).
[18] S. Weinfurtner, E. W. Tedford, M. C. J. Penrice, W. G. Unruh, and G. A. Lawrence, Phys. Rev. Lett. **106**, 021302 (2011).
[19] L.-P. Euvé, F. Michel, R. Parentani, and G. Rousseaux, Phys. Rev. D **91**, 024020 (2015).
[20] L.-P. Euvé, S. Robertson, N. James, A. Fabbri, and G. Rousseaux, arXiv:1806.05539.
[21] O. Lahav, A. Itah, A. Blumkin, C. Gordon, S. Rinott, A. Zayats, and J. Steinhauer, Phys. Rev. Lett. **105**, 240401 (2010).
[22] C.-L. Hung, V. Gurarie, and C. Chin, Science **341**, 1213 (2013).
[23] J. Steinhauer, Nat. Phys. **10**, 864 (2014).
[24] T. G. Philbin, C. Kuklewicz, S. Robertson, S. Hill, F. König, and U. Leonhardt, Science **319**, 1367 (2008).

[25] D. Vocke, C. Maitland, A. Prain, K. E. Wilson, F. Biancalana, E. M. Wright, F. Marino, and D. Faccio, Optica **5**, 1099 (2018).
[26] B. Cropp, S. Liberati, and R. Turcati, Phys. Rev. D **94**, 063003 (2016).
[27] R. Dey, S. Liberati, and R. Turcati, Phys. Rev. D **94**, 104068 (2016).
[28] L. Giacomelli and S. Liberati, Phys. Rev. D **96**, 064014 (2017).
[29] I. Kaur and S. Ghosh, arXiv:1810.04860 [Phys. Rev. Lett. (to be published)].
[30] C. Barceló, S. Liberati, and M. Visser, Int. J. Mod. Phys. D **12**, 1641 (2003).
[31] S. Fagnocchi, S. Finazzi, S. Liberati, M. Kormos, and A. Trombettoni, New J. Phys. **12**, 095012 (2010).
[32] U. R. Fischer and R. Schützhold, Phys. Rev. A **70**, 063615 (2004).
[33] S.-Y. Chä and U. R. Fischer, Phys. Rev. Lett. **118**, 130404 (2017).
[34] T. Bravo, C. Sabin, and I. Fuentes, EPJ Quantum Techno. **2**, 3 (2015).
[35] D. Hartley, T. Bravo, D. Rätzel, R. Howl, and I. Fuentes, Phys. Rev. D **98**, 025011 (2018).
[36] J. Steinhauer, Nat. Phys. **12**, 959 (2016).
[37] J. R. M. de Nova, K. Golubkov, V. I. Kolobov, and J. Steinhauer, arXiv:1809.00913.
[38] U. Leonhardt, Ann. Phys. (Amsterdam) **530**, 1700114 (2018).
[39] D. Hartley, C. Käding, R. Howl, and I. Fuentes (to be published).
[40] P. J. Steinhardt, Phil. Trans. R. Soc. A **361**, 2497 (2003).
[41] Y. Fujii and K. Maeda, Classical Quantum Gravity **20**, 4503 (2003).
[42] G. Domènech and M. Sasaki, Int. J. Mod. Phys. D **25**, 1645006 (2016).
[43] J. O. Dickey, P. L. Bender, J. E. Faller, X. X. Newhall, R. L. Ricklefs, J. G. Ries, P. J. Shelus, C. Veillet, A. L. Whipple, J. R. Wiant, J. G. Williams, and C. F. Yoder, Science **265**, 482 (1994).
[44] M. Bartelmann, Classical Quantum Gravity **27**, 233001 (2010).
[45] E. G. Adelberger, J. H. Gundlach, B. R. Heckel, S. Hoedl, and S. Schlamminger, Prog. Part. Nucl. Phys. **62**, 102 (2009).
[46] C. Burrage and J. Sakstein, J. Cosmol. Astropart. Phys. 11 (2016) 045.
[47] C. Burrage and J. Sakstein, Living Rev. Relativity **21**, 1 (2018).
[48] D. E. Bruschi, C. Sabín, A. White, V. Baccetti, D. K. L. Oi, and I. Fuentes, New J. Phys. **16**, 053041 (2014).
[49] L. Pitaevskii and S. Stringari, *Bose-Einstein Condensation* (Oxford University Press, New York, 2003).
[50] C. Barceló, S. Liberati, and M. Visser, Living Rev. Relativity **8**, 12 (2005).
[51] M. Visser and C. Molina-Paris, New J. Phys. **12**, 095014 (2010).
[52] I. Shammass, S. Rinott, A. Berkovitz, R. Schley, and J. Steinhauer, Phys. Rev. Lett. **109**, 195301 (2012).
[53] U. Schneider, L. Hackermuller, J. P. Ronzheimer, S. Will, S. Braun, T. Best, I. Bloch, E. Demler, S. Mandt, D. Rasch, and A. Rosch, Nat. Phys. **8**, 213 (2012).
[54] J. D. Bekenstein, Phys. Rev. D **48**, 3641 (1993).
[55] K. Koyama, Rep. Prog. Phys. **79**, 046902 (2016).
[56] P. Bull *et al.*, Phys. Dark Universe **12**, 56 (2016).
[57] J. Woithe, G. J. Wiener, and F. F. Van der Veken, Phys. Educ. **52**, 034001 (2017).
[58] G. W. Horndeski, Int. J. Theor. Phys. **10**, 363 (1974).
[59] J. Khoury and A. Weltman, Phys. Rev. Lett. **93**, 171104 (2004).
[60] J. Khoury and A. Weltman, Phys. Rev. D **69**, 044026 (2004).
[61] H. Yukawa, Proc. Phys. Math. Soc. Jpn. **17**, 48 (1935).
[62] M. E. Peskin and D. V. Schroeder, *An Introduction to Quantum Field Theory* (Addison-Wesley, Reading, 1995).
[63] H. Dehnen, H. Frommert, and F. Ghaboussi, Int. J. Theor. Phys. **31**, 109 (1992).
[64] E. Gessner, Astrophys. Space Sci. **196**, 29 (1992).
[65] T. Damour and A. M. Polyakov, Nucl. Phys. **B423**, 532 (1994).
[66] M. Pietroni, Phys. Rev. D **72**, 043535 (2005).
[67] K. A. Olive and M. Pospelov, Phys. Rev. D **77**, 043524 (2008).
[68] P. Brax, C. van de Bruck, A.-C. Davis, and D. Shaw, Phys. Rev. D **82**, 063519 (2010).
[69] K. Hinterbichler and J. Khoury, Phys. Rev. Lett. **104**, 231301 (2010).
[70] K. Hinterbichler, J. Khoury, A. Levy, and A. Matas, Phys. Rev. D **84**, 103521 (2011).
[71] C. Burrage, A. Kuribayashi-Coleman, J. Stevenson, and B. Thrussell, J. Cosmol. Astropart. Phys. 12 (2016) 041.
[72] P. Brax, C. van de Bruck, A.-C. Davis, B. Li, and D. J. Shaw, Phys. Rev. D **83**, 104026 (2011).
[73] G. R. Dvali, G. Gabadadze, and M. Porrati, Phys. Lett. B **485**, 208 (2000).
[74] A. Nicolis, R. Rattazzi, and E. Trincherini, Phys. Rev. D **79**, 064036 (2009).
[75] A. I. Vainshtein, Phys. Lett. **39B**, 393 (1972).
[76] J. K. Bloomfield, C. Burrage, and A.-C. Davis, Phys. Rev. D **91**, 083510 (2015).
[77] C. Burrage and J. Khoury, Phys. Rev. D **90**, 024001 (2014).

Quantum-enhanced screened dark energy detection

Own contribution: The idea of constructing a detector for constraining conformally coupled screened scalar field models was conceived in discussions between Tupac Bravo, Ivette Fuentes and myself, extending the ideas of Tupac Bravo to a new problem. I derived the main results comprising the quantum Fisher information and the simple expressions for the bounds. The full bounds appearing in the exclusion plots were derived by me and Christian Käding, and I produced the exclusion plots. The current publication draft was written by me and Christian Käding. All other authors contributed to discussing the interferometer scheme and correcting the draft.

Quantum-enhanced screened dark energy detection

Daniel Hartley,[1,*] Christian Käding,[2,3] Richard Howl,[4] and Ivette Fuentes[4]

[1] *Faculty of Physics, University of Vienna, Boltzmanngasse 5, 1090 Wien, Austria*
[2] *National Research University Higher School of Economics, 101000, Moscow, Russia*
[3] *School of Physics & Astronomy, University of Nottingham, University Park, Nottingham NG7 2RD, United Kingdom*
[4] *School of Mathematical Sciences, University of Nottingham, University Park, Nottingham NG7 2RD, United Kingdom*

(Dated: October 3, 2019)

We propose an experiment based on a Bose-Einstein condensate interferometer for strongly constraining fifth-force models. Additional scalar fields from modified gravity or higher dimensional theories may account for dark energy and the accelerating expansion of the Universe. These theories have led to proposed screening mechanisms to fit within the tight experimental bounds on fifth-force searches. We show that our proposed experiment would greatly improve the existing constraints on these screening models by many orders of magnitude, entirely eliminating the remaining parameter space of the simplest of these models.

General relativity (GR) has remained a tremendously successful theory, producing accurate physical predictions consistent with the barrage of experiments and observations conducted over the last century. Despite this success, there are still many open problems within GR and apparent limitations of the theory itself. Amongst modified theories of gravity aiming to address these problems, scalar-tensor theories (e.g. Brans-Dicke theory [1], see also [2]) are some of the most widely studied. Modified theories of gravity like $f(R)$-gravity can additionally be shown to be equivalent to scalar-tensor theories, and higher dimensional theories (e.g. string theory) predict the existence of effective scalar field modes in 4-dimensional spacetime due to compactifications of the extra dimensions [3].

Modifications of gravity gained even greater attention after the accelerated expansion of the Universe was discovered [4, 5] and the puzzle of dark energy (DE) - the energy that supposedly drives this expansion - arose. Consequently, there have been several proposed explanations for the nature of DE based on scalar-tensor theories (see e.g. [6, 7] for an overview of models). Some of these models are predicted to cause a fifth force, which is in contradiction with observations and experiments [8–10]. Consequently, some of these models have already been ruled out by observations [11]. However, models with a so-called "screening mechanism" [12] have features that supress the effects of the additional scalar fields in regions of high matter density. A screening mechanism would allow additional scalar fields to contribute to dark energy while the coupling to matter as a fifth force still evades experimental constraints.

Cold atom systems have proven to be invaluable tools in precision metrology. From practical applications such as ultra-high precision clocks [13] to more fundamental experiments searching e.g. for deviation from the equivalence principle [14–16], the high degree of control and low internal noise afforded by cold atom systems makes them an ideal testing ground. Many scalar-tensor theories assume a conformal coupling between the metric tensor and the scalar field, and cold atom systems have been found to be well suited to studying these particular models in experiments (e.g. in atom interferometers [17, 18]) and analogue gravity simulations [19]. Atom interferometry experiments currently provide the tightest constraints on some of these models [12, 20].

In this Letter, we propose using a guided Bose-Einstein condensate (BEC) interferometer scheme to further constrain these conformally coupled screened scalar field models. Guided is used in this context to refer to atoms held in a trap for all or most of the interferometer scheme, rather than being in free fall. For this scheme, we consider a guided BEC interferometer as currently demonstrated in experiments. The main advantage of this scheme is a longer integration time: a trapped BEC can be held near a source object for much longer than atoms in a ballistic trajectory. We show that the constraints on the above screened scalar field models could be improved by many orders of magnitude.

The models we consider here come from scalar-tensor theories of gravity [2]. As stated above, an additional scalar field Φ may be coupled to the metric tensor conformally in these theories, such that ordinary matter fields evolve according to the conformal metric

$$\tilde{g}_{\mu\nu} = A^2(\Phi)\, g_{\mu\nu} \tag{1}$$

for some conformal factor $A^2(\Phi)$, where $g_{\mu\nu}$ is the normal GR metric. The equilibrium state of the Φ field is determined by minimising an effective potential [7, 12, 21]

$$V_{\text{eff}}(\Phi) = V(\Phi) + A(\Phi)\,\rho, \tag{2}$$

where $V(\Phi)$ is the self-interaction potential of the model and ρ is the ordinary matter density.

We specifically consider two prominent examples of fifth force models with screening mechanism, namely the chameleon field [21, 22] and the symmetron field (first described in [23–28] and introduced with its current name in [29, 30]). These models have been investigated in atom interferometry experiments as the thick wall of a vacuum chamber can shield its interior from outside effects [17, 31], allowing the ultra-high vacuum to simulate the low density conditions of empty space resulting in long range (and thus measurable) chameleon or symmetron forces.

The chameleon field model is described by the conformal coupling [21]

$$A^2(\Phi) = \exp[\Phi/M_c] \tag{3}$$

and the potential

$$V(\Phi) = \Lambda^4 \exp[\Lambda^n/\Phi^n]. \tag{4}$$

The parameter M_c determines the strength of the chameleon-matter coupling. This parameter is essentially unconstrained but is plausibly below the reduced Planck mass $M_{Pl} \approx 2.4 \times 10^{18}$ GeV$/c^2$. The self-interaction strength Λ determines the contribution of the chameleon field to the energy density of the Universe, as the potential can be expanded as $V \approx \Lambda^4 + \Lambda^{4+n}/\Phi^n$. This energy density can drive the accelerated expansion of the Universe observed today if $\Lambda = \Lambda_{DE} \approx 2.4$ meV. Finally, different choices of the parameter n define different models, where $n \in \mathbb{Z}^+ \cup \{x : -1 < x < 0\} \cup 2\mathbb{Z}^- \setminus \{-2\}$ produces valid models with screening mechanisms. The two most commonly studied chameleon models are those where $n = 1$ or -4 [12].

The effective mass of the chameleon field in equilibrium is determined by the minimum of its effective potential, i.e. $m_c^2 = \left|\partial^2 V_{\text{eff}}/\partial\Phi^2\right|_{\Phi=\Phi_{\text{min}}}$. The position of the effective potential minimum (and thus effective mass) depends on the ordinary matter density ρ (see Supplemental Material for a detailed demonstration). In regions of low density, e.g. the intergalactic vacuum, the chameleon is light and mediates a long range force. In regions of high density, e.g. in a laboratory, the chameleon becomes massive and the force becomes short-ranged, making it challenging to detect with fifth force tests.

The symmetron model has a conformal coupling and a potential given by [29]

$$A^2(\Phi) = \exp\left[\Phi^2/2M_s^2\right] \tag{5}$$

and

$$V(\Phi) = -\frac{\mu^2}{2}\Phi^2 + \frac{\lambda_s}{4}\Phi^4 \tag{6}$$

respectively. As for the chameleon, M_s gives the symmetron-matter coupling and λ_s determines the self-interaction strength. Unlike the chameleon, the symmetron effective potential has a $\mathbb{Z}_2$ symmetry which can be spontaneously broken in environments of low matter density (see Supplemental Material). This allows the symmetron to obtain a non-vanishing effective mass in regions where the ambient matter density is below the critical density $\rho^* = \mu^2 M_s^2$. The symmetron field has a vanishing vacuum expectation value in high density regions ($\rho > \rho^*$) and thus a vanishing force. Consequently, the parameter μ determines the scale of the symmetron-matter decoupling.

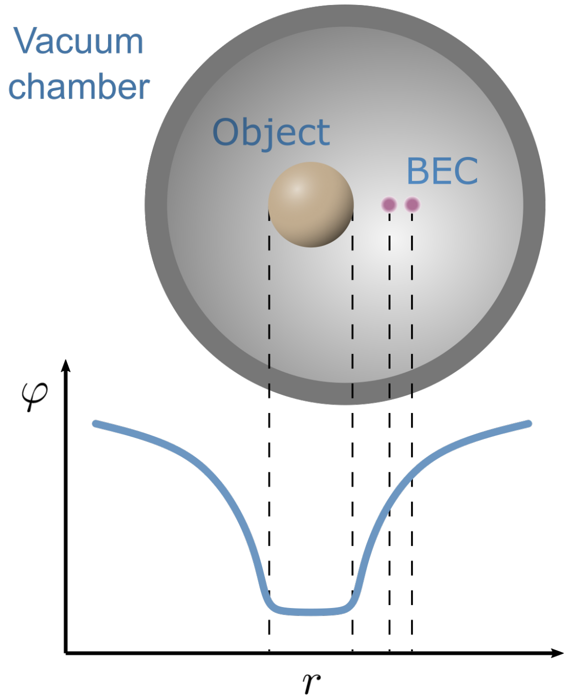

FIG. 1. A schematic diagram of the vacuum chamber overlaid on the field profile of a chameleon field around a spherical source object. The separation of the BEC components is greatly exaggerated.

We propose to use a BEC interferometer held near some source mass to constrain the chameleon and symmetron models (Fig. 1). The lowest order gravitational effect of the source mass is a gravitational redshift, which manifests as a position dependent global phase. The lowest order potential fifth force effect is a modification of this global phase by a position dependent value. This total global phase θ is given by (see Supplemental Material)

$$\theta(r) = \frac{mc^2 T}{2\hbar}\left[\frac{r_s}{r} - 2\log A(\Phi(r))\right] \tag{7}$$

where r_s is the Schwarzschild radius of the source object, m is the mass of each atom in the BEC, T is the time and A is the conformal factor defined as above. A BEC coherently split into parts would measure the phase gradient and thus field gradient in an interference measurement. The other contributions from the environment (e.g. the gravity of the Earth) could be subtracted with differential measurements or a dual interferometer scheme where measurements are performed near to and far from the source object.

BEC-based interferometers are not a new concept, and have already been proposed and demonstrated (e.g. [32–36], see also [37] and references therein). Coherent splitting of a BEC into spatially separated clouds has been implemented both with atom chips [32, 34, 38] (chips printed with an electrode structure allowing for the generation of magnetic and radio-frequency fields very close to an atom cloud) and in free space [39]. Recombination and interference of the separated clouds is typically achieved by turning the trapping potential off and letting the clouds expand into each other as they fall [37]. An alternative scheme has been recently realised, where the two condensate parts are brought into contact via Josephson tunnelling through a low potential barrier [40]. This acts as a beam splitting operation, and the interference contrast is projected onto a mean atom number difference between the two wells.

The optimal sensitivity of a measurement maximised over all possible measurement schemes is given by the quantum Fisher information (QFI) through the quantum Cramér-Rao bound (QCRB) [41–43]. Since the QFI gives the best possible sensitivity in estimating a parameter, optimised over all possible forms of measurement, the QCRB trivially follows as

$$(\Delta\kappa)^2 \geq \frac{1}{NH(\kappa)} \tag{8}$$

where $\Delta\kappa$ is the absolute error in estimating the parameter κ due to some measurement, $H(\kappa)$ is the QFI for estimating the parameter κ and N is the number of measurements performed.

Gaussian states cover the majority of easily experimentally accessible states such as coherent states, thermal states and squeezed states. Calculating the QFI for Gaussian states is simple as Gaussian states have a straightforward description in terms of their first and second moments [44–46].

Let θ_- be the accumulated phase difference between two arms of a BEC interferometer. The QFI for estimating θ_- with a fully condensed $\mathcal{N}_0$-atom BEC is given by

$$H(\theta_-) = \mathcal{N}_0 \tag{9}$$

which scales with the standard quantum limit (SQL) [47].

We now consider some experimental limitations to the schemes proposed in this Letter and use these to calculate the expected sensitivity of our schemes to constraining the chameleon and symmetron models. Typical BEC experiments condense clouds consisting of $10^4 - 10^6$ atoms, although condensates of up to 10^8 atoms have been demonstrated with sodium [48], and up to 10^9 atoms has been demonstrated with hydrogen [49, 50]. For estimating the sensitivity of this detector, we assume an initial BEC with 10^6 atoms.

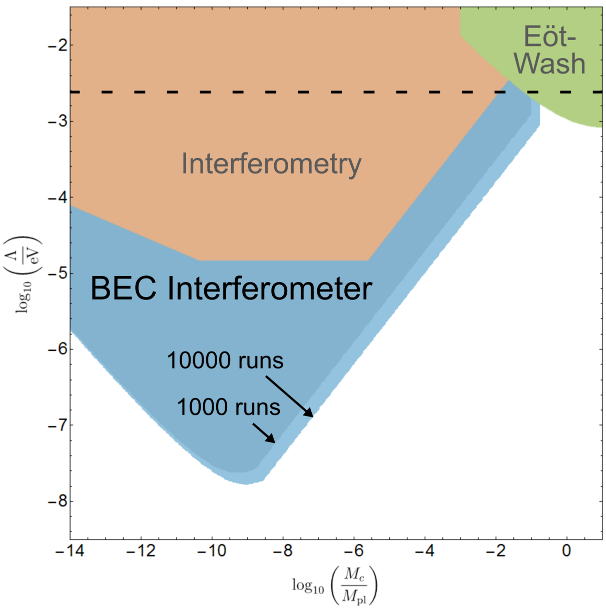

FIG. 2. Constraints for the parameter space of the chameleon model $n = 1$. The brown area corresponds to constraints from atom interferometry and the green area to those from Eöt-Wash experiments [12, 20]. The dotted line indicates the DE scale $\Lambda = 2.4$ meV. New constraints predicted in this work are coloured in blue, where dark blue corresponds to 1000 runs and light blue corresponds to 10000 runs.

The maximum integration time of our proposed detector is set by the mutual coherence time of the components of the split BEC. Mutual coherence times up to 500 ms have been demonstrated with atom chips [51, 52], so we will estimate the integration time of our detector to be 500 ms.

We do not consider the effects of technical noise in the trapping potential or other sources of experimental noise. While we expect that these sources of noise will contribute substantially to the achievable sensitivity of any detector, any substantive analysis will strongly depend on the details of the experimental implementation which we also leave to future work.

The expected new bounds on the chameleon and symmetron models from an implementation of our proposed schemes are presented in Figs. 2 - 4. Together with the numbers given above, we use the same experimental dimensions as in [53] for ease of comparison. Specifically, we consider a spherical vacuum chamber of radius $L = 5$ cm and vacuum pressure 6×10^{-10} Torr. The source object is an aluminium sphere with a radius of $R = 9.5$ mm. The effective distance between the object and the BEC is 8.8 mm, and we assume that the two parts of the BEC

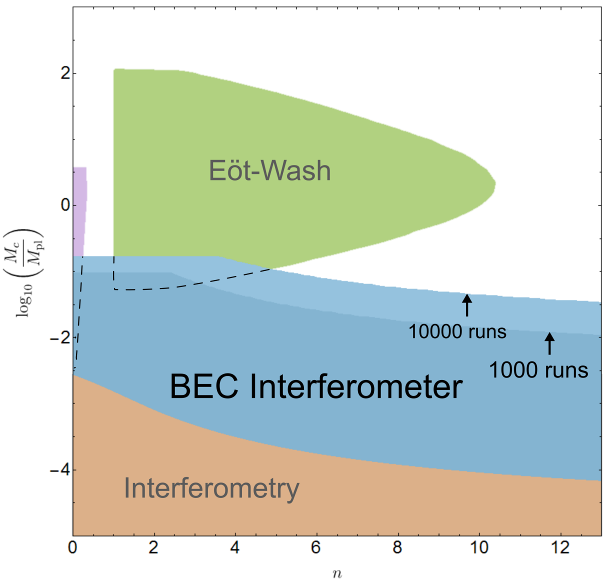

FIG. 3. Constraints for the value of M_c for positive n chameleon models at $\Lambda = 2.4$ meV. The brown area corresponds to constraints from atom interferometry, the green area to those from Eöt-Wash experiments, and the violet area represents constraints from astrophysics [12, 20]. New constraints predicted in this work are coloured in blue, where dark blue corresponds to 1000 runs and light blue corresponds to 10000 runs.

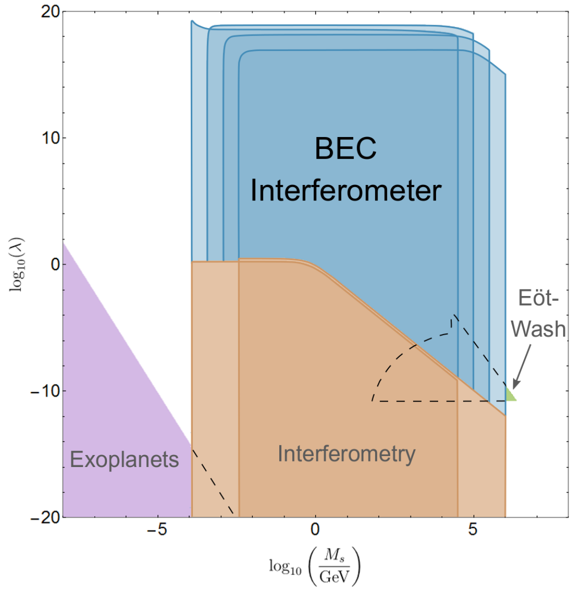

FIG. 4. Constraints for the parameter space of the symmetron model. The brown area corresponds to constraints from atom interferometry, the green area to those from Eöt-Wash experiments, and the violet area represents constraints from exoplanet astrophysics [12, 20]. New constraints predicted in this work for a BEC interferometer are coloured in blue. Different shades of blue correspond to $\mu = 10^{-4}$, $10^{-4.5}$, 10^{-5} and $10^{-5.5}$ eV in natural units respectively.

are split by 100 μm. With clever trap positioning, the distance between the object and the BEC may eventually be limited by the strength of the van der Waals or Casimir-Polder forces, but these are not relevant at the 10 mm scale.

Fig. 2 shows the predicted new constraints for one of the most popular screening models - the chameleon with $n = 1$. There it can be seen that the BEC interferometry scheme would be able to improve existing constraints for this model by up to 3 orders of magnitude and close the gap between former interferometry and Eöt-Wash experiment constraints on the DE scale $\Lambda = 2.4$ meV. This amounts to ruling out the simplest chameleon model as a model of dark energy.

Figure 3 shows constraints for the value of M_c over different values of positive n chameleon models and for $\Lambda = \Lambda_{\rm DE} = 2.4$ meV. Our scheme would improve existing interferometry constraints by more than 2 orders of magnitude and close the gap to Eöt-Wash for $n \leq 5$.

The predicted constraints on the parameter space of the symmetron model are shown in Fig. 4. We expect that our proposed experiment would improve the existing constraints by between 16 and 26 orders of magnitude in λ across the entire accessible range of M_s.

For a summary of the accessible areas of and detailed constraints on the parameter space for both the chameleon and symmetron models, see the Supplemental Material.

While we have only considered chameleon and symmetron screening models, it should be stressed that constraints for any other type of conformally coupled scalar field could be obtained in a similar manner, e.g. for galileons [54] or dilatons [55, 56].

To bring this proposal into reality, future work will focus on optimising the experimental implementation. Any subsequent implementation of our proposal will either discover $n = 1$ chameleon fields at the cosmological energy density or completely rule them out, along with greatly improving the bounds on other screened scalar models.

The authors thank C. Burrage, B. Elder and A. L. Báez-Camargo for helpful comments, and C. Burrage and J. Sakstein for providing their constraint plot files. The authors acknowledge financial support from the Austrian Science Fund (FWF) through project code W 1210-N25, the University of Nottingham, and the John Templeton Foundation through Grant No. 58745. The opinions expressed in this publication are those of the authors and do not necessarily reflect the views of the John Templeton Foundation.

* Corresponding author: daniel.hartley@univie.ac.at

[1] C. Brans and R. H. Dicke, Phys. Rev. **124**, 925 (1961).
[2] Y. Fujii and K. Maeda, *The scalar-tensor theory of gravitation*, Cambridge Monographs on Mathematical Physics (Cambridge University Press, 2007).
[3] I. K. Wehus and F. Ravndal, Int. J. Mod. Phys. **A19**, 4671 (2004), arXiv:hep-ph/0210292 [hep-ph].
[4] S. Perlmutter *et al.* (Supernova Cosmology Project), Astrophys. J. **517**, 565 (1999), arXiv:astro-ph/9812133 [astro-ph].
[5] A. G. Riess *et al.* (Supernova Search Team), Astron. J. **116**, 1009 (1998), arXiv:astro-ph/9805201 [astro-ph].
[6] T. Clifton, P. G. Ferreira, A. Padilla, and C. Skordis, Phys. Rept. **513**, 1 (2012), arXiv:1106.2476 [astro-ph.CO].
[7] A. Joyce, B. Jain, J. Khoury, and M. Trodden, Phys. Rept. **568**, 1 (2015), arXiv:1407.0059 [astro-ph.CO].
[8] J. O. Dickey, P. L. Bender, J. E. Faller, X. X. Newhall, R. L. Ricklefs, J. G. Ries, P. J. Shelus, C. Veillet, A. L. Whipple, J. R. Wiant, J. G. Williams, and C. F. Yoder, Science **265**, 482 (1994).
[9] E. G. Adelberger, B. R. Heckel, and A. E. Nelson, Annu. Rev. Nucl. Part. S. **53**, 77 (2003).
[10] D. J. Kapner, T. S. Cook, E. G. Adelberger, J. H. Gundlach, B. R. Heckel, C. D. Hoyle, and H. E. Swanson, Phys. Rev. Lett. **98**, 021101 (2007).
[11] M. Ishak, Living Rev. Rel. **22**, 1 (2019), arXiv:1806.10122 [astro-ph.CO].
[12] C. Burrage and J. Sakstein, Living Rev. Rel. **21**, 1 (2018), arXiv:1709.09071 [astro-ph.CO].
[13] A. D. Ludlow, M. M. Boyd, J. Ye, E. Peik, and P. O. Schmidt, Rev. Mod. Phys. **87**, 637 (2015).
[14] D. Schlippert, H. Albers, L. L. Richardson, D. Nath, H. Heine, C. Meiners, E. Wodey, A. Billon, J. Hartwig, C. Schubert, N. Gaaloul, W. Ertmer, and E. M. Rasel, Proceedings of the 50th Rencontres de Moriond "Gravitation: 100 years after GR", La Thuile (Italy) (2015).
[15] C. Overstreet, P. Asenbaum, T. Kovachy, R. Notermans, J. M. Hogan, and M. A. Kasevich, Phys. Rev. Lett. **120**, 183604 (2018).
[16] D. Becker, M. D. Lachmann, S. T. Seidel, H. Ahlers, A. N. Dinkelaker, J. Grosse, O. Hellmig, H. Müntinga, V. Schkolnik, T. Wendrich, A. Wenzlawski, B. Weps, R. Corgier, T. Franz, N. Gaaloul, W. Herr, D. Lüdtke, M. Popp, S. Amri, H. Duncker, M. Erbe, A. Kohfeldt, A. Kubelka-Lange, C. Braxmaier, E. Charron, W. Ertmer, M. Krutzik, C. Lämmerzahl, A. Peters, W. P. Schleich, K. Sengstock, R. Walser, A. Wicht, P. Windpassinger, and E. M. Rasel, Nature **562**, 391 (2018).
[17] C. Burrage, E. J. Copeland, and E. A. Hinds, JCAP **1503**, 042 (2015), arXiv:1408.1409 [astro-ph.CO].
[18] M. Jaffe, P. Haslinger, V. Xu, P. Hamilton, A. Upadhye, B. Elder, J. Khoury, and H. Müller, Nature Physics **13**, 938 (2017).
[19] D. Hartley, C. Käding, R. Howl, and I. Fuentes, Phys. Rev. D **99**, 105002 (2019).
[20] C. Burrage and J. Sakstein, Journal of Cosmology and Astroparticle Physics **2016**, 045 (2016).
[21] J. Khoury and A. Weltman, Phys. Rev. **D69**, 044026 (2004), arXiv:astro-ph/0309411 [astro-ph].
[22] J. Khoury and A. Weltman, Phys. Rev. Lett. **93**, 171104 (2004), arXiv:astro-ph/0309300 [astro-ph].
[23] H. Dehnen, H. Frommert, and F. Ghaboussi, International Journal of Theoretical Physics **31**, 109 (1992).
[24] E. Gessner, Astrophysics and Space Science **196**, 29 (1992).
[25] T. Damour and A. M. Polyakov, Nucl. Phys. **B423**, 532 (1994), arXiv:hep-th/9401069 [hep-th].
[26] M. Pietroni, Phys. Rev. D **72**, 043535 (2005).
[27] K. A. Olive and M. Pospelov, Phys. Rev. D **77**, 043524 (2008).
[28] P. Brax, C. van de Bruck, A.-C. Davis, and D. Shaw, Phys. Rev. D **82**, 063519 (2010).
[29] K. Hinterbichler and J. Khoury, Phys. Rev. Lett. **104**, 231301 (2010), arXiv:1001.4525 [hep-th].
[30] K. Hinterbichler, J. Khoury, A. Levy, and A. Matas, Phys. Rev. **D84**, 103521 (2011), arXiv:1107.2112 [astro-ph.CO].
[31] C. Burrage, A. Kuribayashi-Coleman, J. Stevenson, and B. Thrussell, JCAP **1612**, 041 (2016), arXiv:1609.09275 [astro-ph.CO].
[32] Y. Shin, M. Saba, T. A. Pasquini, W. Ketterle, D. E. Pritchard, and A. E. Leanhardt, Phys. Rev. Lett. **92**, 050405 (2004).
[33] J. E. Debs, P. A. Altin, T. H. Barter, D. Döring, G. R. Dennis, G. McDonald, R. P. Anderson, J. D. Close, and N. P. Robins, Phys. Rev. A **84**, 033610 (2011).
[34] T. Berrada, S. van Frank, R. Bücker, T. Schumm, J.-F. Schaff, and J. Schmiedmayer, Nature Communications **4**, 2077 (2013).
[35] H. Müntinga, H. Ahlers, M. Krutzik, A. Wenzlawski, S. Arnold, D. Becker, K. Bongs, H. Dittus, H. Duncker, N. Gaaloul, C. Gherasim, E. Giese, C. Grzeschik, T. W. Hänsch, O. Hellmig, W. Herr, S. Herrmann, E. Kajari, S. Kleinert, C. Lämmerzahl, W. Lewoczko-Adamczyk, J. Malcolm, N. Meyer, R. Nolte, A. Peters, M. Popp, J. Reichel, A. Roura, J. Rudolph, M. Schiemangk, M. Schneider, S. T. Seidel, K. Sengstock, V. Tamma, T. Valenzuela, A. Vogel, R. Walser, T. Wendrich, P. Windpassinger, W. Zeller, T. van Zoest, W. Ertmer, W. P. Schleich, and E. M. Rasel, Phys. Rev. Lett. **110**, 093602 (2013).
[36] G. D. McDonald, C. C. N. Kuhn, K. S. Hardman, S. Bennetts, P. J. Everitt, P. A. Altin, J. E. Debs, J. D. Close, and N. P. Robins, Phys. Rev. Lett. **113**, 013002 (2014).
[37] A. D. Cronin, J. Schmiedmayer, and D. E. Pritchard, Rev. Mod. Phys. **81**, 1051 (2009).
[38] M. Albiez, R. Gati, J. Fölling, S. Hunsmann, M. Cristiani, and M. K. Oberthaler, Phys. Rev. Lett. **95**, 010402 (2005).
[39] D. S. Naik, G. Kuyumjyan, D. Pandey, P. Bouyer, and A. Bertoldi, Quantum Science and Technology **3**, 045009 (2018).
[40] T. Berrada, S. van Frank, R. Bücker, T. Schumm, J.-F. Schaff, J. Schmiedmayer, B. Julía-Díaz, and A. Polls, Phys. Rev. A **93**, 063620 (2016).
[41] S. L. Braunstein and C. M. Caves, Phys. Rev. Lett. **72**, 3439 (1994).
[42] M. G. A. Paris, International Journal of Quantum Information **07**, 125 (2009).
[43] D. Šafránek and I. Fuentes, Phys. Rev. A **94**, 062313 (2016).
[44] A. Monras, Phys. Rev. A **73**, 033821 (2006).
[45] O. Pinel, P. Jian, N. Treps, C. Fabre, and D. Braun, Physical Review A **88**, 040102(R) (2013).

[46] D. Šafránek, A. R. Lee, and I. Fuentes, New Journal of Physics **17**, 073016 (2015).
[47] P. Kok and B. W. Lovett, *Introduction to optical quantum information processing* (Cambridge University Press, 2010).
[48] K. M. R. van der Stam, E. D. van Ooijen, R. Meppelink, J. M. Vogels, and P. van der Straten, Review of Scientific Instruments **78**, 013102 (2007), https://doi.org/10.1063/1.2424439.
[49] D. G. Fried, T. C. Killian, L. Willmann, D. Landhuis, S. C. Moss, D. Kleppner, and T. J. Greytak, Phys. Rev. Lett. **81**, 3811 (1998).
[50] T. Greytak, D. Kleppner, D. Fried, T. Killian, L. Willmann, D. Landhuis, and S. Moss, Physica B: Condensed Matter **280**, 20 (2000).
[51] G.-B. Jo, Y. Shin, S. Will, T. A. Pasquini, M. Saba, W. Ketterle, D. E. Pritchard, M. Vengalattore, and M. Prentiss, Phys. Rev. Lett. **98**, 030407 (2007).
[52] S. Zhou, D. Groswasser, M. Keil, Y. Japha, and R. Folman, Phys. Rev. A **93**, 063615 (2016).
[53] P. Hamilton, M. Jaffe, P. Haslinger, Q. Simmons, H. Müller, and J. Khoury, Science **349**, 849 (2015).
[54] G. R. Dvali, G. Gabadadze, and M. Porrati, Phys. Lett. **B485**, 208 (2000), arXiv:hep-th/0005016 [hep-th].
[55] T. Damour and A. M. Polyakov, Nucl. Phys. **B423**, 532 (1994), arXiv:hep-th/9401069 [hep-th].
[56] P. Brax, C. van de Bruck, A.-C. Davis, B. Li, and D. J. Shaw, Phys. Rev. **D83**, 104026 (2011), arXiv:1102.3692 [astro-ph.CO].

Quantum-enhanced screened dark energy detection: Supplemental Material

Daniel Hartley,[1] Christian Käding,[2,3] Richard Howl,[4] and Ivette Fuentes[4]

[1]*Faculty of Physics, University of Vienna, Boltzmanngasse 5, 1090 Wien, Austria*

[2]*National Research University Higher School of Economics, 101000, Moscow, Russia*

[3]*School of Physics & Astronomy, University of Nottingham, University Park, Nottingham NG7 2RD, United Kingdom*

[4]*School of Mathematical Sciences, University of Nottingham, University Park, Nottingham NG7 2RD, United Kingdom*

(Dated: September 4, 2019)

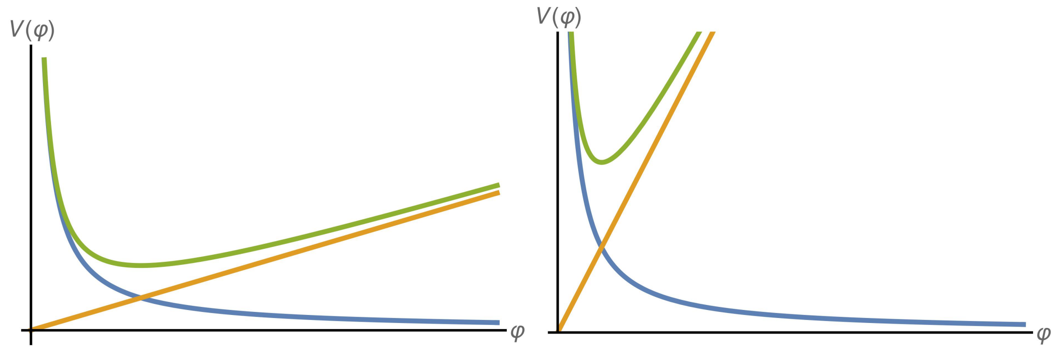

(a) (b)

FIG. 1: $n = 1$ chameleon effective potential for high (left) and low (right) ordinary matter densities plotted in green, with its components plotted in blue and orange.

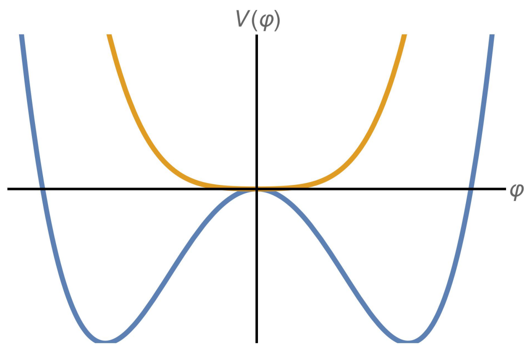

FIG. 2: Symmetron effective potential for high (blue) and low (orange) ordinary matter densities.

EFFECTIVE POTENTIALS FOR THE CHAMELEON AND SYMMETRON MODELS

Fig. 1 compares the chameleon effective potential V_{eff} (in green) in high and low density environments for the $n = 1$ chameleon. The effective potential is given to lowest order by

$$V_{\text{eff}}(\Phi) = \frac{\Lambda^{4+n}}{\Phi^n} + \frac{\rho}{2M_c}\Phi + \mathcal{O}\left(\frac{\Phi^2}{M_c^2}\right). \tag{1}$$

These first two components are plotted in blue and orange respectively for low (Fig. 1a) and high (Fig. 1b) values of ρ. It is reasonable to ignore higher order terms in Φ/M_c as any fifth force effect measured on or near the Earth must be perturbative to be consistent with experimental observations. The effective mass of excitations of the chameleon field is given by

$$m_c^2 = \left|\frac{\partial^2 V_{\text{eff}}}{\partial \Phi^2}\right|_{\Phi=\Phi_{\min}} = 2\Lambda^5 \left(\frac{\rho}{2M_c\Lambda^5}\right)^{3/2} \tag{2}$$

for $n = 1$, which clearly scales with ρ. Therefore, any chameleon force will be screened in high density environments.

Fig. 2 compares the symmetron effective potential for high (orange) and low (blue) density environments. The effective potential is given by

$$V_{\text{eff}}(\Phi) = \frac{1}{2}\left(\frac{\rho}{M_s^2} - \mu_s^2\right)\Phi^2 + \frac{\lambda_s}{4}\Phi^4 \tag{3}$$

from which it is obvious that the $\mathbb{Z}_2$ symmetry ($\Phi \to -\Phi$) is broken when the coefficient of the quadratic term in Φ is negative. This occurs at the critical density $\rho^* = \mu_s^2 M_s^2$. Above this density (Fig. 2, orange curve), the minima of V_{eff} are degenerate at $\Phi = 0$ so there is no fifth force. Below this density (Fig. 2, blue curve), the minima become non-degenerate and non-zero at an effective mass of

$$m_s^2 = 2\left(\mu_s^2 - \frac{\rho}{M_s^2}\right). \tag{4}$$

DERIVATION OF THE LOWEST ORDER EFFECT OF A CONFORMALLY COUPLED SCREENED SCALAR EFFECT ON A BOSONIC FIELD

We begin by modelling our BEC as an interacting massive scalar Bose field $\hat{\Phi}(\boldsymbol{x}, t)$ in a covariant formalism to introduce the background metric in a natural way, following the approach of [1–3]. Note that we do not assume that the BEC has "relativistic" properties such as large excitation energies (i.e. mass energy), high flow velocities (i.e. speed of light) or a strong interaction strength etc., and will later explicitly make "non-relativistic" restrictions.

Following the above references, we describe the evolution of the field operator $\hat{\Phi}$ with the Lagrangian density

$$\mathcal{L} = -\sqrt{-g}\left\{\partial^\mu \hat{\Psi}^\dagger \partial_\mu \hat{\Psi} + \left(\frac{m^2c^2}{\hbar^2} + V\right)\hat{\Psi}^\dagger\hat{\Psi} + U\right\}, \tag{5}$$

where V is the external potential, U is the interaction potential and $g_{\mu\nu}$ is the metric of the background (in general curved) spacetime with determinant g. As is standard in

BEC literature [4, 5], we consider only the leading order 2-particle contact interactions and approximate the interaction strength as

$$U = \frac{\lambda}{2}\hat{\Psi}^{\dagger}\hat{\Psi}^{\dagger}\hat{\Psi}\hat{\Psi}. \tag{6}$$

The interaction strength λ can be related to the s-wave scattering length a_s by

$$\lambda = 8\pi a_s. \tag{7}$$

We can rewrite the field operator $\hat{\Psi}$ as

$$\hat{\Psi} = \hat{\phi}e^{imc^2t/\hbar}. \tag{8}$$

We will later make the assumption that time derivatives of $\hat{\phi}$ are small, i.e. the excitations described by $\hat{\phi}$ have non-relativistic energies.

The appropriate background metric near a sphere of radius R and mass M sourcing screening for the assumed screened scalar field has the line element

$$ds^2 = e^{\zeta^2(r)}\left[-f(r)\,dt^2 + f^{-1}(r)\,dr^2 + r^2 d\Omega^2\right] \tag{9}$$

where $f(r) = 1 - r_s/r$, $r_s = 2GM/c^2$ is the Schwarzschild radius of the object and the conformal factor A has been rewritten as $A^2(\Phi) = \exp\left[\zeta^2(\Phi)\right]$ for notational convenience. Eq. (9) reduces to the Schwarzschild metric when $\zeta^2 \to 0$. The gravitational effect of the Earth is ignored; it is assumed that this can be accounted for either with differential measurements with and without the mass or through a dual interferometer scheme or simply by splitting the interferometer horizontally.

We now convert this Lagrangian to a Hamiltonian density (for readability and ease of interpretation) and make the following assumptions:

1. $|\zeta^2| \ll 1$,

2. $r_s \ll r$,

3. $\left|\partial_t\hat{\phi}\right|/c \ll \left|\partial_i\hat{\phi}\right|$ and

4. $\hbar^2\left|\partial_i\hat{\phi}^{\dagger}\partial_i\hat{\phi}\right| \ll m^2c^2\hat{\phi}^{\dagger}\hat{\phi}$,

where i runs over spatial indices. To lowest order in ζ^2 and r_s/r, the resulting Hamiltonian density is

$$\mathcal{H} = \frac{\hbar^2}{2m}\sum_i \partial_i\phi^\dagger\partial_i\phi + V_{eff}\hat{\phi}^\dagger\hat{\phi} + \frac{1}{2}\lambda_{NR}\hat{\phi}^\dagger\hat{\phi}^\dagger\hat{\phi}\hat{\phi}, \tag{10}$$

where

$$V_{eff} = V_{NR} + \frac{1}{2}mc^2\left[\zeta^2 - \frac{r_s}{r_{avg}}\right]. \tag{11}$$

The potentials have been rescaled in the form

$$V_{NR} = \frac{V}{2m}\,,\ \lambda_{NR} = \frac{\lambda}{2m} \tag{12}$$

as these are the form of the external potential and interaction strength that usually appear in the Gross-Pitaevskii equation (GPE) [4, 5]. The interaction strength λ_{NR} is usually written as g (e.g. in [4]), but we avoid this notation here to avoid confusion with the background spacetime metric.

We have defined r_{avg} as the mean distance of the BEC from the center of the source mass, and expanded r_s/r as

$$\frac{r_s}{r} = \frac{r_s}{r_{avg}+r'} = \frac{r_s}{r_{avg}}\left(1 - \frac{r'}{r_{avg}} + \cdots\right). \tag{13}$$

We can neglect all terms except the first if the BEC trap geometry has a negligible extent in the direction perpendicular to the source mass field gradient. For example, the BEC could be trapped with a cigar-shaped trapping potential oriented perpendicularly to the source mass.

The total field $\hat{\phi}$ can be written in terms of momentum eigenmodes as [4]

$$\hat{\phi}\left(\boldsymbol{r},t\right) = \left[\Psi_0\left(\boldsymbol{r}\right) + \hat{\vartheta}\left(\boldsymbol{r},t\right)\right]e^{-i\mu t/\hbar}, \tag{14}$$

where Ψ_0 corresponds to the momentum ground state, μ is the chemical potential and $\hat{\vartheta}$ contains all higher order modes. We make the Bogoliubov approximation and also assume that the excited modes of the field are negligibly occupied. If the potentials V_{NR} and λ_{NR} are stationary, then the equation of motion for Ψ_0 derived from the above Hamiltonian density is

$$\left[-\frac{\hbar^2}{2m}\nabla^2 + V_{eff} - \mu + \lambda_{NR}\left|\Psi_0\left(\boldsymbol{r}\right)\right|^2\right]\Psi_0\left(\boldsymbol{r}\right) = 0. \tag{15}$$

This is the time-independent GPE with the potential replaced by the effective potential V_{eff}. Since the screened scalar field contribution to V_{eff} is approximately constant across the width of the BEC, this GPE can be solved by splitting the chemical potential into $\mu = \mu_0 + \mu_I$ where μ_0 is the chemical potential when $V_{eff} \to V_{NR}$. The extra term is then given by

$$\mu_I = \frac{1}{2}mc^2\left[\zeta^2 - \frac{r_s}{r_{avg}}\right]. \tag{16}$$

Thus, the lowest order effect on the BEC ground state is a shift in the chemical potential, i.e. a phase shift. Physically, this phase is the gravitational red-shift due to the source mass, and the lowest order contribution of the screened scalar field is a modification of this red-shift. It is also worth noting that this phase shift appears in both the ground state and all excited modes of the BEC in a basis independent way.

ANALYSIS OF THE CONSTRAINT PLOTS IN THE MAIN TEXT

The constraints plotted in Figures 2-4 in the main text are derived from the quantum Cramer-Rao bound for estimating the phase difference in an interferometer. This bound is given by

$$(\Delta\theta_-)^2 \geq \frac{1}{\sqrt{NH(\theta_-)}}. \tag{17}$$

Assuming a null measurement, the bounds on the screening models are given by

$$\frac{1}{\sqrt{NH(\theta_-)}} \geq \frac{mc^2T}{2\hbar}\left(\zeta^2(r_1) - \zeta^2(r_0)\right) \tag{18}$$

for phases measured at r_0 and r_1.

Chameleon constraints, Figures 2 and 3 in the main text

There are three major sections in the BEC interferometer constraints in Fig. 4; the negatively sloped section where $M_c/M_{\rm pl} < 10^{-10}$, the vertical lines bounding the region on the large M_c side of the figure, and the positively sloped section between them.

In the limit of an infinitely wide vacuum chamber, the $n = 1$ chameleon field in the (non-perfect) vacuum has an effective mass

$$m_\infty^2 = 2\Lambda^5\left(\frac{\rho_\infty}{2M_c\Lambda^5}\right)^{3/2} \tag{19}$$

where ρ_∞ is the matter density of the vacuum. When the chameleon field is screened within the source mass, the constraint resulting from a null measurement is given by

$$\frac{1}{\sqrt{NH\left(\theta_-\right)}} > \frac{mc^2T}{2\hbar}\sqrt{\frac{2\Lambda^5}{M_c}}\left(\frac{1}{\sqrt{\rho_\infty}} - \frac{1}{\sqrt{\rho_{obj}}}\right) Re^{m_\infty R/\hbar}\left|\frac{e^{-m_\infty r_1/\hbar}}{r_1} - \frac{e^{-m_\infty r_0/\hbar}}{r_0}\right| \tag{20}$$

where ρ_{obj} is the density of the source object; this corresponds to the negatively sloped section of the Figure 2 constraints.

For larger values of M_c, the infinite vacuum chamber approximation does not hold as the Compton wavelength of the equilibrium chameleon becomes larger than the size of the vacuum chamber. In this case, the field equilibrium inside the vacuum chamber is instead described by [6]

$$\varphi_\infty \to \xi\left(n(n+1)\Lambda^{4+n}R^2\right)^{\frac{1}{n+2}}, \tag{21}$$

where $\xi = 0.55$ is a fudge factor given by the chamber's spherical geometry and vacuum density. The effective mass is set to the radius of the vacuum chamber $m_\infty \to \hbar/R_{\text{vac}}$ and the relevant constraint from a null measurement is

$$\frac{1}{\sqrt{NH\left(\theta_-\right)}} > \frac{mc^2T}{2\hbar}\left(\xi\left[\frac{2\Lambda^5 R_{\text{vac}}^2}{M_c^3}\right]^{1/3} - \sqrt{\frac{2\Lambda^5}{M_c\rho_{obj}}}\right) Re^{R/R_{\text{vac}}}\left|\frac{e^{-r_1/R_{\text{vac}}}}{r_1} - \frac{e^{-r_0/R_{\text{vac}}}}{r_0}\right|. \tag{22}$$

This corresponds to the positively sloped section of Figure 2.

The vertical section occurs when both the massive source and the vacuum in the chamber are screened, which leads to a Λ-independent field profile and

$$\frac{1}{\sqrt{NH\left(\theta_-\right)}} > \frac{mc^2T}{2\hbar}\left(\frac{\rho_{obj}R^3}{3M_c^2}\right) e^{R/R_{\text{vac}}}\left|\frac{e^{-r_1/R_{\text{vac}}}}{r_1} - \frac{e^{-r_0/R_{\text{vac}}}}{r_0}\right|. \tag{23}$$

The horizontal boundaries in Figure 3 for early values of n result from the source and the vacuum both being screened. For larger values of n, the background field profile given in Eq. (21) is used.

Symmetron constraints, Figure 4 in the main text

The value of μ_s to which these constraints apply is limited by the geometry of the proposed experiment, as the Compton wavelength in low density regions is approximately $1/\mu_s$. For the field to evolve to its vacuum minimum within the chamber, the Compton wavelength must be smaller than the vacuum chamber radius. However, if the Compton wavelength is too small then the field is Yukawa supressed. The value of μ_s that this proposed experiment can constrain is restricted by these two conditions to

$$10^{-5.5}\ \mathrm{eV} \lesssim \mu_s \lesssim 10^{-4}\ \mathrm{eV} \tag{24}$$

in natural units.

An object is screened from the symmetron force when its density is above the critical density $\rho_* = \mu_s^2 M_s^2$. The region in M_s that our proposed experiment would constrain is the region where this critical density is between the densities of the source object and the surrouding vacuum. These two density restrictions cause the sharp sides of the excluded regions in both our predicted excluded regions and the atom interferometry exclusion regions in Figure 4.

The curve in the high M_s section of the predicted excluded regions is the area where the critical density and the source object density become comparable. The peak in the low M_s section of the $\mu_s = 10^{-4}$ eV excluded region is caused by a resonance where the Compton wavelength of the symmetron field matches the distance from the object to the BEC.

The wavefunctions of atoms in a BEC are (in the ideal case) spread over the width of the BEC and all overlap. As a first approximation, we consider the BEC to be a region of uniform density as opposed to a collection of discrete objects. The density of the BEC is between that of the vacuum and the source object. When the BEC density is below the critical density, it does not substantially modify the symmetron field profile. When the BEC density is above the critical density, there should in principle be a dip in the symmetron field profile. However, the Compton wavelength of the symmetron is far greater than the width of the BEC in this entire section of the parameter space, so the BEC again does not substantially effect the symmetron field profile. Hence, whether or not the BEC is screened does not play a role in determining the region of parameter space excluded by our proposed experiment.

The full bound is given by

$$\begin{aligned}\frac{1}{\sqrt{NH\left(\theta_-\right)}} > \frac{mc^2T}{2\hbar}\frac{\mu_s^2}{\lambda M_s^2}\left(1-\frac{\rho_\infty}{\mu_s^2 M_s^2}\right)\times \\ \left(2\Gamma\left[\frac{e^{-m_{out}r_0}}{r_0}-\frac{e^{-m_{out}r_1}}{r_1}\right]+\Gamma^2\left[\frac{e^{-2m_{out}r_1}}{r_1^2}-\frac{e^{-2m_{out}r_0}}{r_0^2}\right]\right)\end{aligned} \tag{25}$$

where

$$\Gamma = Re^{m_{out}R} \frac{m_{in}R - \tanh(m_{in}R)}{m_{in}R + m_{out}R\tanh(m_{in}R)} \tag{26}$$

and

$$m_i^2 = 2\left(\mu_s^2 - \frac{\rho_i}{M_s^2}\right). \tag{27}$$

[1] S. Fagnocchi, S. Finazzi, S. Liberati, M. Kormos, and A. Trombettoni, New Journal of Physics **12**, 095012 (2010).

[2] D. Hartley, T. Bravo, D. Rätzel, R. Howl, and I. Fuentes, Phys. Rev. D **98**, 025011 (2018).

[3] D. Hartley, C. Käding, R. Howl, and I. Fuentes, Phys. Rev. D **99**, 105002 (2019).

[4] L. Pitaevskii and S. Stringari, *Bose-Einstein Condensation* (Oxford University Press, 2003).

[5] C. J. Pethick and H. Smith, *Bose-Einstein Condensation in Diulte Gases* (Cambridge University Press, 2002).

[6] B. Elder, J. Khoury, P. Haslinger, M. Jaffe, H. Mller, and P. Hamilton, Phys. Rev. **D94**, 044051 (2016), arXiv:1603.06587 [astro-ph.CO].

Part III

Conclusion

Conclusion

The work presented in this thesis further develops the use of Bose-Einstein condensates as detectors of gravitational phenomena. The combination of low noise, a high degree of control and access to the quantum state makes a Bose-Einstein condensate an ideal platform for precision quantum metrology. Cold atom systems are well established as a platform for gravity-related tests (gravimetry [17], equivalence principle tests [15, 16], fifth force searches [83, 101] etc.) so taking advantage of the benefits of quantum metrology with the manifest and controllable quantum nature of a Bose-Einstein condensate is an obvious (though technically challenging) step forward in precision.

In [1], the simulation of the effect of a gravitational wave on quantised sound waves (phonons) of a Bose-Einstein condensate is investigated. A passing gravitational wave will affect how phonons evolve on a Bose-Einstein condensate (it may in general have both phonon creation and mode-mixing effects [22]) which is utilised in a proposed gravitational wave detector [22].

Two simulations are considered in this paper. The first simulation involves modifying the properties of the Bose-Einstein condensate such that the phonon field evolves as if it were a massless scalar field embedded in a flat space-time with a passing gravitational wave. The second simulation reproduces the equations of motion for the phonon field as if the underlying Bose-Einstein condensate were in the path of a gravitational wave in an otherwise flat space-time.

It is concluded in both cases that both the external potential and the atomic interaction strength in the Bose-Einstein condensate must be modulated to simulate these effects. This interaction strength modulation may be achieved experimentally by exploiting a Feshbach resonance. A Feshbach resonance occurs when the energies of free atom states and bound two-atom states are brought into degeneracy by the application of an external magnetic field, resulting in a divergent s-wave scattering length. By tuning the magnetic field strength near this resonance, the effective scattering length can be controlled. Particular choices of the modulation of the interaction strength and the external trapping potential are shown to achieve the desired simulation parameters for generic far-field gravitational wave profiles. Achieving this gravitational wave simulation is motivated by the aforementioned detector proposal, and the experimental implementation of these results with chosen gravitational wave profile parameters can be used to test the metrological scheme of this detector.

The results of [2] largely follow the techniques of [1], but for conformally coupled screened scalar field models of gravity. A wide array of theories beyond General Relativity and the Standard Model include extra forces and particles for which no experimental evidence has yet been found. To match local experiments and still be cosmologically relevant (e.g. as a partial solution to the cosmological constant problem), these additions to the standard models may possess some screening mechanism which modifies properties such as effective masses and interaction strengths near the Earth or within our solar system. Models with these screening mechanisms can be experimentally constrained from different directions in the parameter space by both local experiments and astrophysical observations and potentially entirely eliminated. Motivated by the proposed detector in [3], the simplest of these models with screening mechanisms are investigated in [2].

These “simplest models” involve extending standard models of the Universe with one extra scalar field mediating a fifth force, which manifests as a conformal coupling to the background metric. The host of astrophysical observations consistent with general relativity suggest that this conformal factor must be perturbative at most. As in [1], the requirements to simulate the evolution of phonons on a Bose-Einstein condensate both as a massless scalar field on a perturbed background space-time and as if the underlying Bose-Einstein condensate bulk were embedded in a perturbed space-time. In contrast with [1], it is found that these two simulations happen to coincide. Perturbations to the interaction strength and external potential applied to the Bose-Einstein condensate are again both needed to implement this simulation, and the form of these perturbations is given for a list of commonly studied screening mechanisms (chameleon, symmetron, dilaton, galileon and D-BIon).

The best current constraints on the conformally coupled screened scalar field models described in the above paragraph are generally given by interferometry experiments with cold atoms [18], so the central result of [3] is a proposed Bose-Einstein condensate interferometer-based detector for the purposes of improving these constraints. As the screening mechanisms for these models are dependent on the local matter density, a massive object creates a gradient in the screened scalar field which may be detected (or the model constrained in the case of no detection) by an interferometer with two arms split in the direction of the gradient. This approach was taken with cold atoms in [83, 102]. The detector proposed in [3] improves on this idea by using a Bose-Einstein condensate held in a trap.

The interaction time of this proposed detector is much greater than that of an atom interferometer, as it is not limited by the gravitational arc of free fall. An atom interferometer is limited by gravity in the sense that it must follow a ballistic trajectory in the region near the source object (with a strong predicted screened scalar field gradient). As the atoms in a non-moving Bose-Einstein condensate evolve, the interaction time of the atoms can potentially be much larger, with this entire time spent in a stronger gradient region. It is shown that combining these advantages and optimisations with current or near-future technical capability would lead to a large improvement in the constraints for models with the chameleon screening mechanism (in the event of a null measurement), entirely eliminating the interesting parameter space of the simplest chameleon model in a single run. Large improvements to the constraints on the symmetron screening mechanism models are also predicted.

Cold atom systems and the quantum control afforded by Bose-Einstein condensates are already impacting current gravity-related metrology and will continue to do so well into the future. The results presented in this thesis continue to show that Bose-Einstein condensates offer an advantageous and testable platform for measurements of gravity. While the experimental implementation of Bose-Einstein condensate based detectors has not yet been achieved, experimental efforts in this direction are currently underway. The protocols outlined in this thesis are possible with current or near-future techniques and the realisation of these detectors is only a matter of time.

Acknowledgements

My gratitude goes to a long list of people. First, to all of the people past and present in the group and the office comprising Ana Lucia Báez Camargo, Luis Cortés Barbado, Tupac Bravo Ibarra, David Edward Bruschi, Karishma Hathlia, Richard Howl, Stephan Huimann, Paul Juschitz, Jan Kohlrus, Max Lock, Dennis Rätzel and sometimes Carlos Pineda. Second, to Christian Käding for the introduction to an interesting field and enthusiasm for new ideas. Third, to my friends in Vienna who are too many to list, who made the last few years overall some of the most enjoyable of my life so far, and without whom I may not have made it through. Fourth, to my family for the passion for curiosity, bottomless and unending support and visits even from the other side of the world. Fifth, to Markus Aspelmeyer for his support, can-do attitude and magic touch. Sixth, to the quantum group administrative staff and to CoQuS in general, for the quick and professional work and the unbelievable level of opportunity and flexibility. Finally, to my supervisor Ivette Fuentes, for the opportunity to work in such a supportive and friendly group.

Bibliography

[1] Hartley, D., Bravo, T., Rätzel, D., Howl, R. & Fuentes, I., 'Analogue simulation of gravitational waves in a $3 + 1$-dimensional Bose-Einstein condensate', *Physical Review D* **98,** 025011, doi:10.1103/PhysRevD.98.025011 (2018).

[2] Hartley, D., Käding, C., Howl, R. & Fuentes, I., 'Quantum simulation of dark energy candidates', *Physical Review D* **99,** 105002, doi:10.1103/PhysRevD.99.105002 (2019).

[3] Hartley, D., Käding, C., Howl, R. & Fuentes, I., 'Quantum-enhanced screened scalar field dark energy detection', arXiv:not.yet (2019).

[4] Abbott, B. P. *et al.*, 'Observation of Gravitational Waves from a Binary Black Hole Merger', *Physical Review Letters* **116,** 061102, doi:10.1103/PhysRevLett.116.061102 (2016).

[5] Abbott, B. P. *et al.*, 'GW170817: Observation of Gravitational Waves from a Binary Neutron Star Inspiral', *Physical Review Letters* **119,** 161101, doi:10.1103/PhysRevLett.119.161101 (2017).

[6] Abbott, B. P. *et al.*, 'Multi-messenger Observations of a Binary Neutron Star Merger', *The Astrophysical Journal* **848,** L12, doi:10.3847/2041-8213/aa91c9 (2017).

[7] Kasen, D., Metzger, B., Barnes, J., Quataert, E. & Ramirez-Ruiz, E., 'Origin of the heavy elements in binary neutron-star mmerger from a gravitational-wave event', *Nature* **551,** 80–84, doi:10.1038/nature24453 (2017).

[8] Pian, E. *et al.*, 'Spectroscopic identification of r-process nucleosynthesis in a double neutron-star merger', *Nature,* 67–70, doi:10.1038/nature24298 (2017).

[9] Abbott, B. P. *et al.*, 'GW151226: Observation of Gravitational Waves from a 22-Solar-Mass Binary Black Hole Coalescence', *Physical Review Letters* **116,** 241103, doi:10.1103/PhysRevLett.116.241103 (2016).

[10] Abbott, B. P. *et al.*, 'GW170104: Observation of a 50-Solar-Mass Binary Black Hole Coalescence at Redshift 0.2', *Physical Review Letters* **118,** 221101, doi:10.1103/PhysRevLett.118.221101 (2017).

[11] Abbott, B. P. *et al.*, 'GW170814: A Three-Detector Observation of Gravitational Waves from a Binary Black Hole Coalescence', *Physical Review Letters* **119,** 141101, doi:10.1103/PhysRevLett.119.141101 (2017).

[12] Abbott, B. P. *et al.*, 'GW170608: Observation of a 19 Solar-mass Binary Black Hole Coalescence', *The Astrophysical Journal* **851,** L35, doi:10.3847/2041-8213/aa9f0c (2017).

[13] Lantz, B. *et al.*, *Instrument Science White Paper 2018* tech. rep. LIGO-T1800133-v4 (LIGO Scientific Collaboration, 2018), https://dcc.ligo.org/LIGO-T1800133/public.

[14] Acernese, F *et al.*, 'Advanced Virgo: a second-generation interferometric gravitational wave detector', *Classical and Quantum Gravity* **32,** 024001, doi:10.1088/0264-9381/32/2/024001 (2014).

[15] Rosi, G. *et al.*, 'Quantum test of the equivalence principle for atoms in coherent superposition of internal energy states', *Nature Communications* **8,** 15529, doi:10.1038/ncomms15529 (2017).

[16] Overstreet, C. *et al.*, 'Effective Inertial Frame in an Atom Interferometric Test of the Equivalence Principle', *Physical Review Letters* **120,** 183604, doi:10.1103/PhysRevLett.120.183604 (2018).

[17] Dos Santos, F. P. & Bonvalot, S., in *Encyclopedia of Geodesy* (ed Grafarend, E.) 1–6 (Springer International Publishing, 2016), doi:10.1007/978-3-319-02370-0_30-1.

[18] Burrage, C. & Sakstein, J., 'Tests of Chameleon Gravity', *Living Reviews in Relativity* **21,** 1, doi:10.1007/s41114-018-0011-x (2018).

[19] Graham, P. W., Hogan, J. M., Kasevich, M. A., Rajendran, S. & Romani, R. W., 'Mid-band gravitational wave detection with precision atomic sensors', arXiv:1711.02225 (2017).

[20] Coleman, J. & the MAGIS-100 Collaboration, 'MAGIS-100 at Fermilab', arXiv:1812.00482 (2018).

[21] Geiger, R. *et al.*, 'Matter-wave laser Interferometric Gravitation Antenna (MIGA): New perspectives for fundamental physics and geosciences', arXiv:1505.07137 (2015).

[22] Sabín, C., Bruschi, D. E., Ahmadi, M. & Fuentes, I., 'Phonon creation by gravitational waves', *New Journal of Physics* **16,** 085003, doi:10.1088/1367-2630/16/8/085003 (2014).

[23] Hawking, S. W., 'Particle Creation by Black Holes', *Communications in Mathematical Physics* **43,** 199–220, doi:10.1007/BF02345020 (1975).

[24] Unruh, W. G., 'Notes on black-hole evaporation', *Physical Review D* **14,** 870, doi:10.1103/PhysRevD.14.870 (1976).

[25] Anglin, J. R. & Ketterle, W., 'Bose-Einstein condensation of atomic gases', *Nature* **617,** 211–218, doi:10.1038/416211a (2002).

[26] Pitaevskii, L. P. & Stringari, S., 'Bose-Einstein Condensation' (Oxford University Press, 2003).

[27] Ludlow, A. D., Boyd, M. M., Ye, J., Peik, E. & Schmidt, P. O., 'Optical atomic clocks', *Reviews of Modern Physics* **87,** 637–701, doi:10.1103/RevModPhys.87.637 (2015).

[28] Pethick, C. J. & Smith, H., 'Bose-Einstein Condensation in Diulte Gases' (Cambridge University Press, 2002).

[29] Jamieson, M. J., Cheung, A. S. C. & Ouerdane, H., 'Dependence of the scattering length for hydrogen atoms on effective mass', *European Physical Journal D* **56,** 181–188, doi:10.1140/epjd/e2009-00280-8 (2010).

[30] Tiesinga, E. *et al.*, 'A Spectroscopic Determination of Scattering Lengths for Sodium Atom Collisions', *Journal of Research of NIST* **101,** 505–520, doi:10.6028/jres.101.051 (1996).

[31] Egorov, M. *et al.*, 'Measurement of *s*-wave scattering lengths in a two-component Bose-Einstein condensate', *Physical Review A* **87,** 053614, doi:10.1103/PhysRevA.87.053614 (2013).

[32] Leo, P. J., Julienne, P. S., Mies, F. H. & Williams, C. J., 'Collisional Frequency Shifts in ^{133}Cs Fountain Clocks', *Physical Review Letters* **86,** 3743, doi:10.1103/PhysRevLett.86.3743 (2001).

[33] Thomas, A. M., *Ultra-cold Collisions and Evaporative Cooling of Caesium in a Magnetic Trap* PhD thesis (University of Oxford, 2004).

[34] Gross, E. P., 'Structure of a quantized vortex in boson systems', *Il Nuovo Cimento* **20,** 454–477, doi:10.1007/BF02731494 (1961).

[35] Pitaevskii, L. P., 'Vortex Lines In An Imperfect Bose Gas', *Soviet Physics JETP* **13,** 646–651 (1961).

[36] Landau, L. D. & Lifshitz, E. M., 'Fluid Mechanics' (Pergamon Press, 1987).

[37] Bogoliubov, N. N., 'On The Theory Of Superfluidity', *Journal of Physics (USSR)* **11,** 23–32 (1947).

[38] Pitaevskii, L. P. & Stringari, S., 'Landau damping in dilute Bose gases', *Physics Letters A* **235,** 398–402, doi:10.1016/S0375-9601(97)00666-X (1997).

[39] Giorgini, S., 'Dagases in dilute Bose gases: A mean-field approach', *Physical Review A* **57,** 2949, doi:10.1103/PhysRevA.57.2949 (1998).

[40] Visser, M., 'Acoustic black holes: horizons, ergospheres and Hawking radiation', *Classical and Quantum Gravity* **15,** 1767–1791, doi:10.1088/0264-9381/15/6/024 (1998).

[41] Fagnocchi, S., Finazzi, S., Liberati, S., Kormos, M. & Trombettoni, A., 'Relativistic Bose-Einstein condensates: a new system for analogue models of gravity', *New Journal of Physics* **12,** 095012, doi:10.1088/1367-2630/12/9/095012 (2010).

[42] Visser, M. & Molina-Paris, C., 'Acoustic geometry for general relativistic barotropic irrotational fluid flow', *New Journal of Physics* **12,** 095014, doi:10.1088/1367-2630/12/9/095014 (2010).

[43] Birrell, N. D. & Davies, P. C. W., 'Quantum Fields in Curved Space' (Cambridge University Press, 1982).

[44] Fulling, S. A., 'Aspects of Quantum Field Theory in Curved Space-Time' (Cambridge University Press, 1989).

[45] Bunch, T. S., Panangaden, P. & Parker, L., 'On renormalisation of $\lambda\phi^4$ field theory in curved space-time', *Journal of Physics A* **13,** 901–932, doi:10.1088/0305-4470/13/3/022 (1980).

[46] Einstein, A., 'Die Feldgleichungen der Gravitation', *Sitzungsberichte der Königlich Preußischen Akademie der Wissenschaften*, 844–847 (1915).

[47] Danzmann, K. & the LISA Consortium, 'The Gravitational Universe', arXiv:1305.5720 (2013).

[48] Sabín, C., Kohlrus, J., Bruschi, D. E. & Fuentes, I., 'Themal noise in BEC-phononic gravitational wave detectors', *European Physical Journal Quantum Technology* **3,** 8, doi:10.1140/epjqt/s40507-016-0046-4 (2016).

[49] Howl, R., Sabín, C., Hackermüller, L. & Fuentes, I., 'Quantum Decoherence of Phonons in Bose-Einstein Condensates', *Journal of Physics B* **51,** 015303, doi:10.1088/1361-6455/aa9622 (2017).

[50] Rätzel, D. & Fuentes, I., 'Testing small scale gravitational wave detectors with dynamical mass distributions', *Journal of Physics Communications* **3,** 025009 (2018).

[51] Howl, R. & Fuentes, I., 'Active Interferometry with Gaussian Channels', arXiv:1902.09883 (2019).

[52] Misner, C. W., Thorne, K. S. & Wheeler, J. A., 'Gravitation' (W. H. Freeman and Company, 1973).

[53] Crisostomi, M. & Koyama, K., 'Vainshtein mechanism after GW170817', *Physical Review D* **97,** 021301, doi:10.1103/PhysRevD.97.021301 (2018).

[54] Manasse, F. K. & Misner, C. W., 'Fermi Normal Coordinates and Some Basic Concepts in Differential Geometry', *Journal of Mathematical Physics* **4,** 735, doi:10.1063/1.1724316 (1963).

[55] Ni, W.-T. & Zimmermann, M., 'Inertial and gravitational effects in the proper reference frame of an accelerated, rotating observer', *Physical Review D* **17,** 1473, doi:10.1103/PhysRevD.17.1473 (1978).

[56] Schutz, B., 'A First Course in General Relativity' (Cambridge University Press, 2009).

[57] Dyson, F. W., Eddington, A. S. & Davidson, C., 'A determination of the deflection of light by the sun's gravitational field, from observations made at the total eclipse of May 29, 1919', *Philosophical Transactions of the Royal Society A* **220,** 571–581, doi:10.1098/rsta.1920.0009 (1920).

[58] Dickey, J. O. *et al.*, 'Lunar Laser Ranging: A Continuing Legacy of the Apollo Program', *Science* **265,** 482–490, doi:10.1126/science.265.5171.482 (1994).

[59] Horndeski, G. W., 'Second-order scalar-tensor field equations in a four-dimensional space', *International Journal of Theoretical Physics* **10,** 363–384, doi:10.1007/BF01807638 (1974).

[60] Fujii, Y. & Maeda, K.-i., 'The Scalar-Tensor Theory of Gravitation' (Cambridge University Press, 2004).

[61] Clifton, T., Ferreira, P. G., Padilla, A. & Skordis, C., 'Modified gravity and cosmology', *Physics Reports* **513,** 1–189, doi:10.1016/j.physrep.2012.01.001 (2012).

[62] Joyce, A., Jain, B., Khoury, J. & Trodden, M., 'Beyond the cosmological standard model', *Physics Reports* **568,** 1–98, doi:10.1016/j.physrep.2014.12.002 (2015).

[63] Khoury, J., 'Alternative to particle dark matter', *Physical Review D* **91,** 024022, doi:10.1103/PhysRevD.91.024022 (2015).

[64] Burrage, C., Elder, B. & Millington, P., 'Particle level screening of scalar forces in $1+1$ dimensions', *Physical Review D* **99,** 024045, doi:10.1103/PhysRevD.99.024045 (2019).

[65] Wehus, I. K. & Ravndal, F., 'Dynamics of the scalar field in five-dimensional Kaluza-Klein theory', *International Journal of Modern Physics A* **19,** 4671–4685, doi:10.1142/S0217751X04020609 (2004).

[66] Ishak, M., 'Testing general relativity in cosmology', *Living Reviews in Relativity* **22,** 1, doi:10.1007/s41114-018-0017-4 (2019).

[67] Burrage, C., Copeland, E. J., Millington, P. & Spannowsky, M., 'Fifth forces, Higgs portals and broken scale invariance', *Journal of Cosmology and Astroparticle Physics* **2018,** 036, doi:10.1088/1475-7516/2018/11/036 (2018).

[68] Postma, M. & Volponi, M., 'Equivalence of the Einstein and Jordan frames', *Physical Review D* **90,** 103516, doi:10.1103/PhysRevD.90.103516 (2014).

[69] Faraoni, V. & Nadeau, S., '(Pseudo)issue of the conformal frame revisited', *Physical Review D* **75,** 023501, doi:10.1103/PhysRevD.75.023501 (2007).

[70] Banerjee, N. & Majumder, B., 'A question mark on the equivalence of Einstein and Jordan frames', *Physics Letters B* **754,** 129–134, doi:10.1016/j.physletb.2016.01.022 (2016).

[71] Pandey, S. & Banerjee, N., 'Equivalence of Jordan and Einstein frames at the quantum level', arXiv:1610.00584 (2016).

[72] Pascual, J., 'Schwerkraft und Weltall: Grundlagen der theoretischen Kosmologie' (Braunschweig: Vieweg, 1952).

[73] Bekenstein, J. D., 'Relation between physical and gravitational geometry', *Physical Review D* **48,** 3641, doi:https://doi.org/10.1103/PhysRevD.48.3641 (1993).

[74] Sakstein, J., 'Disformal theories of gravity: from the solar system to cosmology', *Journal of Cosmology and Astroparticle Physics* **2014,** 012, doi:10.1088/1475-7516/2014/12/012 (2014).

[75] Khoury, J. & Weltman, A., 'Chameleon cosmology', *Physical Review D* **69,** 044026, doi:10.1103/PhysRevD.69.044026 (204).

[76] Dehnen, H., Frommert, H. & Ghaboussi, F., 'Higgs field and a new scalar-tensor theory of gravity', *International Journal of Theoretical Physics* **31,** 109–114, doi:10.1007/BF00674344 (1992).

[77] Hinterbichler, K. & Khoury, J., 'Screening Long-Range Forces through Local Symmetry Restoration', *Physical Review Letters* **104,** 231301, doi:10.1103/PhysRevLett.104.231301 (2010).

[78] Vainshtein, A. I., 'To the problem of nonvanishing gravitational mass', *Physics Letters B* **39,** 393–394, doi:10.1016/0370-2693(72)90147-5 (1972).

[79] Babichev, E. & Deffayet, C., 'An introduction to the Vainshtein mechanism', *Classical and Quantum Gravity* **30,** 184001, doi:10.1088/0264-9381/30/18/184001 (2013).

[80] Dvali, G., Gabadadze, G. & Porrati, M., '4D gravity on a brane in 5D Minkowski space', *Physics Letters B* **485,** 208–214, doi:10.1016/S0370-2693(00)00669-9 (2000).

[81] Nicolis, A., Rattazzi, R. & Trincherini, E., 'Galileon as a local modification of gravity', *Physical Review D* **79,** 064036, doi:10.1103/PhysRevD.79.064036 (2009).

[82] Bloomfield, J. K., Burrage, C. & Davis, A.-C., 'Shape dependence of Vainshtein screening', *Physical Review D* **91,** 083510, doi:10.1103/PhysRevD.91.083510 (2015).

[83] Jaffe, M. *et al.*, 'Testing sub-gravitational forces on atoms from a miniature in-vacuum source mass', *Nature Physics* **13,** 938–942, doi:10.1038/nphys4189 (2017).

[84] Braunstein, S. L. & Caves, C. M., 'Statistical distance and the geometry of quantum states', *Physical Review Letters* **72,** 3439–3443, doi:10.1103/PhysRevLett.72.3439 (1994).

[85] Kok, P. & Lovett, B. W., 'Introduction to optical quantum information processing' (Cambridge University Press, 2010).

[86] Paris, M. G. A., 'Quantum Estimation for Quantum Technology', *International Journal of Quantum Information* **7,** 125–137, doi:10.1142/S0219749909004839 (2009).

[87] Giovannetti, V., Lloyd, S. & Maccone, L., 'Advances in quantum metrology', *Nature Photonics* **5,** 222–229, doi:10.1038/nphoton.2011.35 (2011).

[88] Giovannetti, V., Lloyd, S. & Maccone, L., 'Quantum Metrology', *Physical Review Letters* **96,** 010401, doi:10.1103/PhysRevLett.96.010401 (2006).

[89] Adesso, G., Ragy, S. & Lee, A. R., 'Continuous Variable Quantum Information: Gaussian States and Beyond', *Open Systems & Information Dynamics* **21,** 1440001, doi:10.1142/S1230161214400010 (2014).

[90] Andersen, U. L., Gehring, T., Marquardt, C. & Leuchs, G., '30 years of squeezed light generation', *Physica Scripta* **91,** 053001, doi:10.1088/0031-8949/91/5/053001 (2016).

[91] Demkowicz-Dobrzański, R., Banaszek, K. & Schnabel, R., 'Fundamental quantum interferometry bound for the squeezed-light-enhanced gravitational wave detector GEO 600', *Physical Review A* **88,** 041802, doi:10.1103/PhysRevA.88.041802 (2013).

[92] Arvind, Dutta, B., Mukunda, N. & Simon, R., 'The real symplectic groups in quantum mechanics and optics', *Pramana* **45,** 471–497, doi:10.1007/BF02848172 (1995).

[93] Weedbrook, C. *et al.*, 'Gaussian quantum information', *Reviews of Modern Physics* **84,** 621, doi:10.1103/RevModPhys.84.621 (2012).

[94] Šafránek, D., *Gaussian quantum metrology and space-time probes* PhD thesis (University of Nottingham, 2016).

[95] Pinel, O. *et al.*, 'Ultimate sensitivity of precision measurements with intense Gaussian quantum light: A multimodal approach', *Physical Review A* **85,** 010101, doi:10.1103/PhysRevA.85.010101 (2012).

[96] Marian, P. & Marian, T. A., 'Uhlmann fidelity between two-mode Gaussian states', *Physical Review A* **86,** 022340, doi:10.1103/PhysRevA.86.022340 (2012).

[97] Pinel, O., Jian, P., Treps, N., Fabre, C. & Braun, D., 'Quantum parameter estimation using general single-mode Gaussian states', *Physical Review A* **88,** 040102, doi:10.1103/PhysRevA.88.040102 (2013).

[98] Monras, A., 'Phase space formalism for quantum estimation of Gaussian states', arXiv:1303.3682 (2013).

[99] Šafránek, D., Lee, A. R. & Fuentes, I., 'Quantum parameter estimation using multi-mode Gaussian states', *New Journal of Physics* **17,** 073016, doi:10.1088/1367-2630/17/7/073016 (2015).

[100] Wang, X.-B., Hiroshima, T., Tomita, A. & Hayashi, M., 'Quantum information with Gaussian states', *Physics Reports* **448,** 1–111, doi:10.1016/j.physrep.2007.04.005 (2007).

[101] Jaeckel, J. & Roy, S., 'Spectroscopy as a test of Coulomb's law: A probe of the hidden sector', *Physical Review D* **82,** 125020, doi:10.1103/PhysRevD.82.125020 (2010).

[102] Hamilton, P. *et al.*, 'Atom-interferometry constraints on dark energy', *Science* **349,** 849–851, doi:10.1126/science.aaa8883 (2015).